

**EXPERIMENTAL STUDIES ON
INTERMEDIATE PYROLYSIS OF
LIGNOCELLULOSIC BIOMASS
COCONUT SHELLS**

THESIS

Submitted in partial fulfilment of the requirements for the degree of

DOCTOR OF PHILOSOPHY

By

KIRAN KUMAR D

(Reg. No. 148018ME14F18)



DEPARTMENT OF MECHANICAL ENGINEERING
NATIONAL INSTITUTE OF TECHNOLOG KARNATAKA,
SURATHKAL, MANGALORE-575025

May, 2021

**EXPERIMENTAL STUDIES ON
INTERMEDIATE PYROLYSIS OF
LIGNOCELLULOSIC BIOMASS
COCONUT SHELLS**

THESIS

Submitted in partial fulfilment of the requirements for the degree of

DOCTOR OF PHILOSOPHY

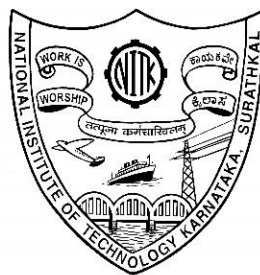
By

KIRAN KUMAR D
(Reg. No. 148018ME14F18)

Under the Guidance of

Dr. Veershetty Gumtapure

Associate Professor

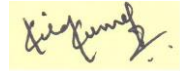


DEPARTMENT OF MECHANICAL ENGINEERING
NATIONAL INSTITUTE OF TECHNOLOG KARNATAKA,
SURATHKAL, MANGALORE-575025

May, 2021

DECLARATION

I hereby *declare* that the thesis entitled “**EXPERIMENTAL STUDIES ON INTERMEDIATE PYROLYSIS OF LIGNOCELLULOSIC BIOMASS COCONUT SHELLS**” which is being submitted to the **National Institute of Technology Karnataka, Surathkal** in partial fulfilment of the requirements for the award of the degree of **Doctor of Philosophy** in Mechanical Engineering is a *bonafide report of the research work carried out by me*. The material contained in this thesis has not been submitted to any University or Institution for the award of any degree.



Kiran Kumar D

Reg. No. 148018ME14F18

Department of Mechanical Engineering

Place: NITK, Surathkal

Date: 29-05-2021

CERTIFICATE

This is to *certify* that the thesis entitled “**EXPERIMENTAL STUDIES ON INTERMEDIATE PYROLYSIS OF LIGNOCELLULOSIC BIOMASS COCONUT SHELLS**” submitted by **Kiran Kumar D (Register Number: 148018ME14F18)** as the record of the research work carried out by him, *is accepted as the Research Thesis submission* in partial fulfilment of the requirements for the award of degree of **Doctor of Philosophy**.

Research Guide

Dr. Veershetty Gumtapure

Associate Professor

Dept. of Mechanical Engineering

NITK, Surathkal

Chairman –DRPC

Dr. Kulkarni S M

Head of the Department

Dept. of Mechanical Engineering

NITK, Surathkal

ACKNOWLEDGEMENT

This thesis has been written as a part of Ph.D. work by Kiran Kumar Dasari at the National Institute of Technology Karnataka (NITK), Surathkal at the department of mechanical engineering. Professor Veershetty Gumtapure has been the main supervisor throughout this work.

I owe a lot of gratitude to all the people whom have been involved and influenced the progress of this work and my personal development as a researcher. First of all I would like to thank Dr. Veershetty Gumtapure for being my main and competent feedback throughout this work. Your door has always been open and you have always spent time discussing issues of all sizes, ranging from professional to personal. You have been as much a friend as an employer to me in these last years, and for this I am very grateful. Many thanks also to the Research Progress Assessment Committee Dr. Saikat Dutta, Department of chemistry and Dr. Kumar G N, Department of Mechanical engineering. I cherish your views on my work and your often alternative view on my work helped shape this work to be much more thorough. I especially thank Vayu oils and gases, Bangalore for allowing performing pyrolysis experiments and IIT Bombay, IIT Madras, IISC Bangalore SAIF lab for chemical analysis.

I acknowledge my thanks to Prof. Gangadharan KV, Prof. Narendranath S, Prof. Shrikanth S Rao and Prof. Kulkarni S M, Head of department of mechanical engineering 2014-2016, 2016-2018, 2018-2020 and 2021- current respectively for extending administrative facility for tranquil progress of my Ph.D. work. I express my heartfull thanks to The Director of NITK Surathkal providing the grants/funds to carry out this research work. I also thank all the non-supporting staff of NITK for their help and support provided during the work.

Research scholars Sunil, Vinay Kumar, Sharath B O, Ritesh Tiwari and Navya from department of chemistry support the work on hydrodeoxygenation. Narendran G from department of mechanical engineering and Kiran Kumar from department of electrical and electronics engineering and support the work on development of dye sensitised solar cell, I appreciate your eager in learning and understanding the challenges of this work.

Research scholars team Suhas U, Narendran G, Vishweshwara PS, Avadhooth walunji, Santosh , Jagadish C, Rudramurthy BV, Madaganda biradar, Nutan Prasad BS, Shankar kodate, Deepak, Pradeep badiger, Praveen TR, Raghavendra , Kezia buruga, Pratibha, Chaitanya Nayak. I appreciate this opportunity, and I think we ended up with a nice output during this Ph.D. work.

During the daily struggles with experimental facilities, analytical equipment, and similar I would like to point out Saikat Dutta, for his patience and pleasant assistance in any issue, small or large. You were an irreplaceable help in this work and a phenomenal support in building of the high pressure reactor. You helped me shape my catalytic experiments and the experimental setups to wher they are today. Your refreshing points of view were very much appreciated and I enjoyed the informal discussion I had with many of you. Also, Sib sankar mal from department of chemistry deserves a notice for his good spirit and always helpful attitude.

Gourish Hiremath, Sandeep Rajoli, Madhu Bisa, Vineeth kumar MG, Shivaprasad karadi, Venkat reddy, Natraj KH, Sandeep MK, Santosh sherigar, Veer sidda reddy, Vinay kumar chuncha, Prashanth HR, Mahesh G, Venu gopal, Basavaraj wali, Sudarshan Kodiya, Richard Mathew, Ravi Narayana, Ganesh mesta, Kavya, Priyanka B, Anusha K, Devandra, Gananeshawar Achar, Harsha N and Tilak Reddy AT, you people have been core friends for as long as I can remember. You have supported me the past fifteen years and always tried to listen interested when I talked about my education and work, despite I often had the feeling that you did not have a clue about the context. Yatish RG, Raneetha Thomas, Rakesh, Uday, Shruthi siddegowda, Rashmi kurli, Siddu patil, Nalina Murthy, Jayalakshmi K for all the good times we shared and hopefully will share in the future. Also the closed ones Arun, Puneeth DR, Arundathi, Ranjith M should be mentioned, despite you left my life way to early carry you still was a big part of it until the very last moment. We should have shared a future of experiences together as friends, but unfortunately life did not intent it this way. May you ever rest in peace my dear friend.

My mother, Father and sister have supported me all the way in my life. I am forever grateful; to be of such a warm family.

Last but not least heartfelt thanks are directed towards my nephew and niece: Likith and Pranishka. Elder Sister Vijayalakshmi Dasari, you have been my solid support in all periods of this work. You never got tired of listening to my often nerdy talk about work and supported me in my enthusiasm. Your love is one of the most important things in my life and I hope it will never fade.

I hope I have not forgotten anybody, if so it was not ill intended.

Sincerely,

Kiran Kumar Dasari

ABSTRACT

In the present scenario, the energy sectors and individual entrepreneurs can opt for a new way of producing energy using the most abundant renewable energy sources available in the form of lignocellulosic agricultural waste. Among the lignocellulosic biomass, agricultural residues, coconut shells are carbon-rich and sustainable resources. In 2016-17, global coconut production has potentially exceeded upto 22 billion nuts. India is the world's third largest producer of coconuts after Indonesia and the Philippines. The total amount of coconut shell residue in India is as high as 2887 (kt/year). If used properly, coconut shells can generate 157 MW of potential power. The literature review showed that limited research studies have been conducted on the yield of the product from coconut pyrolysis. The novelty of current work is to envisage the methodology by intermediate pyrolysis to obtain a high quality of exhaustive end products which could be used as fuel or as raw material for value added chemicals. Pyrolysis is a thermal decomposition technology which decomposes carbonaceous bio wastes into liquids, gases, and char (solid residue) in the absence of oxygen.

The thermochemical conversion of agricultural waste residues coconut shell is considered in the overall study through intermediate pyrolysis process. It is a fixed bed pilot scale reactor heated externally with the help of electric heaters. In this work experiments were conducted at elevated temperature 550-575 °C, three major end products are solid (Bio-char), liquid (Bio-oil/Tar) and pyro gases. The bio-oil resulted from intermediate pyrolysis was analysed for chemical composition using, Fourier transform infrared (FT-IR) spectra and gas chromatography mass spectroscopy (GC-MS). Additionally, bio-tar was separated into saturate, aromatic resin and asphaltene (SARA) fractions by using the column chromatography with the combination of n-pentane, toluene and ethanol solvents. The SARA fractions were further characterized by FT-IR spectra, elemental analysis and nuclear magnetic resonance (NMR) analysis.

Challenges in using bio-oil as drop-in fuel or as a fuel additive include high moisture content, lower heating value, and low thermal stability. Besides, the bio-oils have limited miscibility with conventional petroleum fuels due to the presence of polar compounds like alcohols and carbonyl compounds. The storage stability of bio-oils is typically low due to the presence of compounds with reactive functional groups. Therefore, the bio-oil was upgraded for better physicochemical and elemental properties prior use. Hydrodeoxygenation (HDO) has attracted considerable attention as an efficient way of removing oxygen atoms from bio-oil rich in oxygenated compounds. Although several works have reported HDO chemistry on various bio-oils, HDO chemistry has never been applied to coconut shell derived pyrolytic oil. The bio-oil was upgraded with mild thermal and catalytic hydrodeoxygenation (HDO) and compares the elemental properties of the upgraded bio-oil samples. The higher heating value (HHV) of cr-CSPO was found to be 16.46 MJ/kg. The thermal and catalytic upgrading was performed at 250 °C, 30 bar of hydrogen pressure, a reaction time of 3 h, and a stirring speed of 350 rpm. In the case of catalytic upgrading, 10% of catalysts Ru-C and Pd-C (10 wt.% of cr-CSPO) were used as the catalyst.

Also, the developed activated charcoal is implemented as counter electrode in demonstrating Dye Sensitised Solar Cell (DSSC) using naturally available sensitizer. In addition, Dye Sensitised Solar Cell based current and temperature sensors were developed for highly remote optoelectronics applications. Anthocyanin dye extracted from pomegranate juice generated maximum current of 10 mA/cm². The characteristics of the cell were performed with different optic filters wavelength ranging 400-650 nm and the maximum efficiency was developed for wavelength of 443nm.

Keywords – Biomass; Lignocellulosic; Coconut shells; Intermediate pyrolysis; Bio-oil; Bio-char; Chromatography; Infrared spectra; Hydrodeoxygenation; Pomegranate; Optical filter; Dye sensitised solar cell.

TABLE OF CONTENTS

.....	i
ABSTRACT	i
NOMENCLATURE	vii
ABBREVIATIONS	ix
LIST OF FIGURES	i
LIST OF TABLES	v
CHAPTER 1	1
INTRODUCTION	1
1.1 OVERVIEW	1
1.2 BIOMASS	2
1.3 MAIN COMPONENTS OF BIOMASS	3
1.3.1 Cellulose	5
1.3.2 Hemicellulose.....	6
1.3.3 Lignin.....	7
1.4 DIFFERENT BIOMASS FEEDSTOCKS	8
1.4.1 Coconut waste residues (CWR).....	8
1.5 BIOMASS CONVERSION METHODS	11
1.6 THERMOCHEMICAL CONVERSION	11
1.6.1 Pyrolysis.....	12
1.6.2 Types of pyrolysis	12
1.6.3 Bio-oil	14
1.6.4 Bio-char	14
1.7 STRUCTURE OF THE REPORT	15
CHAPTER 2	16
LITERATURE REVIEW	16
2.1 LIGNOCELLULOSIC BIOMASS PYROLYSIS	17
2.2 HEAVY OIL (TAR) SOLVENT EXTRACTION	23
2.3 CATALYTIC UPGRADATION OF BIO-OIL	25
2.4 DYE SENSITISED SOLAR CELLS	28
2.5 SCOPE AND OBJECTIVES OF THE WORK	31
CHAPTER 3	32
RESEARCH METHODOLOGY	32

3.1 MATERIALS AND METHODS	32
3.2 INSTRUMENTS USED FOR ANALYSIS.....	32
3.2.1 Thermo gravimetric analysis (TGA) of coconut shell powder	32
3.2.2 Thermo gravimetric analysis (TGA) of bio-oil.....	32
3.2.3 Elemental analysis.....	33
3.2.4 Fourier transform infrared radiation (FT-IR) analysis	34
3.2.5 Gas chromatography and mass spectroscopy (GC-MS).....	34
3.2.6 Nuclear magnetic resonance (NMR).....	34
3.2.7 Characterization by analytic techniques	35
3.2.8 Indium tin oxide glass (ITO)	35
CHAPTER 4.....	36
INTERMEDIATE PYROLYSIS OF AGRICULTURAL WASTE COCONUT SHELLS IN A PILOT SCALE SYSTEM FOR PRODUCING SUSTAINABLE FUELS AND CHARACTERISATION OF BIO-OIL AND BIO-CHAR	36
INTRODUCTION	36
4.1 FEEDSTOCK PREPARATION	37
4.2 PYROLYSIS PROCEDURE.....	37
4.3 RESULTS AND DISCUSSION.....	38
4.3.1 Thermogravimetric analysis of coconut shells.....	38
4.3.2 Elemental analysis.....	40
4.3.3 Fourier transform infrared spectroscopy (FT-IR) analysis	40
4.3.4 Gas chromatography and mass spectroscopy analysis	44
4.4 CHARACTERIZATION OF BIO-CHAR.....	46
4.5 BY-PRODUCTS PER METRIC TON OF COCONUT SHELLS	47
CHAPTER 5.....	51
FRACTIONATION OF TAR OF COCONUT SHELL PYROLYSIS BY SOLVENT EXTRACTION AND ADSORPTION CHROMATOGRAPHY	51
INTRODUCTION	51
5.1 EXPERIMENTAL.....	51
5.2 GAS CHROMATOGRAPHY AND MASS SPECTROSCOPY	52
5.3 ISOLATION OF COCONUT SHELL BIO-TAR	53
5.4. RESULTS AND DISCUSSIONS.....	54
5.4.1 Chemical analysis	54
5.4.2 Nuclear magnetic resonance (NMR) analysis.....	57
CHAPTER 6.....	61

UPGRADING OF COCONUT SHELL-DERIVED PYROLYTIC BIO-OIL BY THERMAL AND CATALYTIC HYDRO-DEOXYGENATION	61
INTRODUCTION.....	61
6.1 MATERIALS AND METHODS	63
6.2 PYROLYSIS OF CSPO	64
6.3 REACTION CONDITIONS FOR THERMAL AND CATALYTIC UPGRADING.....	64
6.3.1 Experimental procedure	64
6.4 RESULTS AND DISCUSSIONS	65
6.4.1 Characterization of cr-CSPO, th-CSPO, and ca-CSPO	65
6.4.2 Elemental analysis	66
6.4.3 Analysis by fourier transform infrared spectroscopy (FT-IR).....	70
6.4.4 Thermo gravimetric analysis (TGA).....	73
6.5 CATALYTIC HYDRODEOXYGENATION (HDO) OF PYROLYSIS OIL	75
6.5.1 Gas chromatography –mass spectroscopic (GC-MS) analysis.....	75
6.5.2 Nuclear magnetic resonance (NMR) analysis	79
CHAPTER 7	82
COCONUT SHELL ACTIVATED CARBON-BASED DYE-SENSITIZED SOLAR CELL FOR DEVELOPMENT OF HIGHLY SENSITIVE TEMPERATURE AND CURRENT SENSOR	82
INTRODUCTION.....	82
7.1 EXPERIMENTAL METHODOLOGY	83
7.1.1 Preparation of TiO ₂ photo anode	83
7.1.2 Preparation of POM dye	83
7.1.3 Preparation of carbon.....	83
7.1.4 Carbon coated counter electrode	84
7.2 DSSC ASSEMBLY.....	85
7.3 DSSC SENSOR CHARACTERIZATION SETUP.....	85
7.4 SYNTHESIS AND CHARACTERIZATION OF DSSC MATERIALS	86
7.5 CHARACTERISATION OF SEM AND XRD	88
7.6 RESULTS AND DISCUSSIONS	89
7.6.1 Current and voltage characteristics.....	89
CHAPTER 8	93
CONCLUSIONS.....	93

REFERENCES.....	97
APPENDIX.....	112
List of Publications and Conference Contributions.....	120
BIO-DATA	122

NOMENCLATURE

LIST OF SYMBOLS, UNITS AND GREEK WORDS

Symbol	Description
%	Percentage
Ω	Omega
μ	Micro
\AA	Angstrom
atm	Atmosphere
cSt	Centistokes
g	Gram
l	Litre
GPa	Gigapascal
h	Hour
kg	Kilogram
kt	Kiloton
m	Meter
mg	Milligram
min	Minute
Hz	Hertz
MJ	Megajoules
mm	Millimeter
mA	Milliampere
cm	Centimeter
MPa	Megapascal
wt.	Weight
Mt	Metric ton

MW	Megawatt
nm	Nanometer
s	Second
kV	Kilovolt
TW	Terrawatt
V	Voltage
θ	Theta, contact angle
eV	Electron volt
$^{\circ}\text{C}$	Degree Celsius
ml	Millilitre

ABBREVIATIONS

AC	Ash content
ANOVA	Analysis of variance
BC	Bio-char
BET	Brunauer–Emmett–Teller analysis
C ₂ H ₆	Ethane
C ₃ H ₈	Propane
CAGR	Compound annual growth rate
ca-Ru-C-CSPO	Catalyst - Ruthenium on activated carbon - coconut shell pyrolysis oil
ca-Pd-C-CSPO	Catalyst - Palladium on activated carbon - coconut shell pyrolysis oil
CCl ₄	Carbon tetrachloride
CH ₂ O	Formaldehyde
CH ₃ OH	Methanol
CH ₄	Methane
CO	Carbon monoxide
Co	Cobalt
CO ₂	Carbon dioxide
cr-CSPO	Crude coconut shell pyrolysis oil
CS	Coconut shells
CSBT	Coconut shell bio-tar
CSPO	Coconut shell pyrolysis oil
DCM	Dichloromethane
DOP	Degree of polymerization
DSC	Differential scanning calorimetry
DSSC	Dye sensitized solar cell
DTA	Differential thermal analysis
DTG	Differential thermal gravimetric
FC	Fixed carbon

FTIR	Fourier transform and infrared
GC-MS	Gas chromatography mass spectroscopy
GPC	Gel permeation chromatography
H ₂ O	Water
H/C	Hydrogen carbon ratio
HCOOH	Formic acid
HDO	Hydro-deoxygenation
HHV	Higher heating value
HPLC	High performance liquid chromatography
HTH	High temperature hydrogenation
IPP	Intermediate pyrolysis process
IREDA	Indian renewable energy development agency limited
ITO	Indium tin oxide
KOH	Potassium hydroxide
LHSV	Liquid hour space velocity
LTH	Low temperature hydrogenation
mol	Mole
Mo	Molybdenum
MSW	Municipal solid waste
MC	Moisture content
NIR	Near infrared spectroscopy
NIST	National Institute for Standards and Technology
NMR	Nuclear magnetic resonance
NO	Nitric oxide
O/C	Oxygen to carbon ratio
Pt	Platinum
Pd-C	Palladium on activated carbon
POM	Pomegranate
ppm	Parts per million
rpm	Revolutions per minute
Rh	Rhodium

Ru-C	Ruthenium on activated carbon
SAIF	Sophisticated Analytical Instrument Facility
S/C	Steam carbon ratio
SEM	Scanning electron microscopy
SO ₂	Sulphur dioxide
TEM	Transmission electron microscopy
TGA	Thermo-gravimetric analysis
TiO ₂	Titanium dioxide
VC	Volatile content
WHSV	Weight hour space velocity
XRD	X-ray diffraction

LIST OF FIGURES

Figure 1.1 Lignocellulosic biomass fractionation tree	4
Figure 1.2 The composition of wood, illustrating the structure of lignocellulosic biomass. © Per Hoffmann, Oskar Faix and Ralph Lehnen	4
Figure 1.3 Primary products of cellulose polymer	5
Figure 1.4 Primary products of hemicellulose polymer	6
Figure 1.5 Primary products of lignin polymer	7
Figure 1.6 Degradation of biomass pyrolysis polymers of agricultural residue coconut shell	9
Figure 1.7 Thermochemical conversion methods	11
Figure 2.1 A survey of publications related to lignocellulosic biomass in last decade	16
Figure 2.2 A survey of publications related to lignocellulosic residue coconut shells in last decade	17
Figure 4.1 Physical representation of pyrolysis process. coconut shells as grey, gases/voids as white, liquids and chars as black.....	38
Figure 4.2 Thermo gravimetric analysis of coconut shell	39

Figure 4. 3 Fourier transform infrared spectra of coconut shell pyrolysis-oil.....	41
Figure 4.4 Gas chromatography mass spectroscopy spectra of coconut shell pyrolysed oil.....	45
Figure 4.5 Scanning electron micrograph at 500 x magnification of bio-char.....	47
Figure 5.1 Gas chromatography and mass spectroscopy spectra of coconut shell bio-tar.....	53
Figure 5.2 Schematic pictorial view of isolation of coconut shell bio-tar	53
Figure 5.3 Pictorial views of saturate, aromatic, resin and asphaltene fractions of coconut shell bio-tar	55
Figure 5.4 Overview of fourier transform infrared spectra of four fractions	56
Figure 5.5 Microscopic image of bio-asphalt.....	57
Figure 5.6 ¹ H Nuclear magnetic resonance of saturate fraction	59
Figure 5.7 ¹ H Nuclear magnetic resonance of aromatic fraction.....	59
Figure 5.8 ¹ H Nuclear magnetic resonance of resin fraction.....	60
Figure 5.9 ¹ H Nuclear magnetic resonance of asphaltene fraction	60
Figure 6.1 Pyrolysed coconut shell oil upgraded tested conditions.....	63

Figure 6.2 High-pressure reactor.....	65
Figure 6.3 Elemental analysis of cr-CSPO, th-CSPO ca-PdC-CSPO and ca-RuC-CSPO at 250 °C.	66
Figure 6.4 Elemental analysis and yield of ca-Pd-C-CSPO at various reaction temperatures.....	67
Figure 6.5 Elemental analysis and yield of ca-Ru-C-CSPO at various reaction temperatures.....	67
Figure 6.6 Elemental analysis and yield of thermally upgraded CSPO at various reaction temperatures.	68
Figure 6.7 Higher heating value of ca-Ru-C, ca-Pd-C and th-CSPO at 200 250 and 300 °C.....	69
Figure 6.8 Yields of ca-Ru-C, ca-Pd-C and th-CSPO at 200, 250 and 300 °C.....	70
Figure 6.9 FTIR spectrum of cr-CSPO.....	71
Figure 6.10 Overlaid FTIR spectra of cr-CSPO, th-CSPO, ca-Ru-C-CSPO and ca-Pd-C-CSPO	73
Figure 6.11 Overlayed TGA graph of cr-CSPO, th-CSPO, and ca-CSPO.	74
Figure 6.12 Proton NMR of th-CSPO at 250 °C.....	80
Figure 6.13 Proton NMR of ca-Ru-C-CSPO at 250 °C.....	81

Figure 6.14 Proton NMR of ca-Pd-C-CSPO at 250 °C.....	81
Figure 7.1 Schematic layout of natural POM dye DSSC.....	84
Figure 7.2 Actual photograph of the constructed natural POM dye DSSC	85
Figure 7.3 Characterization of photo electrode and counter electrode, (a) TiO ₂ coating, (b) activated carbon coated counter electrode, (c) worn out photo electrode, (d) worn out counter electrode condition, (e) porous surfaces in photo electrode, (f) TiO ₂ photo electrode after POM dye adsorption, (g, h) SEM details of the porous structures.....	87
Figure 7.4 Scanning electron microscopic images, (a) TiO ₂ and (b) activated carbon	88
Figure 7.5 X-ray diffraction pattern of activated carbon	89
Figure 7.6 I-V characteristic curve of dye sensitised solar cell with different optical filters and one without optical filter	89
Figure 7.7 Open circuit voltage decrement of POM based dye sensitised solar cell at increased temperatures.....	90
Figure 7.8 Open circuit voltage versus current for dye sensitised solar cell with POM sensitizer.	90

LIST OF TABLES

Table 1.1 Coconut growing countries as on 2016.....	10
Table 1.2 Different types of pyrolysis of wood product yields.....	13
Table 3.1 Chemicals used in experiments and analysis.....	33
Table 4.1 Comparative ultimate analysis with different biomass materials	42
Table 4. 2 Fourier transform infrared analysis of CSPO	44
Table 4.3 Chemical composition of coconut shell pyrolysed oil	45
Table 4.4 Analysis of coconut shell and bio-char	46
Table 4. 5 Cost analysis	48
Table 5.1 Elemental analysis of coconut shell bio-tar.....	52
Table 5.2 Chemical compounds of coconut shell bio-tar	52
Table 5.3 Elemental compositions of SARA fractions from coconut shell bio-tar.....	55
Table 5.4 Comparison of yields of different feedstocks with present study.....	56
Table 5.5 Functional group distribution from ¹ H NMR spectral integration of four fractions using Chemical shift region (ppm)	58

Table 6.1 Frequencies of bond vibrations in the FTIR spectra of th-CSPO and ca-CSPO	72
Table 6.2 Gas chromatography and mass chromatography of CSPO at 575 °C	75
Table 6. 3 Gas chromatography and mass chromatography of ca-Ru-C-CSPO	76
Table 6.4 Gas chromatography and mass chromatography of ca-Pd-C-CSPO.....	77
Table 6.5 Functional group distribution from ¹ H NMR spectral integration using Chemical shift region (ppm)	80

CHAPTER 1

INTRODUCTION

In this introduction, global energy agricultural waste residues issues are discussed. The pyrolysis of biomass is considered an important step in the renewable energy mix. Then, a brief introduction to pyrolysis, a thermochemical conversion pathway for biomass, is given. This chapter highlights the challenges of a bio-economic transformation that can play significant role in bioenergy. The present research was carried out on agricultural residues of coconut shells are presented in this thesis report. Finally, the structure of the thesis is outlined at the end of this chapter.

1.1 OVERVIEW

The world is very ancient and human origins are mysterious and insecure. The Sun radiates approximately 100,000 terawatts of energy to the earth, about 10,000 times more than the energy consumption of the world today. In addition to develop a more sustainable future, the use of renewable energies like biomass and solar energy are gradually being seen as a favourable alternative for the current energy demand and to overcome the global warming crises (Dasari et al. 2019). Over the past several decades, fossil fuels have been the primary source of carbon-based energy and transportation fuels in the world. Due to the increasing demand, depletion of fossil fuel reserves and irreversible environmental degradation, there has been a coordinated effort in developing cleaner and greener fuels (Abdelfattah et al. 2018). Currently in India no industrial process exists to economically convert lignocellulosic biomass to renewable fuels and chemicals.

With a population of more than 1.37 billion, India has a population density of 325 residents per square kilometer and lives in 7,935 towns. India produces 62 million tons of mixed waste per year (recyclable and non-recyclable), of which less than 60% are collected and about 15% processed (Kumar et al. 2017). By 2031, the amount of waste is expected to increase, with an average annual growth rate of 4%. It is expected that by 2047, 1,400 square kilometers of landfills will be required for

landfilling of increasing volumes of mixed waste. This space is roughly equivalent to the three most populous cities in India: the total area of Chennai, Hyderabad and Mumbai. Burning waste is the third leading cause of greenhouse gas emissions in India. Combustion of waste releases CO, NO_x, SO_x and carcinogenic hydrocarbons into the air. India alone emits 6% of household waste methane emissions (global average emissions are 3%) (Planning Commission, 2014). In order to protect the environment, efforts are being made to recover coconut waste and use it for value-added applications. India reaffirmed in the Paris agreement that it would reduce emissions intensity by 35% and increase energy production capacity by 40% from renewable sources. By 2022, India is committed to building 175 GW through renewable energy (Swaminathan et al. 2018). Agricultural waste residues and other biomass raw materials are significant for the production of renewable activated carbon. In particular, the use of electrical energy produced by sustainable resources such as lignocellulosic raw materials will decrease the impact on human toxicity (up to 60%) and on global warming (up to 80%).

1.2 BIOMASS

Globally, biomass is the 4th largest energy source after coal, oil and natural gas, accounting for about 14% of the global primary energy consumption. Biomass is the only renewable carbon source that is widely available in nature and can be used to produce fuels and value-added chemicals. In this context, biomass is an organic material derived from plants. Biomass generally refers to organic matter based on carbon, hydrogen and oxygen from plants or animals. Biomass is produced by photosynthesis of plants. Photosynthesis process converts light energy into chemical energy in the form of sugar (Saxena et al. 2009).

As a result, biomass and its derivatives can potentially diversify energy resources and mitigate environmental impacts. The use of biomass and its components as fuel is considered to be carbon neutral, as biomass fixes carbon dioxide in the atmosphere in the form of sugar as it grows. Therefore, when biomass is burned as a fuel, there is no net in the carbon dioxide produced. They have gained appreciable consciousness in the fields of chemistry, engineering and agriculture. Basic knowledge about biomass and bio-oil as biomass derivatives is extracted from the

literature and discussed in this and subsequent chapters to determine the context of this study.

The use of biomass as energy source is of particular interest because of the following anticipated benefits:

- ❖ Biomass is a renewable, potentially sustainable and relatively environmentally friendly source of energy;
- ❖ A large number of different feedstocks are available from biomass;
- ❖ Significant use of biomass will prolong the usage of the fossil fuels supply;
- ❖ The sulfur content of biomass fuels is negligible, so it does not lead to SO₂ emissions that cause acid rain;
- ❖ The combustion of biomass generates less ash than coal combustion and the resulting ash can be used as a field soil additive; (Saxena et al. 2009)
- ❖ The effective way to utilize the municipal solid wastes (MSW), agricultural and forestry residues as a resource for the production of energy and that will reduce the problems associated with the disposal of wastes;
- ❖ Biomass supplies clean renewable energy that can improve environmental, economic and energy securities;
- ❖ The use of biomass could be a way to reduce the formation of more CO₂ in the atmosphere because it does not raise the level of CO₂ in the atmosphere; in particular, energy crops and agricultural residues.

1.3 MAIN COMPONENTS OF BIOMASS

Lignocellulosic biomass especially non-edible lignocellulosic biomass and cellulosic waste, is considered by many to be a rich, inexpensive and renewable carbon source that can be a commercially competitive and promising alternative to fossilized carbon. Figure 1.1 shows the biomass fractionation tree. The structure and composition of biomass varies depending on species, genetic characteristics, age, environmental conditions, and parts of the plant. Figure 1.2 illustrates the structure and composition of the wood. In general terrestrial lignocellulosic biomass mainly comprises three biopolymers; namely cellulose (40-60 wt.%), hemicellulose (20-40

wt.%) and lignin (10-25 wt.%) (Yang et al. 2007; Frolander and Rodsrud 2011 and Han et al. 2019).

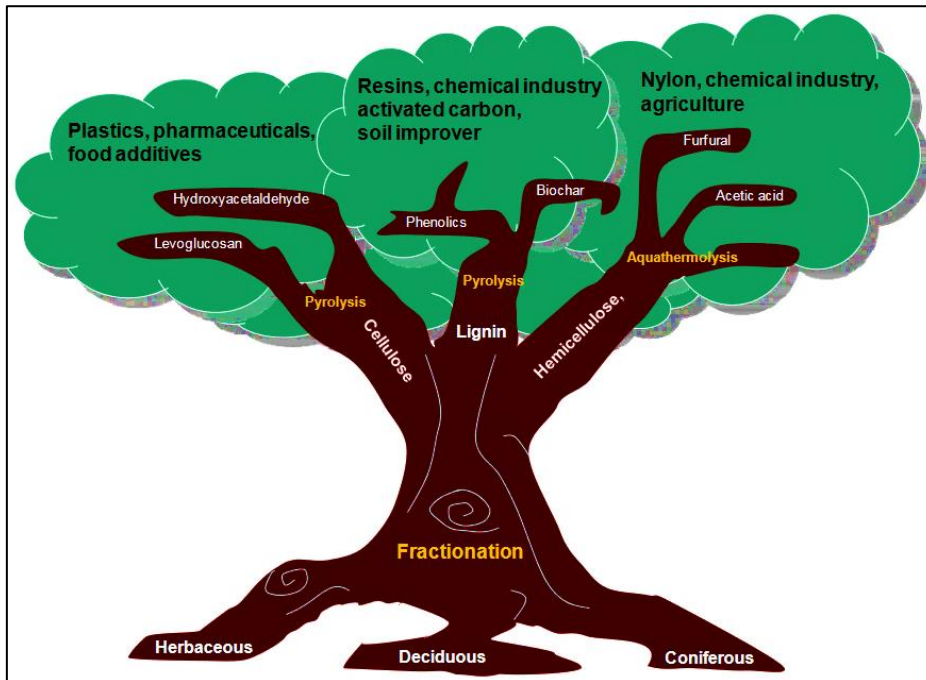


Figure 1.1 Lignocellulosic biomass fractionation tree

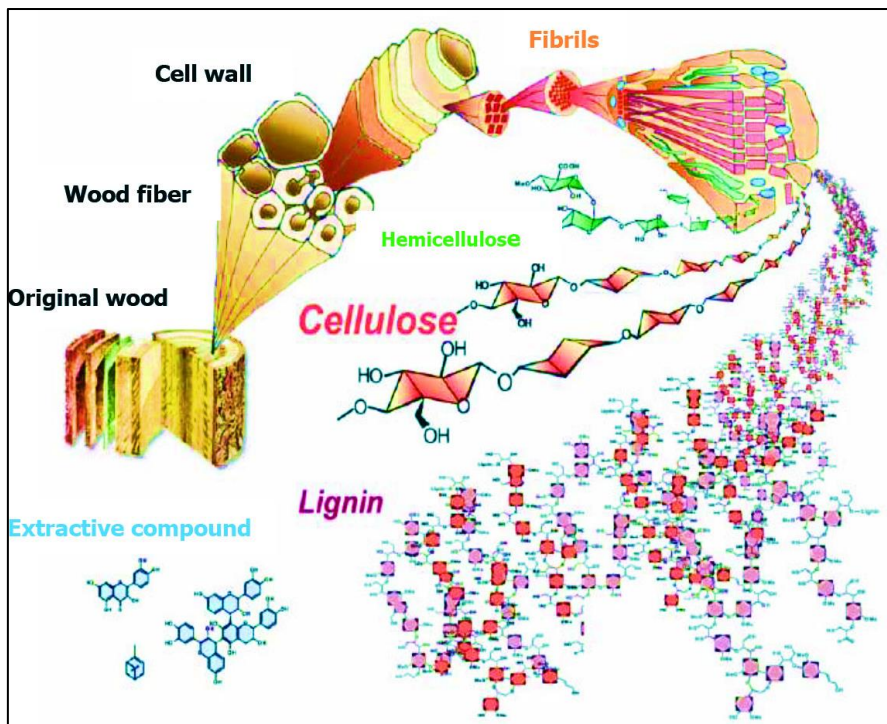


Figure 1.2 The composition of wood, illustrating the structure of lignocellulosic biomass. © Per Hoffmann, Oskar Faix and Ralph Lehnen

1.3.1 Cellulose

Cellulose is an organic compound whose main constructional compound is assorted with other polysaccharides and lignin on the cell wall of plant. Cellulose is a polysaccharide composed of a linear combination of d-glucose units linked to each other by $\beta(1\rightarrow4)$ glycosidic bonds. Compounds of two glucose molecules called cellobiose are the basic building blocks of cellulose linear polymers. The usual chemical formula of cellulose is represented by $(C_6H_{10}O_5)_x$, where x is the degree of polymerization (DOP) and represents the number of glucose groups. Cellulose has high DOP and has a strong tendency to form intermolecular and intramolecular H_2 bonds, and aggregation of linear chains of molecules within microfibrils produces crystalline structure. Intramolecular and intermolecular hydrogen bonding from substituents ($-OH$ and $-CH_2OH$) imparts high strength to cellulose. The primary products of cellulose are shown in figure 1.3. Cellulose produces CO_2 , CO , H_2O , CH_2O , and $C_5H_4O_2$ (Anca-Couce et al. 2016).

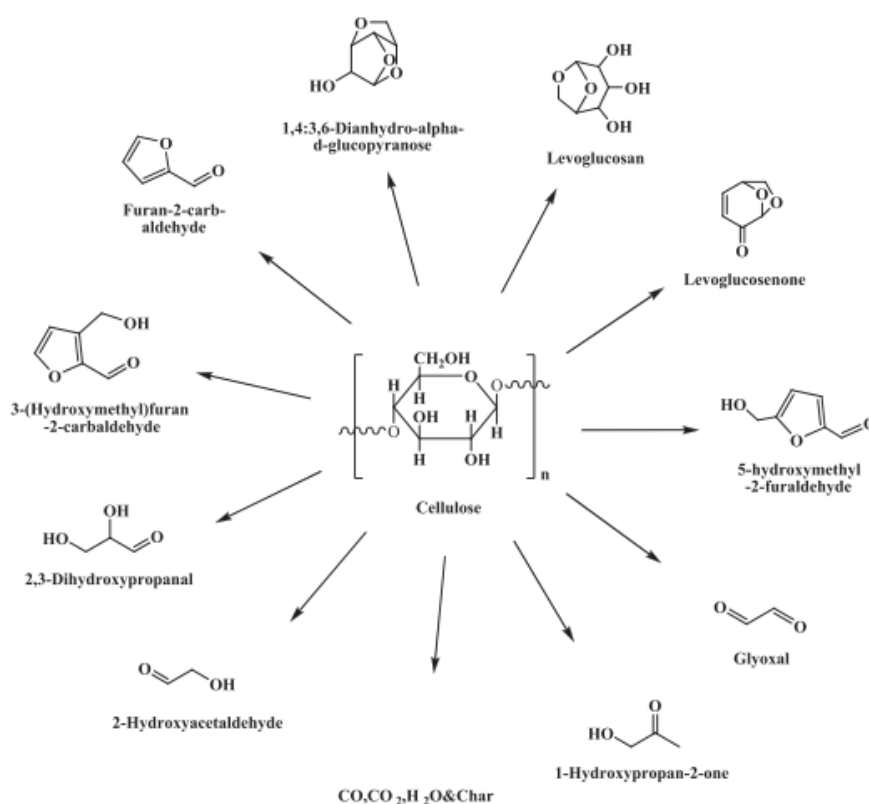


Figure 1.3 Primary products of cellulose polymer

1.3.2 Hemicellulose

Hemicellulose is a multiplex heteropolysaccharide consisting mostly of pentoses (xylose and arabinose) and hexoses (galacturonic, glucuronic and methylglucuronic). Unlike cellulose, hemicelluloses are amorphous that has lower degree of polymerization. The general formula of hemicellulose is $(C_5H_8O_4)_x$. Hemicellulose composed of sugars and the most copious hemicelluloses are xylans and glucomannans. Xylan is a good representative of hemicellulose from hardwood and glucomannan from hemicellulose of softwood. Xylose is the most copious monosaccharide in xylan, but its content depends on raw material. Since it may arise from the composition, the hemicellulose in the hardwood consists importantly pentose sugar, while the hexose in the softwood is more. The primary products of hemicellulose are shown in figure 1.4. Xylan only produces CO_2 , CO , H_2O , CH_2O , CH_3OH , $HCOOH$ (Wang et al. 2017).

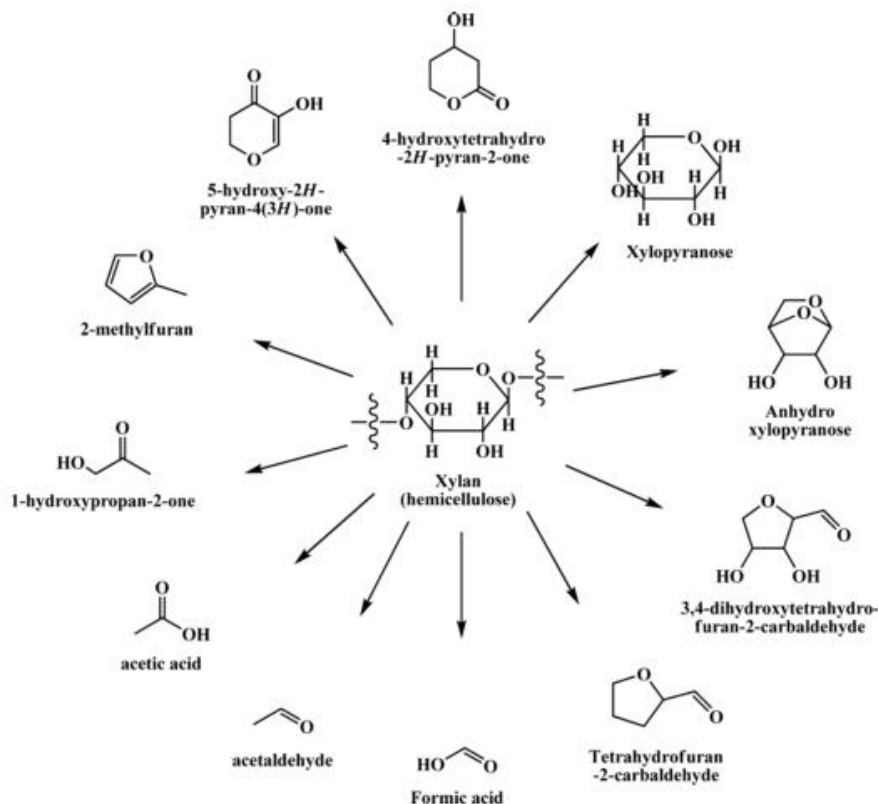


Figure 1.4 Primary products of hemicellulose polymer

1.3.3 Lignin

Lignin is an aromatic substance, 3D and transverse bound phenol polymer which is composed of random mixture of phenylpropane units substituted "hydroxyl" and "methoxy" linked differently. These phenylpropane monomers are classified into guaiacyl, syringyl and p-hydroxyphenyl units. Lignin is mainly present in the outer layer of the fiber and is responsible for the stiffness of the structure and keeps the polysaccharide fibres together. For lignocellulosic biomass, the percentage of lignin is reported to be as high as 40%. Cellulose microfibrils are surrounded by hemicellulose, and the voids are seen with lignin. Lignin acts as a link between hemicellulose and cellulose in the cell wall (Mohan et al. 2006). The primary products of lignin are shown in figure 1.5.

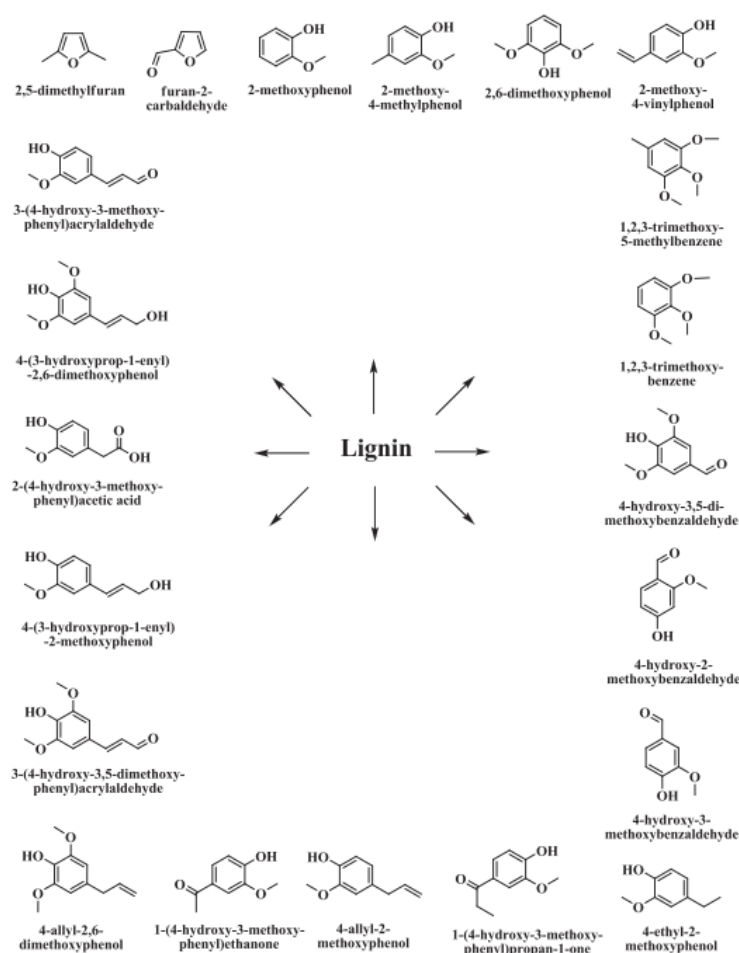


Figure 1.5 Primary products of lignin polymer

1.4 DIFFERENT BIOMASS FEEDSTOCKS

The different types of agricultural waste and lignocelluloses materials which are effective and very inexpensive, such as corncob, hazelnut shell, pruning mulberry shoot, olive stone, Jojoba seed, sawdust, coconut shell, wood, hazelnut bagasse, kenaf fiber, bamboo, rice husk, petai, groundnut shell, paper mill sludge, prosopis (*Prosopis juliflora*), coconut husk, jatropha husk, tamarind wood, pistachio-nut, sugarcane bagasse, jackfruit peel, and many others (Yahya et al. 2009).

1.4.1 Coconut waste residues (CWR)

The huge agricultural residues generated by many developing countries are mainly used as an energy source for converting fuel. Coconut (*Cocos nucifera*) has been a cash crop in humid tropical countries for decades with an annual global production of 62.5 million tons (Mt). Coconut is a high-quality agricultural product. Coconut is an ideal plantation planted in more than 90 countries around the world. Indonesia (18.3 Mt), Philippines (15.3 Mt) and India (11.9 Mt) are the top three leading coconut producing countries. World coconut production has crossed about 22 billion nuts in 2016-17. India accounts for 22.34 % of the global coconut production and is a major player in the global coconut trade. Overall coconut production is increasing every year and is expected to increase further with increasing global demand (Fardyanti et al. 2018). This will out-turn in enormous quantity which may lead to destruction and creates environmental problems if not used properly. The production of coconut fruit generates large quantities of waste, namely coconut husks and coconut shells (CS). Among all known plant organs, high-density raw materials such as the drupe fruit endocarps (shells) of olives, eastern black walnut and coconut have the highest lignin content, and the endocarp produces energy comparable to coal (Radhakrishnan et al. 2016). The CS is solid lignocellulosic agricultural residue that can be considered a fuel. The CS has lower ash content, making it supreme for ease handling and meagre collision on the environment. The CS is comparatively homogeneous to hardwood in chemical structure; although the lignin content is excessive and the cellulose content is lower, with an apparent density of 0.6-0.7 g / cm³ and a moisture content of about 10 % (Govind Raj and Alias Joy 2009).

The coconut shell consists of cellulose (20-36 wt.%), hemicellulose (24-49 wt.%) and lignin (29-30 wt.%), which can be easily converted into high products by thermal conversion techniques. The degradation of agricultural residue coconut shells is shown (figure 1.6). The process of pyrolysis of CS comprises three stages, dehydration, degradation and pyro-condensation (Zhang et al. 2016).

Coconut meat has various commercial uses (cosmetics, shower gels, shampoo, etc.), industrial (flavourings, medicinal and nutraceutical) and domestic (foods, cooking oils, pest control products, etc). Coconuts, shells and husks have local characteristics, especially in India (eg., handicrafts, home furnishing, mattresses, etc.) and are prospective for materials such as activated carbon, bio-fibres, heavy metal bio sorbents, particleboards, etc., (Ting et al. 2016).

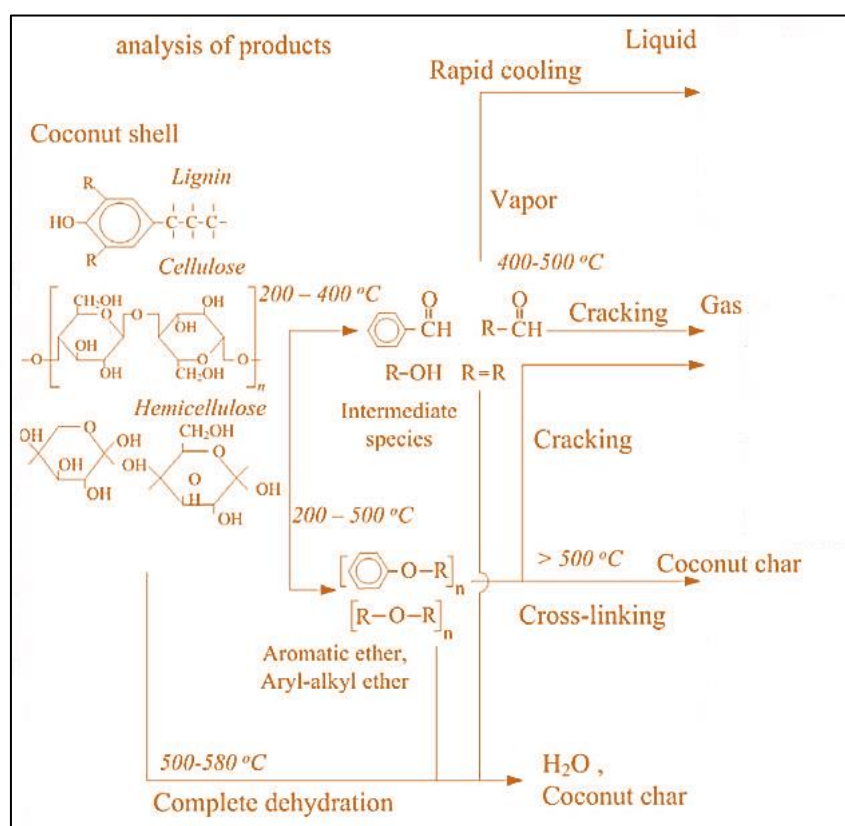


Figure 1.6 Degradation of biomass pyrolysis polymers of agricultural residue coconut shell

The total available coconut shell residue is up to 2887 (kt/year). If used correctly, coconut shells can generate a potential power of 157 MW. The coconut processing business has not yet been fully developed in India. The major countries

growing coconuts are enlisted in table 1.1. The CS pyrolysis produces bio-oil from which value-added products and chemical raw materials can be extracted and also a carbon-rich solid product called bio-char (BC). In addition to absorptive applications, BC can also be used as a catalyst carrier and fertilizer base material (Murugan and Gu 2015).

Table 1.1 Coconut growing countries as on 2016

Sl No.	Country	Area (hectare)	Production (Million nuts)	Productivity (Nuts/hectare)
1	F.S Micronesia	18	60	3,333
2	Fiji	64	159	2,484
3	India	2,088	22,167	10,616
4	Indonesia	3,441	13,934	4,049
5	Jamaica	16	100	6,250
6	Kenya	77	254	3,299
7	Kiribati	23	198	8,609
8	Malaysia	85	505	5,941
9	Marshall Islands	8	38	4,750
10	Papua Guinea	221	1,483	6,710
11	Philippines	3,565	13,825	3,878
12	Samoa	99	267	2,697
13	Solomon Islands	38	100	2,632
14	Srilanka	440	3,011	6,843
15	Thailand	184	686	3,728
16	Tonga	26	56	2,154
17	Vanuatu	92	699	7,598
18	Vietnam	165	1,471	8,915
19	Other Countries	1,256.00	8,115	6,461
	Total	11,906	67,128	5,638

Source: Asian and Pacific Coconut Community (APCC) Statistical Year Book of 2016

1.5 BIOMASS CONVERSION METHODS

A number of transformation protocols has been established to take advantage of biomass raw materials characteristic and have been reviewed (Czernik and Bridgwater, 2004; Mohan et al. 2006). There are different ways to transform biomass into biofuels, which are: biochemical transformation and thermochemical conversion. Some widely used biochemical conversion techniques are anaerobic digestion, saccharification and hydrolysis. Thermochemical conversion includes four sub-categories: liquefaction, pyrolysis, gasification, and combustion. The schematic path for thermochemical conversion is shown in figure 1.7.

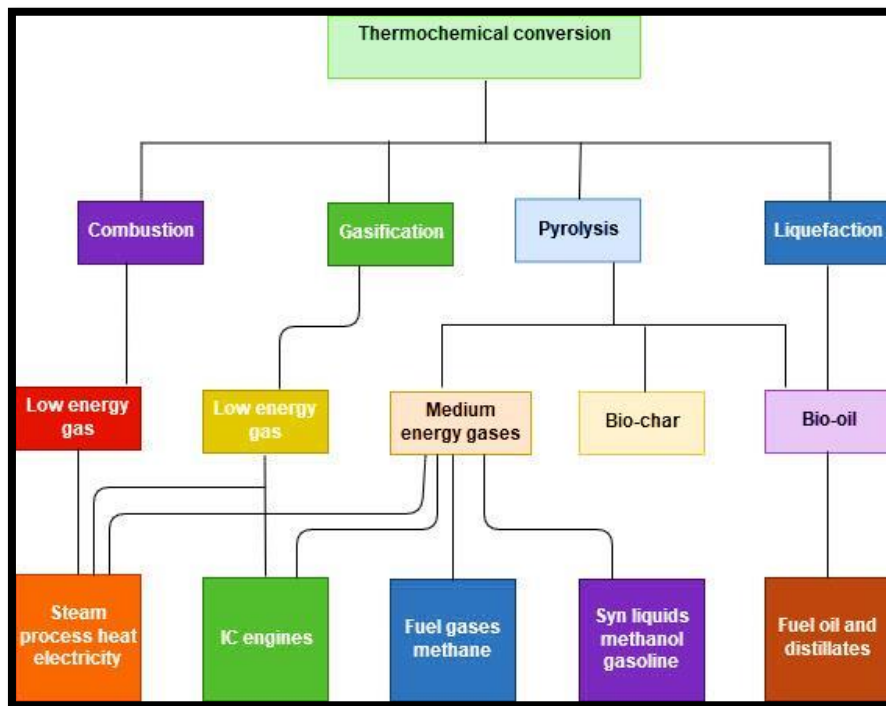


Figure 1.7 Thermochemical conversion methods

1.6 THERMOCHEMICAL CONVERSION

Thermochemical transformation involves many methods that can give rise to useful fuels and chemicals from a variety of bio-renewable materials at high temperatures. All forms of biomass can also be gasified, pyrolysed and combusted to produce other useful chemicals and produce energy. As a transformation, pyrolysis can be defined as the chemical change that occurs when biomass is heated without

oxygen. In addition, pyrolysis is considered to be the basic chemical reaction of the gasification and combustion processes.

1.6.1 Pyrolysis

Pyrolysis is considered to be a promising thermochemical technique because it can effectively convert biomass advanced fuels, which is important for the substitution of fossil fuels. Pyrolysis of biomass produces combustible gases, liquids and solids. Gaseous product contains CH_4 , and are mainly found in natural gas, biogas and coal mine gas. It is a high-quality gas fuel and is significant feedstock in construction of syngas and other chemicals. Liquids are upgraded to generate alternative fuels or value-added products. These are also used as chemical feedstock. Products derived from the pyrolysis of liquid biomass include binders, phenol and liquid fuels or resins (Trinh et al. 2013). Solid carbon can be used directly in the production of activated carbon, batteries and electrode assemblies.

Wood biomass is the ancient energy form used by humans. Certain types of raw materials have a significant proportion of inorganic matter. This inorganic material produces ash concentrations ranging from 1% in softwood to 15% in herbal biomass and agro-industrial residues (Phusunti et al. 2009). Traditionally, biomasses are directly used for heating and cooking by combustion, or indirectly converted to gaseous and liquid fuels by conversion techniques. Because of the variety of forms of biomass fuels, they can be used for several of purposes, like power generation, transforming to fuel vehicles, and producing process heat for industrial applications.

1.6.2 Types of pyrolysis

For different applications, the pyrolysis can be operated as slow, intermediate or fast pyrolysis depending upon the operating conditions such as mainly residence time and temperature. The end products are mixture of condensable gas, bio-oil and bio-char depending on the operating conditions and raw materials. The yields in the different types of pyrolysis process are shown in table 1.2.

Slow pyrolysis is a batch process, performed under low temperature and slow heating, which can extend the residence time. This process is more resistant to water

content in the raw material. Carbonization is the slow pyrolysis of the non-condensing biomass of the pyrolysis products. It is the ancient biomass processing method for charcoal production; and is performed where BC is the needed. The volatiles are not generally condensed in this type, but can be used to provide the necessary heat for operation, by direct or indirect heating. The heating rate is reported to be as low as 0.1-2 °C/min. Moisture affects the characteristics of charcoal, which helps to produce activated carbon through pyrolysis. Moisture content in charcoal production is usually 15-20%. The size of the raw material can vary from the size of the briquette to that of the whole logs. Although wood is the main raw material for slow pyrolysis, other raw materials such as cashew nut shells and palms have been reported (Antal and Gronli 2003; Stamatov et al. 2006).

Table 1.2 Different types of pyrolysis of wood product yields

Type	Fast	Intermediate	Slow
Temperature (°C)	~500	~500	~400
Residence time (s)	~1	~10-30	~60
Liquid yield (%)	75	50 % in 2 phase	30 % in 2 phase
Solid yield (%)	12	25	35
Gas yield (%)	13	25	35

Intermediate pyrolysis is performed at elevated temperature 300-600 °C. Compared to fast pyrolysis, the tar yield and viscosity of the liquid product obtained from intermediate pyrolysis is low. More controlled chemical reactions take place in intermediate pyrolysis and provides a wide range of variations for process optimization. Bio-oil yields (up to 55%) can be obtained in this type, large size raw material (coarse, chopped, shredded or grated) is acceptable (Hornung 2014; Murugan and Gu 2015; Tripathi et al. 2016).

Fast pyrolysis is a leading technology that is gaining increasing attention due to growing interest in the production of liquid fuels from biomass. The importance of fast pyrolysis is to eliminate the by-products from further cracking into non-condensable compounds. During fast pyrolysis, operating conditions need to be over-

exact controlled to yield higher liquid product (bio-oil). The main precondition for fast pyrolysis is high heat transfer rate, which is attained by fine grinding the raw material. The feedstock is heated at elevated temperature (450-600 °C) for a short time (usually less than 2 s). The bio-oil yield of fast pyrolysis of wood is recorded to be as high as 75% based on dry feed. Because the reaction takes place in a short residence time, not only the chemical kinetics, but also the rate of heat and mass transfer is important. The transformation phenomenon plays a critical role in deciding the chemical properties of the product. The desired product can be attained by controlling the operating conditions to optimal values (Bridgwater 1994; Hornung 2014).

1.6.3 Bio-oil

The pyrolytic liquid, also known as bio-oil, is a multiplex mixture composed of more than 400 compounds including carboxylic acids, aldehydes, esters, acetals, hemiacetals, alcohols, olefins, aromatics, phenolics, nitrogen- and sulfur-containing heterocycles (Ruddy et al. 2014; Gollakota et al. 2016). The chemical structure of bio-oil depends on the feedstock, reaction parameters during the pyrolytic liquefaction, and the storage conditions. Crude bio-oil generally has low heating value, high oxygen content, high viscosity, poor thermal, oxidative, and storage stability. Therefore, bio-oils cannot be used directly as engine fuels without prior upgrading; however, it may be used in boilers and furnaces for process heating applications (Mortensen et al. 2011; Lehto et al. 2014). The bio-oil produced during the pyrolysis of CS has a strong pH and is abrasive due to the appearance of phenolic compounds. Phenol is actually of economic value and can be used as a disinfectant, resin, pesticide, explosive, drug and dye (Fardyanti et al. 2018).

1.6.4 Bio-char

Production of bio-char depends on pyrolysis method, process parameters, raw material, and operating environment (Park et al. 2008; Mui et al. 2010; Gopakumar et al. 2015). The BC obtained during the pyrolysis process does have high energy, which sometimes is compared to coal and used as a direct fuel in industry. In addition to the production of bio-char, it was found that the properties of bio-char will change with

different process conditions. Obviously, in order to obtain the maximum bio-char production, the process parameters of biomass pyrolysis must be optimized. The high carbon content and microporous structure of biochar make it practical for a variety of industrial applications. In agriculture, it is mainly used to enhance the soil quality. Adding BC to the soil can increase the rate of carbon segregation, which gradually decreases the decomposition of nutrients and improves soil quality. At purification industry, the heavy metals such as, Cr, Ni, Cd, Hg and Pb are removed (Mohan et al. 2011), and contrasting chemicals tetracycline, phenol also removed in economical manner (Mohan et al. 2009; Deveci and Kar 2013), etc. The textile industry always emits different types of dyes and pigments, which pollutes the water inherently and causes major health issues. Bio-char can be used successfully and economically in the elimination of textile dyes and pigments. Bio-char can be used as fuel in power generation, because it has high percentage of carbon (Rangabhashiyam et al. 2013). Activated carbons are sometimes referred to as “future materials”, because of their proven performance in many process applications such as, coffee decaffeination, (Sirichote et al. 2002), decolourization (Li et al. 2015), deodorization and aroma removal (Sahu et al. 2010), treatment of drinking water (Jeswani et al. 2015), industrial flue gas cleaning and air conditioning (Perrich et al. 2018).

1.7 STRUCTURE OF THE REPORT

This research report mainly consists of eight chapters includes: **Chapter 1**, Introduction gives brief idea about research area. **Chapter 2**, Literature review elucidates the open literature available on bio-oil and bio-oil upgrading strategies and dye sensitised solar cells. In **Chapter 3**, the research methodology followed is discussed. **Chapter 4**, Provides the experimental studies on intermediate pyrolysis of coconut shells and their characterisation. **Chapter 5**, Provides the isolation of tar by solvent extraction and adsorption chromatography. **Chapter 6**, Discusses the experimental studies on upgradation of bio-oil using different catalysts in high pressure reactor at different temperatures. **Chapter 7**, Provides the application of solid bio-char in fabricating dye sensitised solar cell and **Chapter 8**, Discusses the overall conclusions.

CHAPTER 2

LITERATURE REVIEW

The energy crisis and environmental pollution are global problems. Every country is effectively working together to ensure a better future for humanity. Lignocellulosic agricultural waste coconut shells are used throughout this research for the study of intermediate pyrolysis of biomass. The literature on the different types of pyrolysis of general biomass and reactors are carried out. A survey of publications (Elsevier) related with lignocellulosic biomass and coconut shells in the last decade are given in figures 2.1 and 2.2. The survey indicates that there is potential increase in the study of biomass energy utilization. Mainly literature survey is carried out on lignocellulosic biomass, heavy oil solvent extraction, catalytic upgradation of bio-oil and dye sensitised solar cell to explore the utilization of lignocellulosic agricultural waste residue coconut shells.

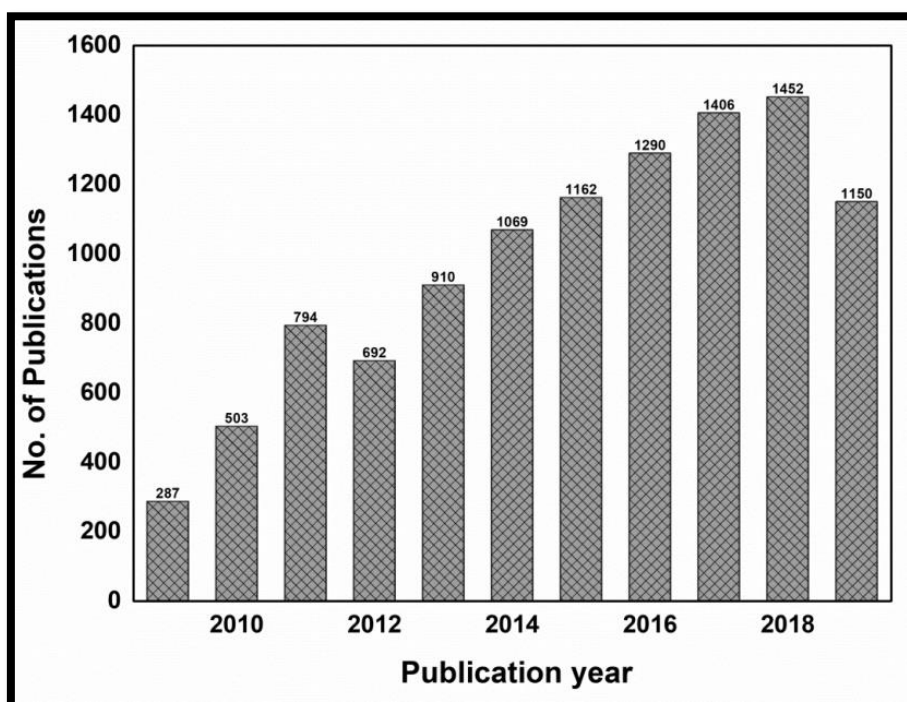


Figure 2.1 A survey of publications related to lignocellulosic biomass in last decade

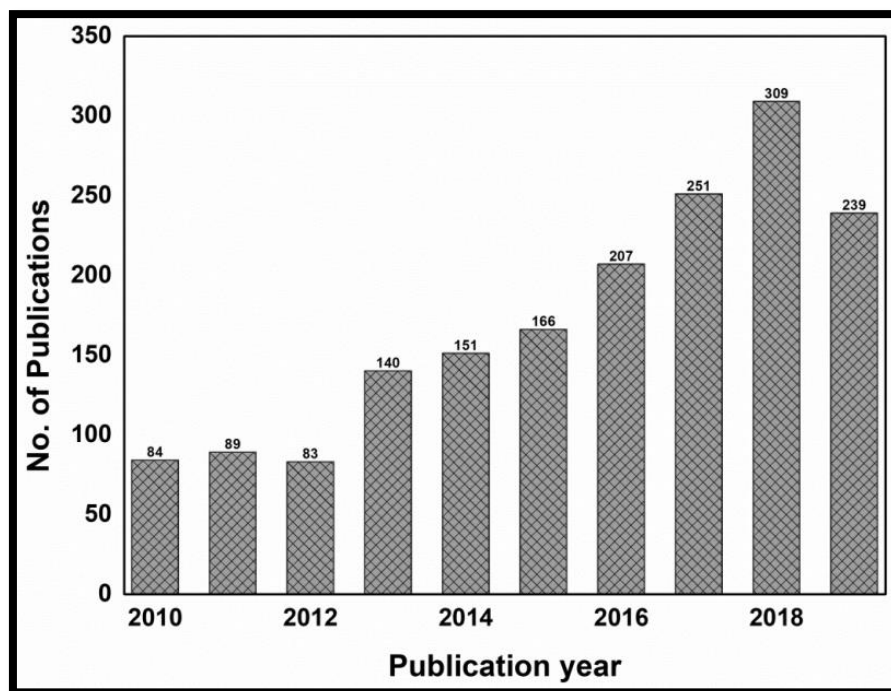


Figure 2.2 A survey of publications related to lignocellulosic residue coconut shells in last decade

2.1 LIGNOCELLULOSIC BIOMASS PYROLYSIS

Warnijati et al. (1996) studied the pyrolysis of coconut shells in a concentric reactor with three tubes. The use of amalgamation of internal and external heating in a concentric three-tube reactor improves energy efficiency. It was found from the analysis that the coconut shell contains 9.69% moisture, 0.83% ash, 29.62% lignin and 59.86% cellulose material. Due to higher temperatures and longer pyrolysis times, more tar is produced. Finally, at an optimal time of 95 min and a temperature of 579 °C, 19.53% of charcoal, 5.22% of tar, and 0.16% of light oil were produced. The overall goal of this study was to improve energy efficiency.

Yorgun et al. (2001) studied the flash pyrolysis of sunflower oil cake for obtaining liquid fuel. A fast pyrolysis experiment of sunflower (*Helianthus annuus*) oil cake was operated in a tubular transport reactor under an inert gas of nitrogen (N₂) atmosphere. The parameters like pyrolysis temperature, particle size and purge gas flow rate on product yield were investigated, optimum yield of bio-oil was 45% at final pyrolysis temperature of 550 °C with a particle size of 0.425 to 0.850 mm and a nitrogen flow rate of 300 cm³/min. The bio-oil mixture contained aliphatic and

aromatic hydrocarbons having the empirical formula $\text{CH}_{1.512}\text{O}_{0.175}\text{N}_{0.070}$, molar ratio H/C 1.73 and molar ratio O/C 0.175 under optimal conditions. Flash pyrolysis increases the oil yield by 20% by considering the Heinze retort. The authors concluded, the obtained pyrolysis oil can be provided as a biofuel, so the obtained liquid product can be directly used as a source of low-grade fuel, or it can be upgraded to a higher-quality liquid fuel.

Lappas et al. (2002) examined the biomass pyrolysis, in a circulating fluidized bed (CFB) reactor for the production of fuels and chemicals. CFB unit is capable of conventional and catalytic biomass pyrolysis with appropriate solids selection. Experimental system had the essential characteristics: rapid mixing of the biomass with the solid heat carrier in the mixing zone, short residence times in the riser reactor and rapid cooling of the steam in the heat exchanger. The ability and flexibility of continuous operation and the use of catalysts as circulating solids are the advantages of this unit. Charcoal and gas can be produced in high yields by catalytic biomass pyrolysis, of which oxidized gaseous compounds dominate (CO_2 and CO). It was found from this study that catalytic biomass pyrolysis produces additional water, coke and gas compared to conventional pyrolysis. When the S/B ratio is increased, the liquid product obtained contains more water, less oxygenates, more hydrocarbons, and less heavy oxides. The result shows that silica sand, commercial fluid catalytic cracking catalyst and a ZSM-5 additive show satisfactory stability when liquid products were produced by catalytic biomass pyrolysis.

Manuel et al. (2002) proposed a vacuum pyrolysis method for sugarcane bagasse, in which 30 and 34 wt.% bio-oil (anhydrous bagasse) can be recovered by this method. Compared to pyrolysis tests performed in pilot reactors, pyrolysis tests performed on a laboratory scale yielded more bio-oil (34.4 vs. 30.1 wt.%) and charcoal (19.4 vs. 25.7 wt.%). The obtained bio-oil is a challenging matrix for chemical, nutritional and pharmaceutical uses. When subjected to an accelerated aging test at 80 °C, the bio sensitivity of bio-oil extracted from sugarcane bagasse is similar to that obtained from other biomass materials. Bio-oil obtained from bagasse pyrolysis was found to be a potentially valuable liquid fuel: low ash content (0.05 wt.%), relatively low viscosity (4.1 cSt at 90 °C), and high calorific value (22.4

MJ/kg) and low levels of methanol insoluble (0.4 wt.%). The obtained charcoal yield was 20 to 26% by weight (anhydrous bagasse).

Onay and Kockar et al. (2003) described flash pyrolysis experiments on a rapeseed sample to determine the effects of pyrolysis temperature, heating rate, particle size, and sweep gas flow on product yields and its chemical composition. The flash pyrolysis was carried out in a tubular transport reactor. The maximum oil yield of 73% was obtained at the temperature of 550 to 600 °C, with particle size range of 0.6 to 1.25 mm and at a nitrogen gas flow rate of 100 cm³/min. Additionally, emphasized that there is a great need for pyrolysis technologies because they can produce denser fuel and easier to transport than raw materials. Chromatographic and spectral study on pyrolysis oils have shown that the oil produced from rapeseed can be utilized as a sustainable fuel and chemical feedstock.

Ates et al. (2004) studied the fast pyrolysis of sesame straw, it was determined that the temperature was between 400 and 700 °C, the particle size was between 0.224 and 1.8 mm in diameter, the heating rate was between 100 and 700 °C /min and the nitrogen flow rate was between 50 and 800 cm³/min. The obtained oil was separated into the chemical category by adsorption chromatography, and the oil was analysed using an elemental analyser, IR, ¹H-NMR. GC analysis showed that olefins, alkanes and branched hydrocarbons were the main compounds of the pentane soluble fraction. Similarly, the H / C ratio of the n-pentane fraction of the oil was 2.12, which is almost the same as that of gasoline. The data from chemical characterization indicate that the oil produced from sesame straw can be utilized as a potential source of renewable fuel.

Acikgoz et al. (2004) pyrolysed linseed in a fixed bed fast pyrolysis to determine the role of temperature, heating rate, particle size and gas flow rate on the product yields and composition. The obtained liquid yield was 57.7 wt.% at temperature 550 °C; 0.6 mm particle size with gas flow rate of 100 cm³/min and heating rate of 300 °C/min. From spectroscopic studies concluded that oil obtained from linseed can be utilized as renewable fuel and chemical feedstock, with higher heating value of 38.45 MJ/kg.

Onay and Kockar (2004) conducted experiments on rapeseed with two different reactors, fixed-bed Heinze and a well-swept fixed-bed tubular reactor to determine the effects of temperature, heating rate, particle size and gas flow rate on the product yields and composition. The maximum oil yield was 68% in fixed-bed Heinze reactor with heating rate of 300 °C /min where as in well -swept fixed-bed tubular, the oil yield was 51.7 % with heating rate of 30 °C /min. From spectroscopic studies concluded that pyrolytic oil can be used as renewable fuel and chemical feedstock.

Yan et al. (2005) experimentally investigated the effect of temperature on the distribution of gaseous products in pyrolysed palm oil waste. During the experiment, it was observed that temperature has important effect on the pyrolysis of palm oil waste, especially on the distribution of gaseous products. Different pyrolysis rates and gas conversion curves at low (<355 °C) and high (> 355 °C) temperatures indicate that the reaction mechanisms involved are different. When the temperature is below 355 °C, the pyrolysis may be controlled by kinetics, where the pyrolysis rate increases significantly with temperature. Experimental studies using TGA-FTIR and thermodynamic models have shown similar results: the total gas yield increases with increasing temperature, but at the cost of residual carbon. Thermodynamic equilibrium simulations show that H₂, CO₂, CH₄ and CO are the main gaseous products. It can be inferred from the research that H₂ is produced only at high temperatures. At temperatures above 900 °C, the yields of H₂ and CO increase with temperature, with maximum yields of 45 and 30 mol%, respectively. If the temperature is increased, the yields of H₂O, CO₂, and CH₄ will decrease, but will become essentially zero at high temperatures (> 800 °C). This study provides an understanding the effect of temperature on the gases produced by pyrolyzing biomass.

Asadullah et al. (2008) conducted jute stick pyrolysis for obtaining bio-oil using a continuous feed fluidized bed reactor at various temperatures ranging from 300 to 600 °C. The non-condensable gas mixture contains mainly N₂, CO and CO₂. During pyrolysis process, CH₄, C₂H₆, C₃H₈ etc. have also been formed. The study showed that the liquid yield was maximum at 500 °C and density of the liquid was

high (1.11 g/ml) compared to light fuel oil. Due to the presence of some organic acids, such as formic acid, acetic acid, etc., the viscosity of the liquid was found to be 2.34 cP, and the bio-oil was essentially acidic, and the pH and acid value were found to be approximately 4 and 135 mgKOH/g respectively. The moisture content of liquid was 16% by weight. The solids and ash content was 0.02 and 0.03% by weight, respectively.

Zheng et al. (2008) examined the rapid pyrolysis of the cornstalk in a fluidized bed reactor. As the temperature increases, the pyrolysis yield increases. At a pyrolysis temperature of 500 °C, the highest liquid yield produced was 66%. The obtained pyrolysis liquid is complex organic mixture mainly composed of oxygenates, acids and heterocyclic compounds. Pyrolysis liquid is very mildly corrosive to copper and stainless steel. The authors concluded the pyrolysis liquid produced can be directly used as fuel oil for combustion in boilers or furnaces without any upgrade. Direct use of pyrolyzed oil for diesel engines can reduce technology investment. Alternatively, it can be upgraded for use as a vehicle fuel.

Ganapathy et al. (2009) performed experiments on slow pyrolysis of coconut shells in fixed bed reactor and process conditions were optimized to obtain the highest liquid yields. In a reactor with a length of 200 mm, the maximum bio-oil yield produced was at temperature 550 °C with particle size of 1.18-1.80 mm and the constant heating rate of 60 °C /min. Under different process conditions, the yields of the obtained bio-oil, char and gas are 38-44 wt.%, 22-31 wt.% and 30-33 wt.%, respectively.

Natarajan et al. (2009) conducted experiments on rice husk, slow pyrolysis in fixed bed and optimized treatment conditions to obtain the highest liquid yield. The maximum yield of liquid obtained at a temperature 550 °C with a particle size of 0.60-1.18 mm and a constant heating rate of 60 °C /min in a reactor 300 mm long. Under different process conditions, the yields of the obtained bio-oil, charcoal and gases were 22.57 – 31.78 wt.%, 34.17– 42.52 wt.% and 27.75 – 42.26 wt.%, respectively.

Joardder et al. (2011) studied the transformation of coconut shells into bio-oil using fixed bed fire-tube heating reactor and optimized the liquid yield at temperature 450 °C, particle size 0.6 mm and gas flow rate 6 l/min with running time of 1.4 h. The obtained yield of bio-oil was 34.3 wt%. The oil was further characterized for physical and chemical properties to be used as renewable fuel.

Tsai et al. (2007) prepared bio-oil from agricultural by product rice husk in a fixed bed fast pyrolysis reactor. The maximum bio-oil yield was 40 wt.% at 500 °C, with particle size <0.50 mm at heating rate of 200 °C/min and concluded rice husk bio-oil consists most of complex compounds composed of aromatic and carbonyl groups.

Rout et al. (2015) carried pyrolysis experiments on coconut shells in a fixed bed. The optimum temperature was 575 °C with maximum bio-oil yield of 49.5 wt%. The bio-oil mainly composed of aromatic structures followed by aliphatic and heterocyclic compounds. The empirical formula for obtained bio-oil was $\text{CH}_{0.70}\text{N}_{0.06}\text{O}_{0.39}\text{S}_{0.14}$.

Yang et al. (2014) described the intermediate pyrolysis in 20 kg/h pyroformer using wood and barely straw pellets as biomass feed and obtained the bio-oil yield of 34.1 wt.% for wood pellets and 12 wt.% for barely straw pellets. Analysis showed that the bio-oil was rich in heterocyclic and phenolic compounds. The novelty of the work described the recycling of the internal char acted as both heat carrier and catalytic cracking. From analysis it was concluded that wood oil was 3 times higher than that of barely straw oil.

Tinwala et al. (2015) studied intermediate pyrolysis process (IPP) in a bench scale pyrolyser with 8 different agro waste materials. Bio-oil yield ranged from 20.5 to 47.5%, while the carbon-rich solids and pyrolysis gas ranged from 27.5 to 40% and 24.5 to 40.5%, respectively.

The intermediate pyrolysis process developed by Aston University is an improved process over conventional pyrolysis. It reduces the formation of highly molecular tars and provides dry, brittle bio-chars suitable for use in a variety of applications (Patel et al. 2016).

Mohammed et al. (2016) evaluated the effect of temperature on the pyrolysis distribution of bambara peanut shell products (bio-oil, bio-char and non-condensable gases) performed in a fixed-bed reactor. The physicochemical properties of the products have been reported. Calorific value of bio-oil is 25-29 MJ/kg, which contains sugar and other value-added chemicals. Bio-char was rich in carbon and non-condensable gases consisted of CH₄ and CO. The authors conclude that bio-oil can be utilized directly as fuel for boilers, bio-char can be utilized as solid fuel, and non-condensable gases can be used as fuel.

Fardyanti et al. (2018) examined, the bio-oil produced by the pyrolysis of the coconut shell. Liquid products were obtained using an aqueous methanol solution as a diluent. The extraction process was carried out for 60 min and then separated by the two phases, extract phase and the raffinate phase using a separatory funnel. The analysis results concluded that the partition coefficient and yield of phenol extraction are highest at 50 °C and a stirring speed of 250 rpm.

2.2 HEAVY OIL (TAR) SOLVENT EXTRACTION

Aske et al. (2001) examined 18 different crude oils and condensates by Infrared (IR) and near infrared spectroscopy (NIR) techniques. The crude samples were separated by high performance liquid chromatography (HPLC) into four classes particularly saturates, aromatics, resins and asphaltenes, in short the SARA fractions. The ability of the spectroscopic analysis with reference to the SARA fractions are examined by multivariate analysis namely principal component analysis and partial least square analysis. The uncertainties on IR technique were found to be 2.5, 2.2, 1.4 and 1.3 wt% for SARA fractions, respectively. The NIR uncertainties were 2.8, 2.4, 1.4 and 1.0 wt%. The values found were in the same range determined by HPLC.

Akmaz et al. (2011) studied batiraman heavy crude oil for structural characterization and n-heptane was used to separate asphaltene fraction. The solvent was evaporated and collected maltene from filtrate. Fourier transform infrared spectra determined the C=C, C=O, CH₂ and CH₃ groups. The study proposed hypothetical compositions for the SARA fractions. Saturate fractions were composed of long aliphatic compounds. Aromatic fraction was aromatic compounds with aliphatic side

chains. Resin fractions consisted of fused aromatic rings with branched paraffins and polar compounds. Asphaltene was considered as a polymeric fraction.

Kan et al. (2011) investigated two different special metal prepared catalysts (Mo-Co/ γ -Al₂O₃ and W- Ni/ γ -Al₂O₃) used for two stage catalytic hydrogenation of coal tar into free-flowing liquid fuels. The results of hydrogen pressure and liquid hour space velocity on hydrogenation performance were studied. The gasoline (≤ 180 °C) and diesel (180-360 °C) fractions obtained from the oil products were also analysed. It was found that, sulfur content decreased from 1.96 to 0.98 wt.%.

Sun et al. (2011) studied tar obtained by low temperature pyrolysis of coal and it was extracted with petroleum ether by ultrasonic irradiation method. The soluble and insoluble parts were analysed using GC-MS and TG-FTIR techniques. The extracted yield was 61.7 % and the GC-MS results showed that most of the chemical compounds were phenolics, free alkanes and heterocyclic compounds. The TG-FTIR data showed that the volatiles were released in between 110-425 °C. The main gaseous products evolved during the process were phenols, carbon dioxide, water, saturated hydrocarbons, aromatic compounds, oxygen hetero cycles, etc.

Kusy et al. (2012) characterised the brown coal tar obtained from pyrolysis. Cobalt-Molybdenum (Co-Mo) bimetallic catalyst was used for the hydrogenation process. The process was optimised on the temperature 300 °C and pressure of 30 bar. The end products were further characterized and analysed against the GC-MS of starting material. The yield of the end product depends on the operating conditions. Mixture of hydrocarbons was produced and was similar to naphtha cut of petroleum.

Li et al. (2001) optimized the process conditions and micro-kinetics for hydrodesulphurization of coal tar using Box-Behnken design. Experiments were conducted on trickle bed hydrogenation. Analysis of variance (ANOVA) analysis determined the optimum conditions namely temperature 408 °C, pressure of 13.1 MPa, LHSV of 0.32 h⁻¹ and hydrogen to volume ratio of 1,200 L_N/L. The sulphur content was 12-16 mg/kg. The kinetic model was proposed using power law model. The process followed second order kinetics and activation energy (42.15 kJ/mol) was

found lesser than petroleum fractions. The authors concluded that, the model could detect the mass fraction of sulfur quite accurately.

Sun and Zhang (2017) worked on the distillation residues of middle temperature coal tar and analysed chemical composition and structural characterization. The tar was extracted into four fractions, namely saturate (22.5%), aromatic (24.3%), resin (26.5%) and asphaltene (16.9%). The fractions were further characterised for their compositions and chemical structures by using elemental analysis, FT-IR, ^1H NMR. The work concluded that among the four fractions, saturate fraction was rich in long alkyl chains and no heteroatom was found. The molecular weights found to be asphaltene>resin>aromatic.

2.3 CATALYTIC UPGRADATION OF BIO-OIL

Caballero et al. (1996) studied the kinetics of the pyrolysis reaction of Kraft lignin at various heating rates. The pyrolysis was carried out at 450-900 °C for 30 s at a heating rate of 20 °C/ms. The mathematical model applied to the pyrolytic process was in good agreement with the experimental findings. The yields of aromatics, hydrocarbons, CO_2 , and CO increased with temperature.

Niquille and Prins (2006) compared the metal sulfide and noble metal catalysts and analysed the hydrodesulfurization (HDS) of dibenzothiophene (DBT) and 4,6-dimethyldibenzothiophene (4,6-DM-DBT). The platinum catalyst supported on alumina ($\text{Pt}/\text{Al}_2\text{O}_3$) fared better than palladium on alumina ($\text{Pd}/\text{Al}_2\text{O}_3$) for the HDS of DBT and 4,6-DM-DBT. The desulfurization of DBT and 4,6-DM-DBT were faster over $\text{Pt}-\text{Al}_2\text{O}_3$ compared to $\text{Pd}-\text{Al}_2\text{O}_3$.

Wildschut et al. (2010) produced bio-oil from fast pyrolysis within a batch reactor using Ru-C catalyst and demonstrated the recyclability of the catalyst. The yield of bio-oil was 30-55 wt.% and H/C ratio of 1.24 (fresh Ru-C). The H/C ratio marginally reduced to 1.08 in the third cycle.

Zhao et al. (2011) studied guaiacol as a model substrate for pyrolysis liquid on a series of catalysts like $\text{Ni}_2\text{P}/\text{SiO}_2$, $\text{Fe}_2\text{P}/\text{SiO}_2$, MoP/SiO_2 , $\text{Co}_2\text{P}/\text{SiO}_2$, and WP/SiO_2 . The results showed that the primary products for HDO of guaiacol were phenol,

benzene, and anisole. Catechol was found to form as a major product at lower contact times in the case of Co₂P and WP transition metal phosphide catalysts. However, at higher contact time, the formation of catechol was not observed.

Ardiyanti et al. (2011) studied the hydro-treatment of the wood-based pyrolysis liquid using mono and bimetallic catalysts based on Pt, Pd, and Rh supported on zirconia in the batch reactor at 350 °C, 20 MPa hydrogen pressure and 4 h reaction time. The yields of the upgraded oil were between 37-47 wt.%, 30-42 wt.% of the aqueous phase, 6-10 wt.% of gaseous fraction, and 2-7 wt.% of solid carbonaceous residue. The oxygen content in the pyrolysis liquid decreased phenomenally from 40.1 wt.% to 7-11 wt.%. The authors concluded; relative yields depend on the type of feedstock used.

Zhu et al. (2013) summarized the strategies for creating mesoporosity in zeolite catalysts and discussed the catalytic applications of mesoporous zeolites in oil refining and natural gas conversion. The authors concluded, mesoporous zeolites exhibited excellent performance in cracking of heavy oil, isomerization, hydrodesulfurization, hydrogenation, dehydroaromatization of methane, dehydration of methanol into dimethyl ether, methanol to olefins, and methanol to hydrocarbons.

Sanna et al. (2015) examined the low-temperature hydrogenation (LTH) of the water-soluble fraction of bio-oil at 125 °C and high-temperature hydrogenation (HTH) at 250 °C using Ru-C and Pd-C catalysts at 50 bar of hydrogen pressure. The weight hour space velocity (WHSV) for Ru-C and Pd-C was 1.5-3 h⁻¹ and 3 h⁻¹, respectively. The end products for LTH were ethylene glycol, propylene glycols, and sorbitol. Small quantities of acetic acid, phenol, and substituted phenols were hydrogenated. In HTH, the sorbitol was hydrogenated into mono and diols. The authors concluded that water-soluble bio-oil could produce alcohols, diols, and oxygenated gasoline additives in a two-stage continuous hydrogenation process. Ruthenium catalyst converts aldehydes, ketones, and sugars to their corresponding alcohols in LTH and can be easily converted to the desired products by HTH.

Saad et al. (2015) examined the catalytic cracking of heavy oil obtained by pyrolysis of rubber wood using HZSM-5 catalyst. The end products were organic

liquid product and gasoline range aromatics. From response surface methodologies, the best yields were found to be around 28 % (organic liquid product) at temperature 536 °C using HZSM-5. The maximum gasoline aromatics were found to be 54 % at temperature 575 °C.

Quan et al. (2017) studied catalytic steam reforming of coconut shell-derived pyrolytic bio-oil using Fe/olivine catalyst in a fixed bed quartz reactor. The results showed that the phenolics presented in the bio-oil were converted into gaseous compounds such as H₂, CO, CO₂, and CH₄. The best parameters for carbon conversion was 97% under 10% loading of the catalyst at the temperature of 800 °C with WHSV= 0.5 and S/C=2.

Boscagli et al. (2018) performed an intermediate pyrolysis of beech-wood and wheat straw and compared the influence of the improved oil by hydrodeoxygenation using Ru-C and NiCu / Al₂O₃ catalysts. Because of its low content of heteroatoms, beech-wood has proven to be a suitable raw material for HDO, and the high sulfur content of wheat straw bio-oil has caused irreversible catalyst poisoning. Ru-C usually consumes more hydrogen than NiCu / Al₂O₃, has higher hydrogenation activity, HDO has higher selectivity to alcohols and hydrocarbons, and NiCu / Al₂O₃ results in higher ketone concentrations. Pyrolysis temperature affects the degree of cracking; higher temperatures result in higher quality pyrolysis oils with lower oxygen mass fractions but lower mass yields. By changing the hydrotreating temperature (80, 150, 250 and 350 °C), different types of compounds can be converted and different degrees of deoxygenation can be achieved. Overall, the results show that for dispersive (or small-scale) applications, especially for heterogeneous feedstocks with high ash content, the use of hot steam filtration for intermediate pyrolysis is an effective alternative to the more commonly used rapid pyrolysis.

Alda-Onggar et al. (2019) prepared Ni and Ir-supported ZrO₂ catalysts by incipient wetness method and investigated the effectiveness of the catalysts on the HDO of model phenolic compounds like isoeugenol, guaiacol, and vanillin. The results showed that the HDO of guaiacol at 250 °C and 3 MPa of hydrogen pressure yielded 36% of cyclohexanol over the Ni/ZrO₂ catalyst. A maximum of 33% yield of

propyl-cyclohexane was observed using Ir/ZrO₂. Vanillyl alcohol was the main product in vanillin HDO at 100 °C.

2.4 DYE SENSITISED SOLAR CELLS

Satya et al. (1997) produced activated carbon from coconut shell char using steam in a fluidized bed reactor. They reported that better activated charcoal was prepared by increasing reaction time, particle size and fluidizing velocity and temperature.

Juan et al. (2009) described the DSSC temperature dependence using total resistance of the cell. They suggest the thermal gradient between the photo anode and counter electrode reduces the total DSSC resistance. This develops similar thermal resistance on both illuminated and dark conditions. This also intended to reduce resistance of counter electrode and accelerate the increased charge transfer kinetics and redox. Further, at increased temperature the conductivity of dye increases. They concluded that increase in temperature reduces the total resistance in which the resistance of photo electrode is not much altered. It is also said that the increased in temperature not much reduces the film total capacitance. It is also found that increases in temperature increases fast electron transfer for 10% (Liu et al. 2007).

Feng et al. (2012) investigated performance of activated carbon as DSSC electrode material by comparing with several other carbon compounds. They confirmed that the increase in efficiency the DSSC is not just due to increased surface area but also with enhanced microporous structures, this makes activated carbon a better candidate.

Kulkarni et al. (2013) prepared activated carbon from coconut shells and used as the adsorbent. Adsorption was carried out in a fluidized bed. Investigation on parametric effects like concentration, fluid flow rate and adsorbent particle size were studied. It was concluded that as the concentration increased, the saturation percentage of the adsorbent increased. In addition, in the case of coconut shell activated carbon, an increase in fluid flow rate will also result in better adsorption. However, it has also been observed that the percent saturation of adsorption decreases

as the particle size of the adsorbent increases. A particle size of 0.420 mm was found to be more favorable.

Das et al. (2015) prepared activated carbon from green coconut shells by chemical activation method. It was used for the removal of CO₂ from flue gas and various inorganic contaminants from waste water. They reported that the adsorption capacity of the chemically activated carbon was found superior than other potentially synthesized method with enhanced surface area and pore size.

Kumar and Bhargava (2015) studied efforts on developing DSSC using carbon from glucose and generated an increased power efficiency by 6.72% within an area of 0.25 cm². It was further extended by implementation of graphitized carbon from sugar free with a generated current density of 8.30 mA/cm² with a cell efficiency of 3.63% .

Mahajan and Femina (2017) synthesised activated carbon from prosopis juliflora wood by carbonization at 600 °C and thermal activation at 800 °C. They studied the activated carbon for its adsorbent chemical and physical properties. It was estimated that the synthesized activated carbon showed a Brunauer–Emmett–Teller (BET) surface area of 748.91 m²/g, pore size of 1.5 nm and micro pore volume of 0.163 cm³/g.

The performance of DSSC is profoundly dependent on the sensitizer and large band gap semiconductor materials such as TiO₂ (Singh and Koiry 2018). TiO₂ are highly advantageous due to its higher adsorption of dye and superior capacity to resist the continuous transfer of electron subjected to solar photons under illumination.

The effectiveness and efficiency of the solar cell is determined majorly by dye absorption spectrum and surface factors of TiO₂ molecules (Feng et al. 2012). Normally, photo anode is set by adsorption of sensitizer dye on TiO₂ layer. In most of the cases the synthesised synthetic sensitizer dyes requires multistage procedures with tedious chromatographic purification methodologies (Sinha et al. 2018).

Apart from the toxicity and recombination issues developed in DSSC, the external factor plays a major role in performance of DSSC practical application. In

particular dependence of DSSC for temperature characteristics. Several investigations were reported on performance of DSSC. But very few highlights the importance of temperature effects. Hogberg et al. (2017) investigated the use of liquid crystal electrolyte for DSSC in elevated temperature . Moreover, with increased cost and toxicity, separate interest in exploring the possibility of using natural dyes for photon absorption.

2.5 SCOPE AND OBJECTIVES OF THE WORK

From the literature review it is understood that the importance of future energy needs relies more on harnessing biomass energy and solar energy in our day-to-day energy systems. Challenges in using biomass-based bio-oil as drop-in fuel or as a fuel additive include high moisture content, lower heating value, and low thermal stability. Besides, the bio-oils have limited miscibility with conventional petroleum fuels due to the presence of polar compounds like alcohols and carbonyl compounds. The storage stability of bio-oils is typically low due to the presence of compounds with reactive functional groups. Therefore, the bio-oil must be upgraded for better physicochemical and elemental properties prior use. Also when solar energy, compared with the existing photovoltaic PV solar cells DSSC provides more optimistic approach on rapidly advancing consumer electronics segment with reduced size and enhanced smartness. As a result, integrating DSSC can potentially redefine the flexible electronics with sophistication at tremendous levels of diversification. Nowadays, sensors and energy sources are implemented in wearable electronics, optoelectronics and bio devices. It is pertinent to mention that the use of DSSC sensors/energy sources on current devices can predominantly reduce the size of flexible devices. This makes the thin film based DSSC a better option for latest compact devices. Therefore, the objectives of the present research work are to:

- Studies on coconut shell using intermediate pyrolysis process oriented for solid and liquid products production of pilot plant and cost analysis of end products of coconut shells.
- Characterization of coconut shell pyrolysed products by sophisticated techniques: Elemental analysis; SEM analysis; XRD; FT-IR; GC-MS; NMR.
- Upgradation of bio-oil by hydrodeoxygenation using Pd-C and Ru-C catalysts
- Coconut shell charcoal-based counter electrode for the development of dye sensitised solar cell (DSSC).

CHAPTER 3

RESEARCH METHODOLOGY

In this chapter, the general chemicals used in the study and analysis are listed. The chapter also includes the analytical and spectroscopic methods used for characterisation of the material.

3.1 MATERIALS AND METHODS

All the chemicals used in the experiments of this work have been listed in Table 3.1. The Intermediate pyrolysis process of coconut shell trial experiments were conducted in Vayu Gases, Oil and Carbons, Bengaluru and collected the coconut shell pyrolysed oil (CSPO) and bio-char. The by products (CSPO and Bio-char) was used for all experimental studies. The collected samples were analysed and reported. The upgradation of bio-oil was conducted on high pressure reactor at Chemistry department lab, National Institute of Technology, Surathkal, Karnataka, India. The research report is based on elemental analysis, FT-IR, NMR and GC-MS analysis of the products, with TGA analysis of feedstock and upgraded oil.

3.2 INSTRUMENTS USED FOR ANALYSIS

3.2.1 Thermo gravimetric analysis (TGA) of coconut shell powder

Thermo-gravimetric analysis (TGA) of CS powder is performed by HITACHI EXSTAR TG/DTA 6300. An accurately weighed 15-20 mg sample was placed in the platinum crucible. The sample was heated from ambient temperature to 600 °C. The experiment was conducted under a constant flow (100 ml/min) of nitrogen gas at a heating rate of 20 °C/min.

3.2.2 Thermo gravimetric analysis (TGA) of bio-oil

Thermo-gravimetric analysis (TGA) of CS pyrolysed and upgraded oil was done using a PerkinElmer Thermogravimetric analyser (TGA 4000). An accurately weighed 15-20 mg sample was placed in the alumina crucible. The sample was heated from ambient temperature to 800 °C. The experiment was conducted under a constant

flow (20 ml/min) of nitrogen gas at a heating rate of 10 °C/min. The analyses were carried out at Chemistry department lab, National Institute of Technology, Surathkal, Karnataka, India

Table 3.1 Chemicals used in experiments and analysis

Sl. No.	Chemicals	Company	Used as
1	Acetone	Lab grade	Cleaning
2	Ethanol	Sigma Aldrich	Diluent
3	n-pentane	Merck	Diluent
4	Toluene (C ₇ H ₈)	Merck	Diluent
5	Potassium Bromide (KBr)	Himedia	Initiator
6	Carbon tetrachloride (CCl ₄)	Merck	Diluent
7	Tetrahydrofuran (THF)	Merck	Diluent
8	Dichloromethane (DCM)	Merck	Diluent
9	Chloroform (CHCl ₃)	Merck	Diluent
10	Palladium on activated carbon (Pd-C)	Otto Chemie	Catalyst
11	Ruthenium on activated carbon (Ru-C)	Sigma Aldrich	Catalyst
12	Titanium dioxide (TiO ₂)	Lab grade	Initiator
13	Ethylene Glycol (CH ₂ OH) ₂	Lab grade	Diluent

3.2.3 Elemental analysis

The elemental analyser was used to determine the composition of the bio-oil (CHNS-O Flash EA 1112 Series). The elemental analysis determines the percentage of carbon, hydrogen and nitrogen. The oxygen was calculated by the difference. The analyses were carried out at SAIF lab, Indian Institute of Technology, Bombay, India.

3.2.4 Fourier transform infrared radiation (FT-IR) analysis

The presence of the organic functional groups present in the bio-oil was identified by FT-IR. The spectra of the bio-oil were identified in the range of 4000-400 cm^{-1} . The liquid and solid obtained from pyrolysis under optimum conditions were tested to analyse the presence of chemical functional groups by Fourier Transform Infrared (FT-IR) spectroscopy. The analyses were carried out at Chemistry department lab, National Institute of Technology, Surathkal, Karnataka, India

3.2.5 Gas chromatography and mass spectroscopy (GC-MS)

The chemical composition of the bio-oil was identified by GC-HRMS. The column containing helium (carrier gas) flowing at a rate of 1.5 ml/min was injected with liquid product of volume 1 μl . The liquid product compounds get ionized at 70 eV, 200 $^{\circ}\text{C}$ and were analysed over a mass electron (m/z) range of 40-700. The result obtained with respect to different retention time and respective mass spectra were plotted and validated with spectral data from National Institute for Standards and Technology (NIST) library.

The chemicals compounds present in the pyrolysis liquids, which have obtained under optimum parameter by pyrolysis process were analysed by Gas chromatography mass spectrometry (GC-MS). The instrumental facility was utilized from Sophisticated Analytical Instrument Facility (SAIF) lab, at Indian Institute of Technology Madras and Indian Institute of Technology Bombay.

3.2.6 Nuclear magnetic resonance (NMR)

NMR analysis identifies the functional groups, hydrogen distribution and carbon aromaticity. The 500 MHz liquid state NMR spectrometer was used to analyse the upgraded coconut shell pyrolysed oil. Chloroform is used as the standard solvent for the analysis. The analyses were carried out at SAIF NMR lab, Indian Institute of Science, Bangalore.

3.2.7 Characterization by analytic techniques

ASTM 3172-07a was followed to proximate analysis bio-char. The BC was characterized by Scanning Electron Microscope (Model: JEOL-JSM-6480LV SEM) with an acceleration voltage of 15 kV. The analyses were carried out at Metallurgical and materials department lab, National Institute of Technology, Surathkal, Karnataka, India. The structures of solid rich carbon were seen by X-ray diffraction (XRD) using a diffractometer by Cu-K α radiation ($\lambda = 1.542 \text{ \AA}$) operating at 40 kV with step size of 0.02° in the range of $10-90^\circ$. The analyses were carried out at Physics department lab, National Institute of Technology, Surathkal, Karnataka, India.

3.2.8 Indium tin oxide glass (ITO)

The Indium tin oxide coated conductive glass is used in the fabrication of dye sensitised solar cell. The ITO glass dimensions: length 50 mm x width 25 mm x thickness 0.7 mm; resistivity 10 ohms; transmittance >0.83 ; procured from Techinstro, Maharashtra, India.

CHAPTER 4

INTERMEDIATE PYROLYSIS OF AGRICULTURAL WASTE COCONUT SHELLS IN A PILOT SCALE SYSTEM FOR PRODUCING SUSTAINABLE FUELS AND CHARACTERISATION OF BIO-OIL AND BIO-CHAR

Solid biomass fuels and agricultural residues can be directly used for energy production, but there is a considerable advantage and interest in converting them into more valuable and more flexible forms of energy in the form of solids, liquids or gases. This chapter focuses on pilot scale intermediate pyrolysis of agricultural residues coconut shells. Pyrolysis is considered from decades in the production of char but it is only last decades the intermediate pyrolysis route is particularly interesting because the solids, liquids and gases are produced with appropriate equal yields and can be easily stored and shipped; they can be used for the production of energy, chemicals or as a source of energy. In this chapter the pilot scale experimental procedure and characterisation of the coconut shell as raw material and coconut shell pyrolysed end products (bio-oil and bio-char) are described using analytical and spectroscopic techniques.

INTRODUCTION

According to Indian Renewable Energy Development Agency Limited (IREDA), biomass is capable of supplementing the coal to the tune of about 260 million tons per year saving about Rs. 250 billion USD (Government of India 2018) (MNRE 2017). The maximum energy used in the industries accounts for around 58% of the total energy consumption. The per-capita utilization of energy has increased by a compound annual growth rate (CAGR) of 3.54 % during 2011-12 to 2016-17 (Ranganadham et al. 2018). However, the excessive use of imported crude oils leads to economic hardship and serious environmental issues. There has been a coordinated effort to develop a renewable alternative to fossilized carbon. Non-food biomass, preferably lignocellulosic wastes, can be an economically-attractive feedstock for

renewable biofuels (Ryu et al. 2009; Ragauskas et al. 2014 and Lee et al. 2016). Thermochemical conversions of biomass into liquid fuels via gasification, pyrolysis, or hydrothermal liquefaction are known (Lee et al. 2016). The carbon-based liquid fuels can be used as renewable drop-in fuels as an additive to petro fuels or as standalone fuel after suitable upgrading (Kabir and Hameed 2017). In India power from biomass combustion, biomass gasification, and bagasse cogeneration reached 9.1 GW installed capacity as of 31 March 2019.

The energy production may be enhanced by using the available lignocellulosic agricultural waste residues. Coconut shells have high energy content and will be a good potential source for pyrolysis. The Intermediate pyrolysis process (IPP) of CS was conducted in a pilot scale system heated externally with electric heater. The optimum temperature for maximum bio-oil and bio-char was at 575 °C. The maximum coconut shell pyrolysis oil (CSPO) yield was 33-38 wt.%. Bio-char and pyrolytic gases were other end products. The end products are characterised by elemental analysis, and spectrographic analysis like Fourier transform infrared (FT-IR), gas chromatography-mass spectrometry (GC-MS). From analysis found that CSPO were rich in phenolic compounds and have higher heating value of 16.75 MJ/kg (dry basis). The yield of char was found to be 30 wt.% and have the heating values similar to sub bituminous coal (29.05 MJ/kg).

4.1 FEEDSTOCK PREPARATION

The coconut shells were sieved to a size of 4 to 5 mm and were naturally pre-dried in the sun for 48-72 h. The coconut shell further dried in oven at 105 °C for 24 h to eliminate moisture. Once moisture was removed, they were loaded into the reactor.

4.2 PYROLYSIS PROCEDURE

The experiments are performed at elevated temperature 575 °C in fixed bed reactor a capacity of 120 kg. The system consists of several components, including an electronic control panel, condenser, water scrubber, gas purification system for separating carbon dioxide and tar, compressed gas storage tank of 12 bar and gas engine generator. The reactor is heated using a three-phase electric heater of 40 kW. The moisture removed coconut shells were introduced into the reactor where the

reduction and cracking of raw material happens. Volatiles are condensed in the condenser by a constant flow of water through condenser and the non-condensable gas was passed through the buffer tank which ensured continuous supply to the customized compressor wherein the gas was compressed to higher pressure. The physical representation of the IPP is shown in the figure 4.1. Three replicate runs were performed. The collected end products were calculated by equations 4.1 and 4.2 respectively. The gas yield (%) was calculated by difference i.e. [100 - (Bio-oil yield (%) + Bio-char yield (%))]. The obtained bio-oil had a density of 929 kg/m³(Appendix-A1.2.5), pH value of 2.93 and kinematic viscosity measured at 40 °C is 3.576 cSt (Appendix-A1.2.6).

$$\text{Bio - oil yield (wt. \%)} = \frac{\text{Final weight of the bio-oil}}{\text{Raw material weight}} \times 100 \quad (4.1)$$

$$\text{Bio - Char yield (wt. \%)} = \frac{\text{Final weight of the bio-char}}{\text{Raw material weight}} \times 100 \quad (4.2)$$

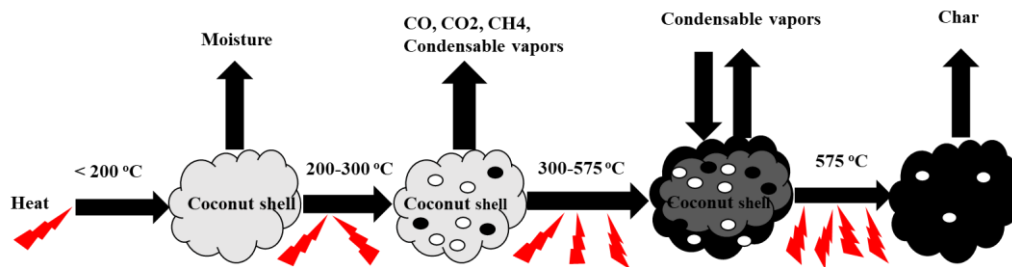


Figure 4.1 Physical representation of pyrolysis process. coconut shells as grey, gases/voids as white, liquids and chars as black

4.3 RESULTS AND DISCUSSION

4.3.1 Thermogravimetric analysis of coconut shells

The thermogravimetric analysis is the measurement of the weight of a sample as a function of temperature or time when the biomass sample is heated in a predefined time temperature program. The thermal image of the coconut shell at 20 °C/min heating rate is as shown (figure 4.2). The TGA and DTG gives the correlation between the mass loss and temperature. From mass loss curve (TG), it is observed 10% of mass loss occurs between ambient to 100 °C due to the vaporisation of

moisture present in the coconut shell powder. As temperature increases further 50% mass loss is seen within the temperature range 260 °C to 381 °C based on the evolution of water, carbon monoxide and other volatile contents present in the sample. Further decomposition is seen up to 600 °C which shows the presence of carbon content and other non-volatile products. The DTG peak shows three peaks, first peak at 100 °C was seen for the removal of the moisture content present in the raw material. The two peaks at 296 °C and 361 °C indicates the mass loss allied with decomposition of volatiles. The temperature range 260-330 °C with the peak 280 °C was due to slow lignin decomposition. The temperature range of thermal devolatilization of cellulose (260-350 °C), hemicellulose (200-280 °C) and lignin (280-500 °C) was reported by Fan et al. 2017).

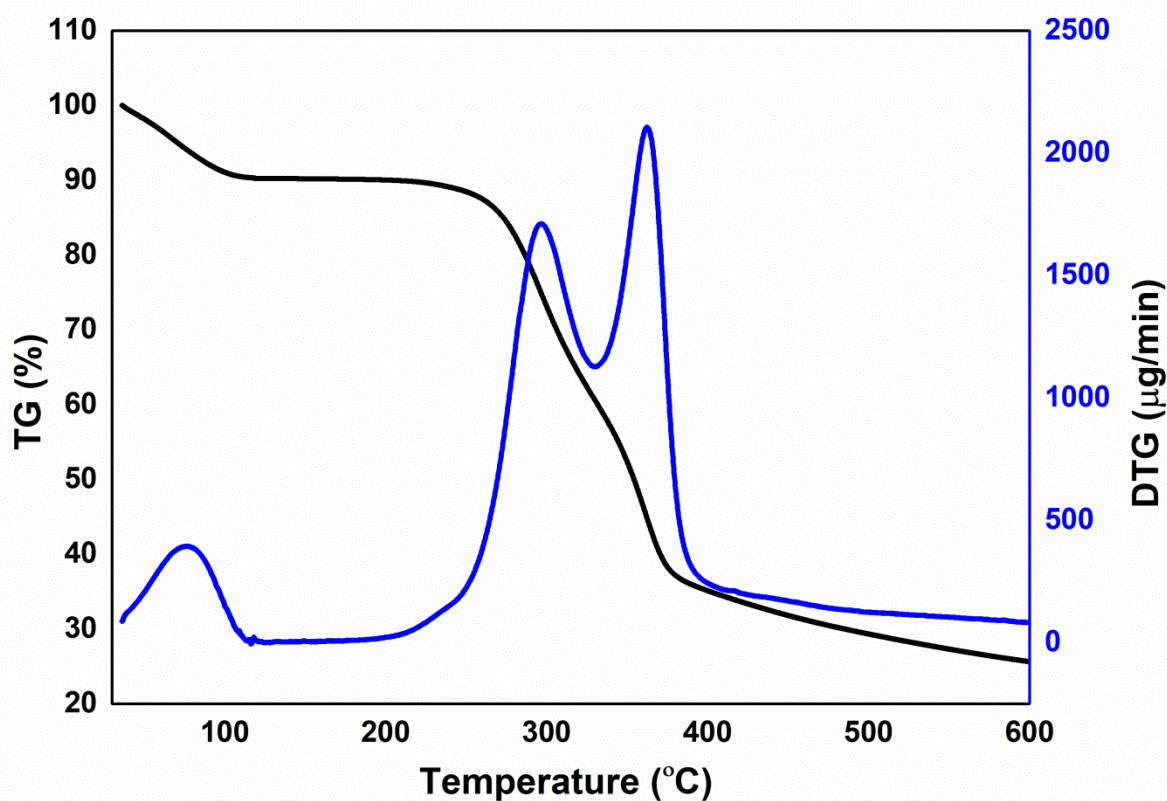


Figure 4.2 Thermo gravimetric analysis of coconut shell

4.3.2 Elemental analysis

The main elemental compounds present in the obtained CSPO i.e., carbon, hydrogen, nitrogen, sulfur, oxygen and estimated H/C, O/C are represented and compared with other biomass materials are presented in table 4.1. The elemental compounds and higher heating value vary with the biomass materials. The fuel energy content is inversely proportional to the amount of oxygen present. The average higher heating value of the CSPO obtained was 16.75 MJ/kg. The obtained result was higher than 11.98 MJ/kg (Venkatesan and Senthilkumar 2015).

4.3.3 Fourier transform infrared spectroscopy (FT-IR) analysis

Figure 4.3 shows the spectra of the CSPO and table 4.2 indicates the wavenumber of CSPO. The results indicate the presence of phenols, ketones, esters and alcohols in bio-oil, based on O-H stretching vibration observed between 3200-3600 cm^{-1} , C=O stretching vibration of 1700 cm^{-1} from ketone or carboxylic acid. Similarly, the stretching vibrations, 1636 cm^{-1} and 1387 cm^{-1} respectively indicates the presence of alkenes and aromatics. The alcohol group identified with C-O stretching at 1273 cm^{-1} , also at band 1016 cm^{-1} show the presence of ether in the bio-oil. Most of the aromatic compound observed on stretching vibration of 756 cm^{-1} . The source of aromatic and aliphatic compounds may be because of polymers present in the CS. The data were compatible when compared with the GC-MS.

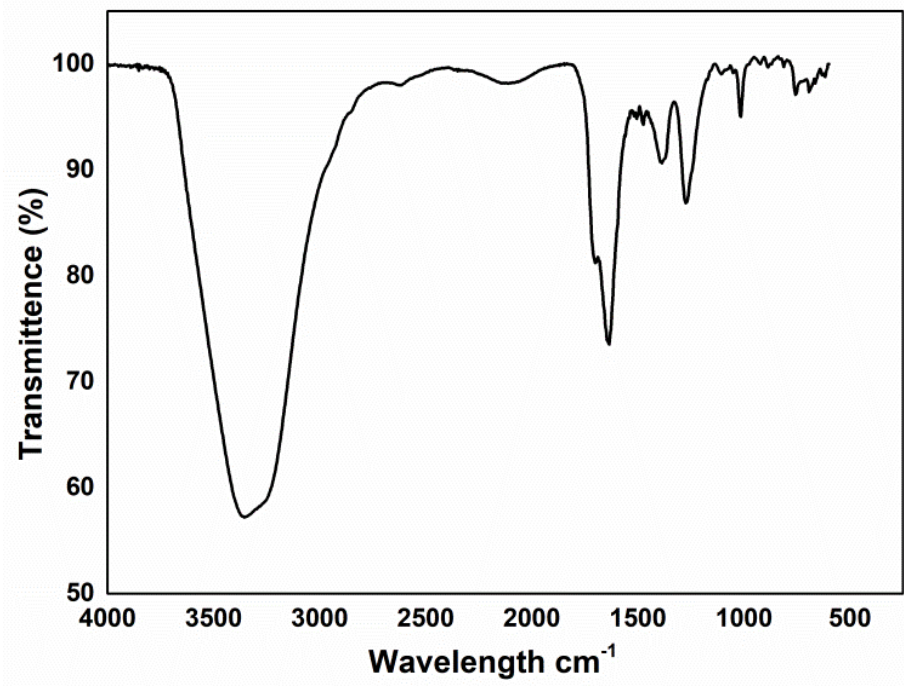


Figure 4. 3 Fourier transform infrared spectra of coconut shell pyrolysis-oil

Table 4.1 Comparative ultimate analysis with different biomass materials

Biomass Type	Carbon (wt.%)	Hydrogen (wt.%)	Nitrogen (wt.%)	Sulfur (wt.%)	Oxygen (wt.%)	H/C ratio	O/C ratio	HHV (MJ/kg)	Reference
Coconut shells	63.45	6.73	0.43	0.17	29.22	1.26	0.35	22.83	(Joardder et al. 2011)
Coconut shells	53.73	6.15	0.86	0.02	39.24	1.36	0.55	20.88	(Kehefez et al. 2010)
Rice husk	50.45	6.58	1.49	0.23	41.25	1.55	0.61	19.91	(Acikgoz et al. 2004)
Coconut shells	59.14	5.47	4.21	0.34	30.84	1.10	0.39	19.75	(Rout et al. 2015)
Wood pellets	55.69	7.93	0.36	-	36.02	1.70	0.49	24.2	(Yang et al. 2014)
Straw pellets	62.57	8.12	1.41	-	27.9	1.55	0.33	28.9	(Yang et al. 2014)
Saw dust	44.8	4.76	0.25		50.19	1.27	0.84	17.62	(Hiloidhari et al. 2014)
Coffee bean	42.56	4.32	0.62		52.5	1.21	0.93	16.68	(Hiloidhari et al. 2014)
Rice straw	39.76	4.51	0.08		55.65	1.35	1.05	16.04	(Hiloidhari et al. 2014)
Coconut shells	46.11	5.9	0.07	0.11	47.95	1.52	0.78	16.75	Present study

Table 4. 2 Fourier transform infrared analysis of CSPO

Wave number (cm ⁻¹)	Assignment	Organic groups
3354	H-bonded O-H stretch (broad strong band)	Alcohol/phenol
1700	C=O stretch (strong)	Ketone or carboxylic acid
1636	C=C stretch (medium)	Alkene
1505	C=C stretch (medium)	Alkene
1474	C=C stretch (medium)	Alkene
1387	C=C stretch (medium)	Aromatic
1273	C-O stretch	Alcohol
1016	C-H bend	Ether
756, 692	C-H bend	Aromatic

4.3.4 Gas chromatography and mass spectroscopy analysis

GC-MS analysis shows the chemical compounds and structural composition of the organic molecules present in the CSPO. The chromatogram of the CSPO is shown in figure 4.4. The compounds were identified by matching the corresponding peak from chromatogram with National Institute of Standards and Technology (NIST) library and were compared with the data reported in the literature. The identified compounds present in the CSPO are represented in the table 4.3 with retention time, peak area percentage and the molecular formula. The obtained CSPO contains various organic groups like esters, acids, alcohols, ketones and other diverse functional groups. The GC-MS analysis contains more than 11 chemical compounds such as 4-hydroxy butanoic acid (4.31 wt.%), phenol (70.81 wt.%), guaiacol (12.06 wt.%), syringol (6.22 wt.%) and others. The obtained CSPO approximately contains >70% of phenolic compounds. This may be due to the decomposition of the lignin content present in the coconut shell (Abnisa et al. 2013; Hasanah et al. 2012). The potential applications of the compounds present in the bio-oil could be utilized like phenols for reagents, plastic and resin industries. Syringol in flavours/fragrances industries, 2-

methoxy-4-methylphenol and 2,6-dimethoxy-4-methylphenol in flavors industries (Sukhbaatar et al. 2009).

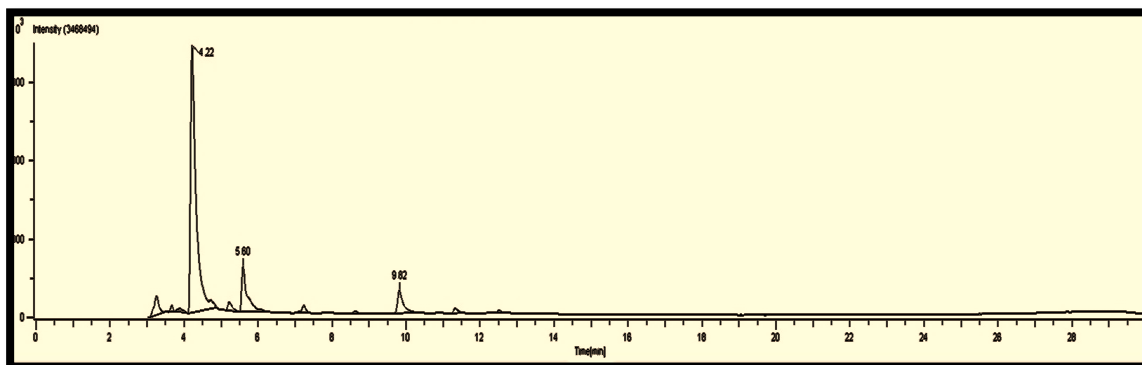


Figure 4.4 Gas chromatography mass spectroscopy spectra of coconut shell pyrolysed oil

Table 4.3 Chemical composition of coconut shell pyrolysed oil

Retention time (min)	Peak area (%)	Molecular formula	Identified compounds
3.26	4.31	C ₄ H ₈ O ₃	Butanoic acid, 4-hydroxy
3.67	0.67	C ₁₀ H ₁₈ O	4-Heptene-3-one,2,5,6-trimethyl-
3.89	0.99	C ₈ H ₁₆ O ₂	1,1-Cyclohexanedimethanol
4.22	70.81	C ₆ H ₆ O	Phenol
5.23	1.81	C ₂₂ H ₂₆ N ₂ O ₆	N-carbobenzyloxy-l-tyrosyl-l-valine
5.6	12.06	C ₇ H ₈ O ₂	Guaiacol
7.23	1.36	C ₈ H ₁₀ O ₂	Cresol
8.62	0.33	C ₉ H ₁₂ O ₂	Phenol, 4-ethyl-2-methoxy-(p-ethylguaiacol)
9.82	6.22	C ₈ H ₁₀ O ₃	Syringol
11.33	1.04	C ₉ H ₁₂ O ₃	1,2,4-Trimethoxybenzene
12.51	0.39	C ₁₀ H ₁₄ OS	Methiocarb-anisole

4.4 CHARACTERIZATION OF BIO-CHAR

The proximate and ultimate analysis are shown in table 4.4, The equations used are shown in Appendix A1.2.2-A1.2.4. It shows that the pyrolysed coconut bio-char contains 88.58 wt.% carbon and has a heating value of 29.56 MJ/kg. These are similar to sub-bituminous coal which has a heating value of 29.05 MJ/kg and a carbon content of at least 73.9%. The biochar obtained with coconut has lower ash and sulfur contents (Yang et al. 2010; Yang et al. 2014 and Rout et al. 2015). When bio-char subjected to electron microscopy scanning at 500x resolution, porous structure is observed which is shown in figure 4.5. The assorted macro pore distribution and rough texture obtained could be applicable for liquid-solid adsorption processes. The formation of pores on the surface of bio-char is mainly due to escape of volatile matter during pyrolysis process. More bio-char pores help in better adsorption for ions and also accommodate space for nutrients and water retention (Nsamba et al. 2015).

Table 4.4 Analysis of coconut shell and bio-char

Ultimate analysis								
Typical Composition	% C	% H	% N	% S	% O	H/C	O/C	HHV (MJ/kg)
Coconut shell	64.23	6.89	0.77	0.50	27.61	1.28	0.32	21.75
Bio-char	88.58	3.11	0.17	0.1	8.04	0.26	0.03	29.56

Typical Composition	Proximate analysis (wt.%)			
	MC	VC	FC	AC
Coconut shell	10.1	75.5	11.2	3.2
Bio-char	3.99	7.35	88.16	0.4

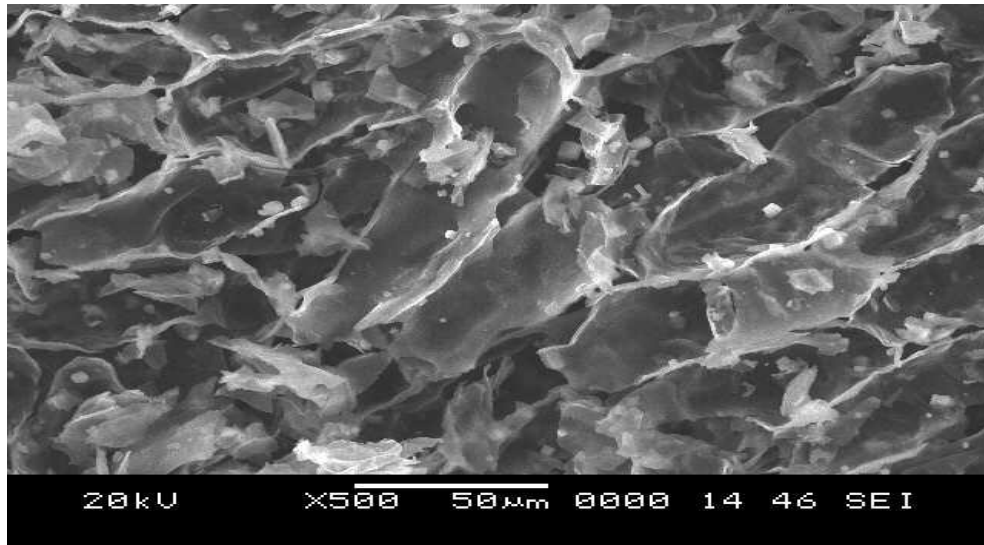


Figure 4.5 Scanning electron micrograph at 500 x magnification of bio-char

4.5 BY-PRODUCTS PER METRIC TON OF COCONUT SHELLS

- | | | |
|--------------------------|---|--|
| 1. a) Bio-char | = | 30% of CS |
| | | b) If transformed to activated carbon ,15% of the total feedstock. |
| 2. Bio-tar | = | 5 to 6% feedstock. |
| 3. Bio-oil | = | 33 to 38%. |
| 4. Non-condensable gases | = | 600 kg total producer gas or
1680 m ³ of gas which can
produce around 2200 units of
power. |

Main composition of the gas includes CH₄, CO, H₂, O₂, CO₂ (little), N₂ (little) and other hydrocarbons. Calorific value of the gas produced will be around 3500 kcal/m³.

Details for ratio of products are estimated through discussion with Vasanth Kumar, 2017 (M/s Vayu Gases, Oils and Carbons Bengaluru- 560091).

Modified Dulong's formula is used to calculate higher heating value based on elemental analysis (Channiwala and Parikh 2002; Tinwala et al. 2015).

$$\text{HHV (MJ/kg)} = (33.5 \times \text{C} + 142.3 \times \text{H} - 15.4 \times \text{O}) \times 0.01.$$

The gas calorific value may be determined by gas chromatography and can be calculated using

$$\text{Calorific value (kcal/m}^3\text{)} = (30 \times \text{CO} + 25.7 \times \text{H}_2 + 85.4 \times \text{CH}_4)$$

Table 4. 5 Cost analysis

1. Production cost

Item	Price	Total cost
Coconut shells (750 kg)	Rs. 8/kg	Rs. 6,000
For 3 labors	Rs. 700/day (wages)	Rs. 2,100
Transportation charges	Rs.1500/day	Rs. 1,500
Miscellaneous charges	Rs. 1,400/day	Rs. 1,400
Production cost per day		Rs. 11,000

2. Revenues

Raw materials	Price	Quantity	Total amount
Pyrolysed bio-oil	Rs. 8/litre	260 litre	Rs. 2,080
Bio-Tar	Rs. 80/litre	40 litre	Rs. 3200
Activated carbon	Rs.70/kg	150 kg	Rs. 10500
Net power available after auxiliary consumption	Rs.5.60/unit	1300 unit	Rs. 7280
Total revenues per day			Rs. 23,060

Note: The pyrolysis product ranges is considered from market survey by Vasanth Kumar, 2017 “Vayu Gases, Oils and Carbons, Bengaluru- 560091” for capacity 750 kg of raw material.

Earnings before interest, taxes, depreciation and amortization (EBIDTA) margin:

$$\text{Total revenues /day} - \text{Production cost /day} = 23,060.00 - 11,000.00 = \text{Rs.12,060 /day.}$$

The calculations for energy generation are as follows.

Total producer gas obtained per day (**750 kg raw material**)

$$= 450 \text{ kg} \times 2.8 \text{ m}^3/\text{kg}$$

$$= 1260 \text{ m}^3 \text{ (after purification of gas with compression for storage)}$$

Total energy content of gas = 1260 x 3500 (considering 3500 kcal/m³ the calorific value of gas)

$$= 44,10,000 \text{ kcal.}$$

For, 1 kWh = ~860 kcal

Considering gas generator efficiency 31%, heat energy required is 2666 kcal/unit, the round of value considered is 2650 kcal/unit energy generation.

Total energy generated per day = 44,10,000 / 2650 = 1664.16 units.

Considering 20% of total energy used for auxiliary consumption gives 332.8 units

Therefore,

Net available electricity to grid = 1664.16 - 332.8 = 1331.36 = ~1330 units.

In general per metric ton of coconut shell can generate 2200 units (kWh) of energy, based on above calculations (Acosta 2018).

Say, if coconut shells are chosen and purchased at a cost of Rs. 8/kg and the total amount for 750 kg will be around Rs. 6000. The plant requires three skilled labours for operation (wages per person Rs. 700/day) and total manpower charges is Rs. 2100 (i.e., 700 x 3) and transportation charges per day may be Rs. 1500 and other miscellaneous includes packing and overhead charges approximately equals Rs. 1400/day. The cost of production per day is around Rs. 11,000/day. To calculate revenue, sensitivity analysis is performed and chosen the best rates accordingly (APPENDIX-A1.1). Sensitivity analysis is a way to predict the outcome of a decision given on the products. It helps in identifying the key variables that are major influence in the cost and benefits. The calculation showed activated carbon Rs. 70/kg; pyrolysed coconut shell oil (Bio-oil) Rs. 8/litre, Bio-Tar Rs. 80/litre and power after captive use

will be Rs. 5.60/unit. The total revenues are around Rs. 23,060/day. The cost and revenue calculations are shown in table 4.5. The EBIDTA margin is the difference of revenue and cost of production which is equal to Rs. 12,060/day.

The main advantage of this pilot plant is, the plant needs less space, less water and can use the raw material available of the season anywhere in India at a very low cost. If 50% of power produced is used for captive use, the remaining 50% can be given to the grid.

CHAPTER 5

FRACTIONATION OF TAR OF COCONUT SHELL PYROLYSIS BY SOLVENT EXTRACTION AND ADSORPTION CHROMATOGRAPHY

In this work, the solvent extraction and column chromatography techniques were followed to separate the coconut shell bio-tar (CSBT) obtained from intermediate pyrolysis of coconut shells at 575 °C. The organic fractions were separated into saturate, aromatic, resin and asphaltene (SARA). Further the SARA products have been characterised by means of Elemental analysis, Fourier transforms infrared technique (FT-IR), and Nuclear magnetic resonance (¹H NMR) spectroscopic analysis.

INTRODUCTION

The negative effect of the thermochemical conversion of biomass is the formation of heavy oil also referred as tar. There is no clear and uniform definition of tar oil, but basically it means the formation of hydrocarbons that can condense in the reactor under operating conditions. The most precise definition is that "tar is a mixture of organic matter produced during the process of thermochemical conversion of biomass". Primary tars, in general the hydrocarbons that are released during pyrolysis, can react with each other to form more developed secondary products with higher molecular weight. Primary tars can also react with the biomass and form char.

5.1 EXPERIMENTAL

Raw material

The coconut shell bio-tar (CSBT) by-product was collected from the pilot plant (Vayu Gases, Oils and Carbons, Bengaluru). Tar by-product obtained from intermediate of pyrolysis of coconut shell, at temperature 575 °C was used as a feedstock. The elemental composition of the CSBT showed the presence of carbon (63.20 wt.%), hydrogen (7.45 wt.%) and nitrogen (0.68 wt.%) and is presented in table 5.1.

Table 5.1 Elemental analysis of coconut shell bio-tar

C (wt. %)	H (wt. %)	N (wt. %)	O* (wt. %)	H/C
63.20	7.45	0.68	28.65	1.4

* Percentage of oxygen was calculated by difference, i.e. [100-(C+H+N)].

5.2 GAS CHROMATOGRAPHY AND MASS SPECTROSCOPY

Gas chromatography and mass spectroscopy analysis shows the chemical compounds and structural compositions of the organic compounds present in the coconut shell bio-tar. The chromatogram of the CSBT is shown in figure 5.1. The compounds were identified by matching the corresponding peak from chromatogram with National Institute of Standards and Technology (NIST) library. The identified compounds present in the CSBT are listed in the table 5.2. with retention time, peak area percentage and the molecular formula. The CSBT obtained contains more than nine chemical compounds such as phenols (~11 wt.%), hydrocarbons (~ 77 wt.%) and other compounds.

Table 5.2 Chemical compounds of coconut shell bio-tar

Retention time (min)	Area wt. %	Chemical compounds	Chemical formula
5.02	3.74	Phenol	C ₆ H ₆ O
6.49	2.00	Phenol, 2-methoxy	C ₇ H ₈ O ₂
8.26	1.78	2-Methoxy-5-methylphenol	C ₈ H ₁₀ O ₂
9.72	2.08	Phenol,4-ethyl, 2-methoxy	C ₉ H ₁₂ O ₂
10.96	2.03	Phenol,2, 6 dimethoxy	C ₈ H ₁₀ O ₃
12.48	0.90	Ethanone, 1-(2,3,4-trihydroxyphenyl)-	C ₈ H ₈ O ₄
29.02	77.26	Tetratetracontane	C ₄₄ H ₉₀
31.22	3.81	Tert-hexadecanethiol	C ₁₆ H ₃₄ S
32.35	4.83	1-nonodecanol	C ₁₉ H ₄₀ O

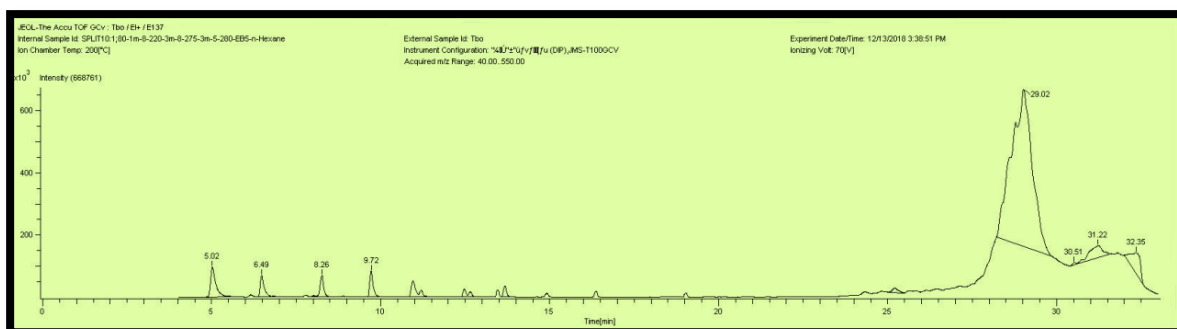


Figure 5.1 Gas chromatography and mass spectroscopy spectra of coconut shell bio-tar

5.3 ISOLATION OF COCONUT SHELL BIO-TAR

Coconut shell bio-tar (CSBT) was isolated into saturate, aromatic, resin and asphaltene. Figure 5.2. shows the clear separation process in the typical schematic pictorial view. Here, 1 g approximately equals 1 ml.

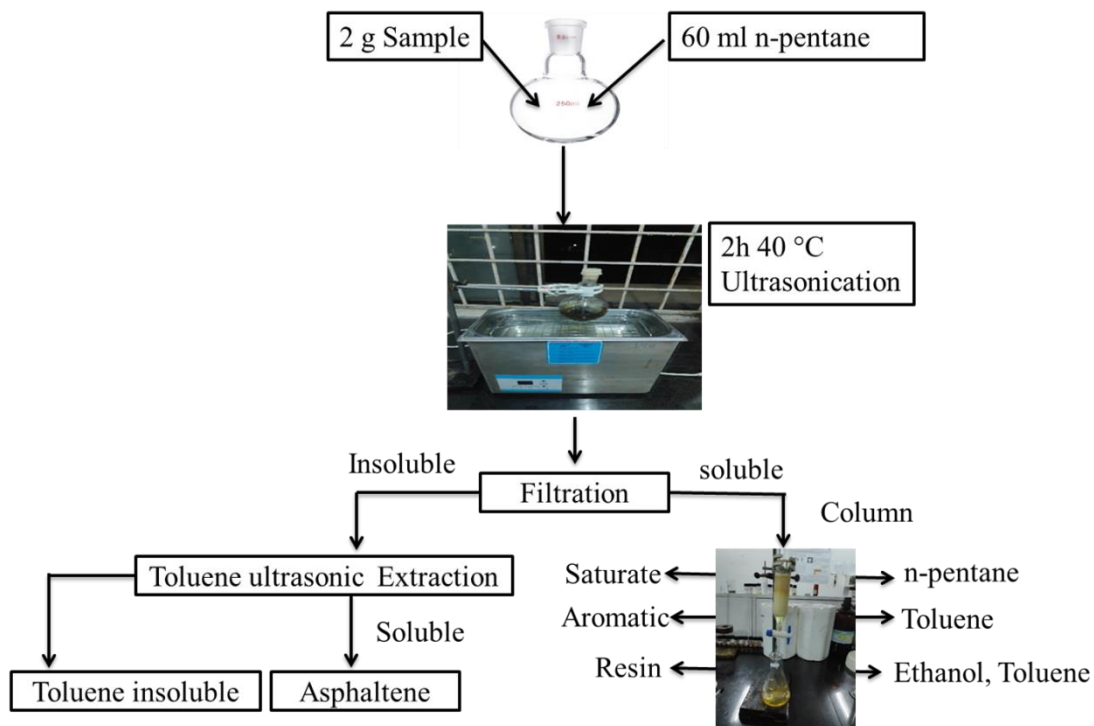


Figure 5.2 Schematic pictorial view of isolation of coconut shell bio-tar

In a 250 ml round bottomed glass pressure vessel, CSBT and n-pentane solvent were added sequentially at volume ratio 1:30. The pressure vessel is sealed and was introduced into ultrasonic bath at temperature 40 °C for 2 h to ensure the maximum content. The vessel was opened and the mixture was cooled and the mixture was filtered through a filter paper (3 µm) to isolate asphaltene. The collected asphaltene fraction was further suspended in hot toluene. Subsequently, the toluene insoluble matter was obtained. The solvent toluene was evaporated under reduced pressure on a rotary evaporator and then the asphaltene fraction was dried in an oven at 80 °C. Consequently, the pentane soluble solution was then separated into SARA fractions followed (Sun and Zhang 2017) as mentioned.

5.4. RESULTS AND DISCUSSIONS

5.4.1 Chemical analysis

The elemental compositions of four fractions saturate, aromatics, resins and asphaltene from CSBT are shown in table 5.3. The results showed that lowest hydrogen content was in asphaltene fraction followed by resin, aromatics and saturate fractions. The H/C ratios confirmed that saturate fractions have higher H/C ratio than other fractions. Asphaltene fraction H/C ratio was lowest. The resin fraction H/C ratio is 1.27 and this almost agrees with asphaltene fraction from many geological origins which show variations between 1.1 and 1.2 confirming low hydrogen content (Rudzinski et al. 2000).

Pictorial view of four fractions from CSBT is shown in figure 5.3. The compositions of the CSBT showed saturate (17.17%), aromatic (18.97%), resin (16.37%), asphaltene (24.77%) and toluene insoluble (1.9%). Overall, 77.28% of starting oil was recovered. The mass loss accounts for the vaporization of saturates and aromatics during evaporation of solvents like pentane and toluene (Aske et al. 2001). Likewise, polar molecules remained absorbed to neutral alumina powder which was not eluted completely.

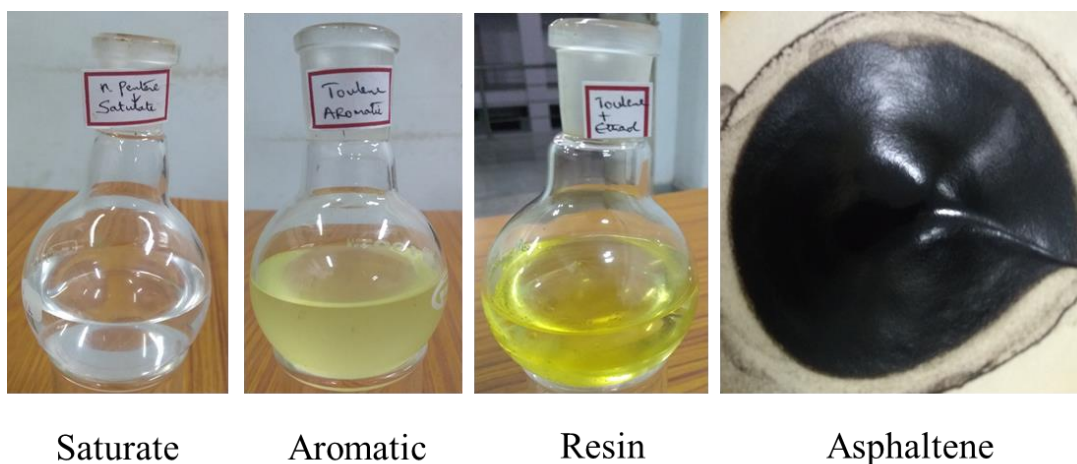


Figure 5.3 Pictorial views of saturate, aromatic, resin and asphaltene fractions of coconut shell bio-tar

Table 5.3 Elemental compositions of SARA fractions from coconut shell bio-tar

Elements	Saturate (wt.%)	Aromatic (wt.%)	Resin (wt.%)	Asphaltene (wt.%)
Carbon	68.75	61.98	68.40	59.11
Hydrogen	8.76	7.01	7.32	5.46
Nitrogen	0.32	0.34	0.55	2.12
Oxygen	22.15	30.65	23.72	33.31
H/C	1.51	1.34	1.27	1.10

Sun and Zhang (2017) followed the same procedure to separate distillation residues of middle-temperature coal tar (DRMCT) and Batiraman heavy crude oil (BHCO) into SARA fractions. The observed weight fractions of DRMCT are shown in table 5.4. The observed weight fractions of BHCO were saturate (19 wt.%), aromatics (26 wt.%), resin (27 wt.%) and asphaltene (28 wt.%). FT-IR analysis determines the functional groups present in four fractions SARA shown in Figure 5.4. Based on FTIR spectrum analysis, the bio-asphalt showed O-H stretching around 3400 cm^{-1} in the FT-IR indicating the presence of phenol and alcohol, C-H stretching groups in uptake IR $2800\text{-}3000\text{ cm}^{-1}$ indicates the presence of aliphatic compound. Bio-asphalt is made from non-petroleum based renewable resources. In this work,

bio-asphalt from bio-oil obtained from coconut shells through intermediate pyrolysis process. Figure 5.5 shows scanning electron microscope (SEM) image there is a porous surface with cavities and spherical particles on the porous surface. Elemental chemical analysis by EDS of structure showed that they consist of a high concentration (68.20 %) of carbon.

Table 5.4 Comparison of yields of different feedstocks with present study

Feedstock	Saturate (wt.%)	Aromatic (wt.%)	Resin (wt.%)	Asphaltene (wt.%)	References
DRMCT	22.5	24.3	26.5	16.9	(Akmaz et al. 2011)
BHCO	19	26	27	28	(Sun and Zhang 2017)
CSBT	17.17	18.97	16.37	24.77	Present study

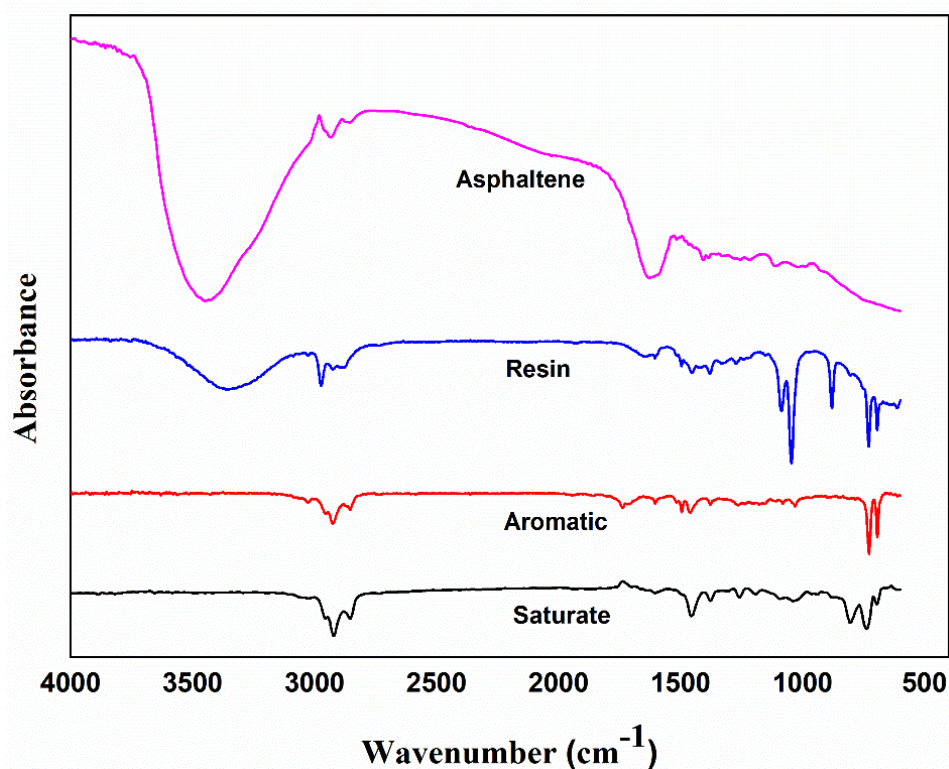


Figure 5.4 Overview of fourier transform infrared spectra of four fractions

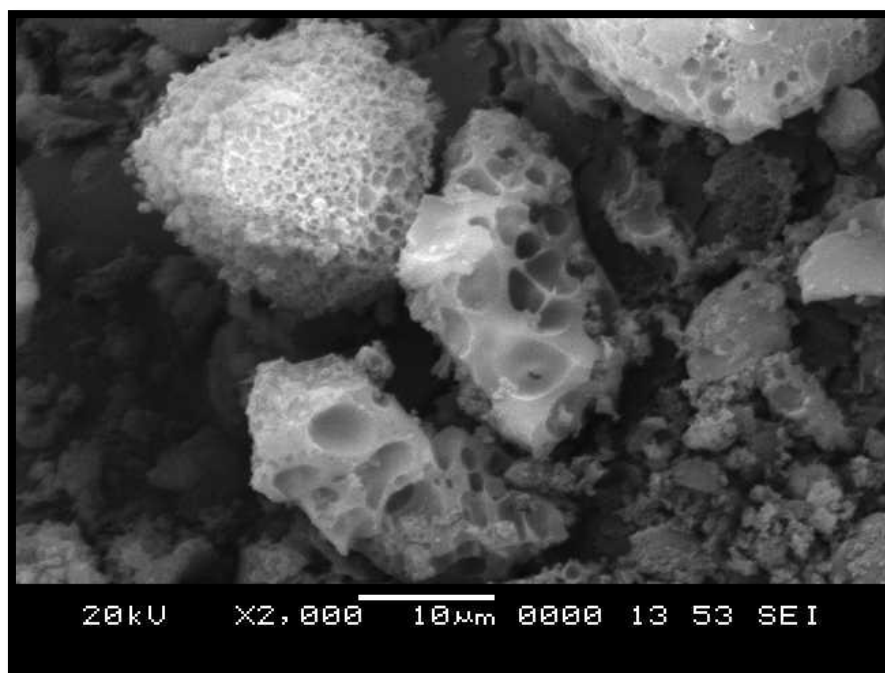


Figure 5.5 Microscopic image of bio-asphalt

5.4.2 Nuclear magnetic resonance (NMR) analysis

In ^1H NMR the four fractions had oxygenated hydrocarbons, such as long chain alcohols, ethers and the resin are kind of a phenolic resin as hydrocarbons were connected because of aromatic regions and it seems to be a complicated mixture. The saturate fraction is hydrocarbon based. In toluene fraction, there were no phenolics found but only some oxygenated compounds showing peaks around 3.5-4.5 ppm in the ^1H NMR and hydrocarbon peak 1-2 ppm was found. From previous studies (Alcaniz-Monge et al. 2011), the distribution of the different H_2 atoms of the SARA fractions is shown in Table 5.5. The saturated fraction contains no amount of aromatic hydrogen. In addition, the total number of hydrogen atoms in the β -position in the saturated fraction is high, approximately 58.55 % (1.5-1 ppm), which shows large quantity of H_2 in the β -position, relative to the aromatic ring, is present in the form of $-\text{CH}_2$ and $-\text{CH}-$ to methyl (Rudzinski et al. 2000) (Rudzinski et al. 2000). The total hydrogen atoms in α -position represent the degree of branching of the aromatic ring in the following order: saturated <aromatic <resin <asphaltene. The minimum value of the saturated fraction is 0.05 % (4.5-1.5 ppm), which may be due to deficient in aromatic structure. In addition, saturated fraction has the highest number of H_2 (39.74

%) around 1.0-0.5 ppm. However, asphaltene fraction has minimum, at 7.1%. By combining the highest value of H₂ in asphaltene of 27.53%, it can be deduced that the methyl group is the main alkyl side chain in the asphaltene. The proton NMR spectra of four fractions are shown in figure 5.6 - 5.9 and the percentages of hydrogen are tabulated (table 5.5)

Table 5.5 Functional group distribution from ¹H NMR spectral integration of four fractions using Chemical shift region (ppm)

Chemical shift region (ppm)	Dominant type of Hydrogen	Percentage of Hydrogen			
		Saturate	Aromatic	Resin	Asphaltene
10 - 6.5	Aromatic hydrogen	-	-	42.13	27.53
4.5 - 3.5	Hydroxyl groups	-	6.0	20.68	32.78
3.0 - 2.0	CH ₃ CH ₂ and CH α to an aromatic ring	-	8.5	22.03	32.51
2.0 - 1.6	CH ₂ and CH β to an aromatic ring	59.12	15.96	-	7.1
1.6 - 0.5	β -CH ₃ , CH ₂ and CH γ to an aromatic ring	40.87	69.36	14.8	-

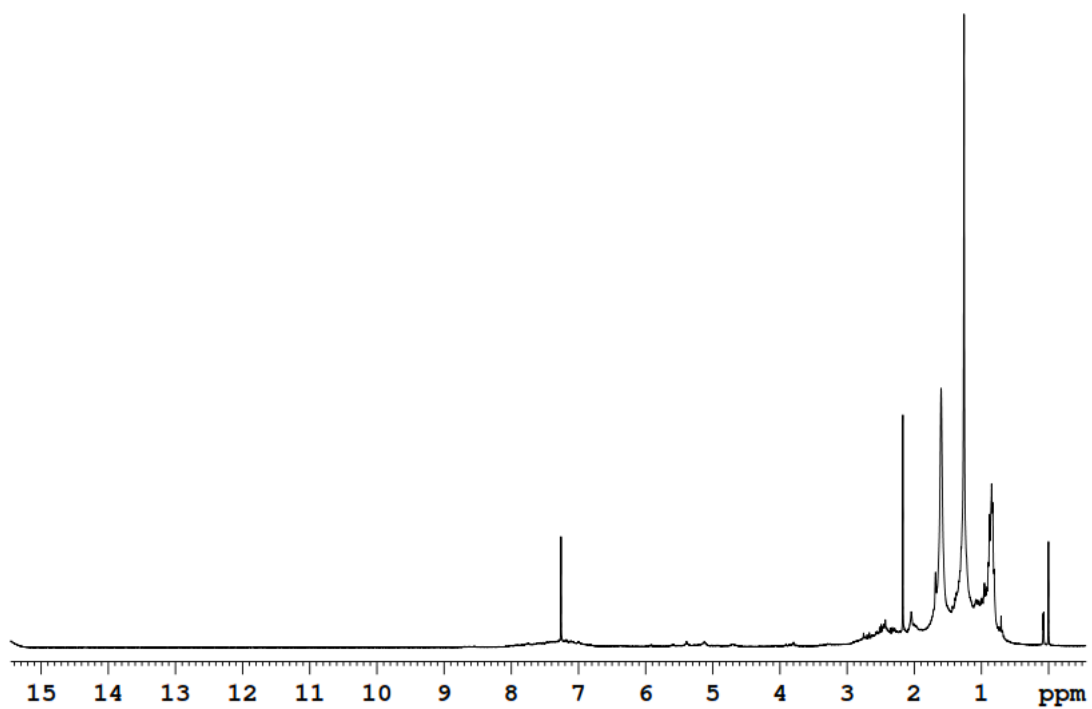


Figure 5.6 ^1H Nuclear magnetic resonance of saturate fraction

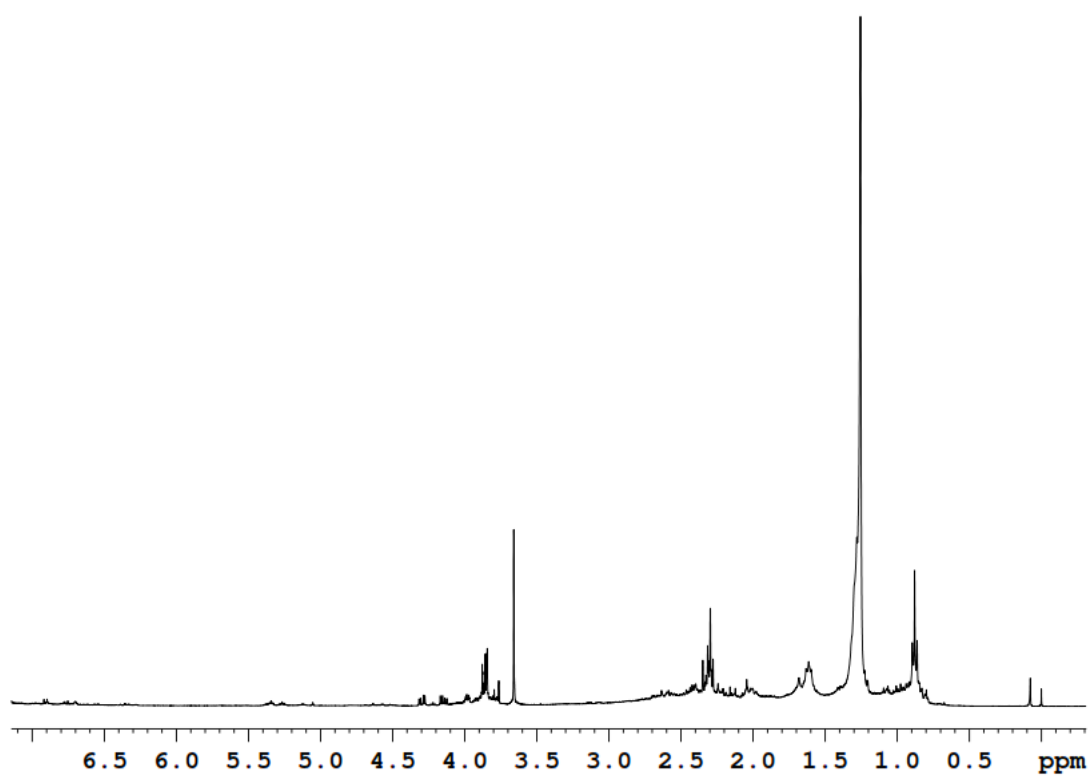


Figure 5.7 ^1H Nuclear magnetic resonance of aromatic fraction

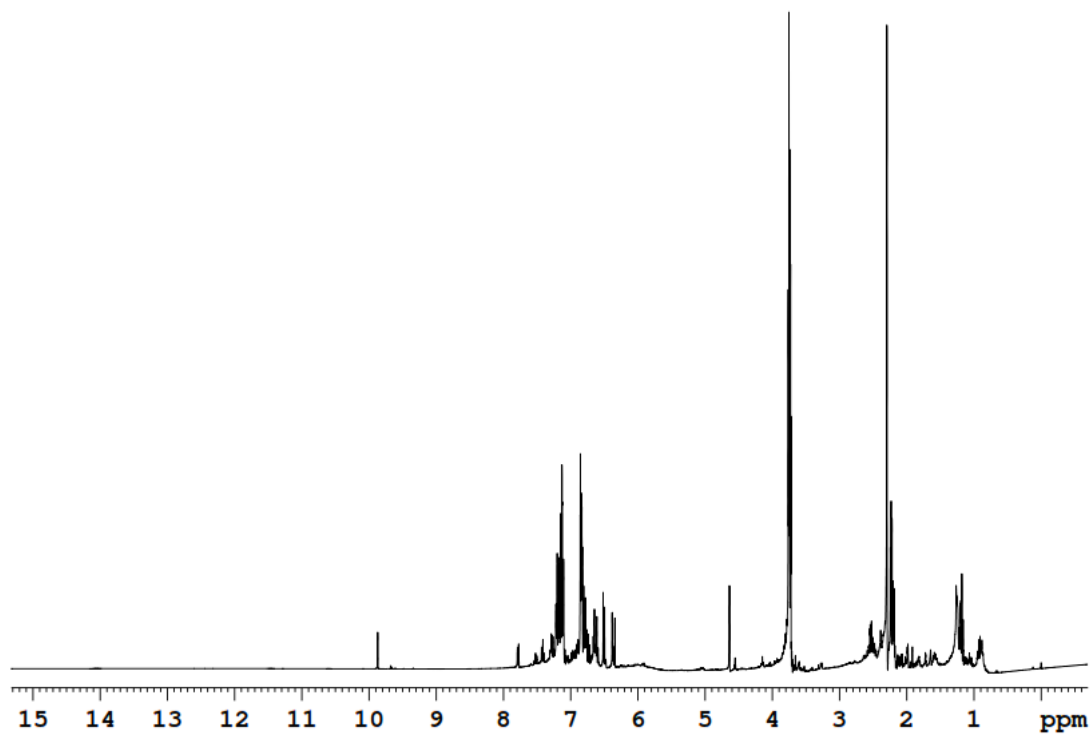


Figure 5.8 ^1H Nuclear magnetic resonance of resin fraction

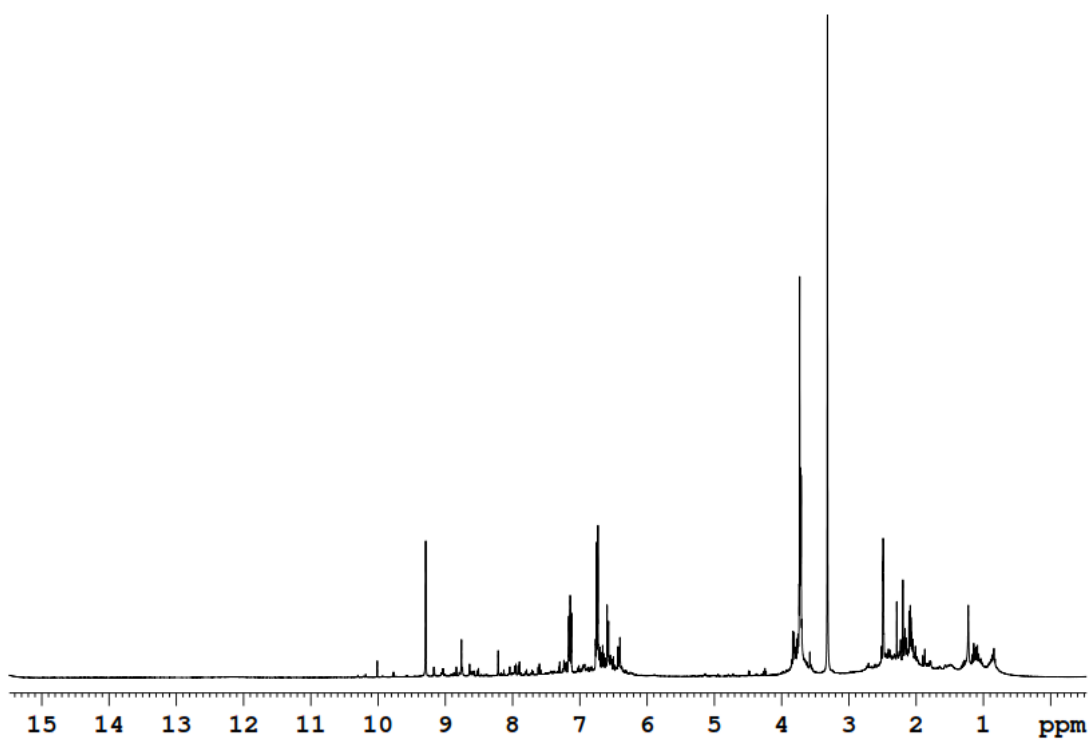


Figure 5.9 ^1H Nuclear magnetic resonance of asphaltene fraction

CHAPTER 6

UPGRADING OF COCONUT SHELL-DERIVED PYROLYTIC BIO-OIL BY THERMAL AND CATALYTIC HYDRO- DEOXYGENATION

In this chapter the coconut shell pyrolysed oil was upgraded using high pressure reactor at different temperatures using ruthenium on activated carbon (Ru-C) and palladium on activated carbon (Pd-C) catalysts with hydrogen gas at 30 bar for 3 h of reaction time and discussed the effects of reaction temperature.

INTRODUCTION

Increasing use of fossil fuels has led to economic recession and environmental depletion. To meet this challenge, much research has been conducted on biofuel production around the world. This indicates that the next generation will reduce dependence on transportation fuels and minimize pollution. Biomass is a carbon-rich renewable resource and environmentally friendly. The liquid product obtained by the thermochemical conversion of biomass is commonly referred to as bio-oil. As a renewable energy source, bio-oil has little carbon dioxide neutrality and therefore contributes little to greenhouse gas emissions (Baratieri et al. 2008; Zheng et al. 2008). Bio-oil is a brown liquid product. Bio-oil is usually formed by thermal depolymerisation and cracking of cellulose, hemicellulose and lignin in the absence of oxygen. The upgrading of bio-oil has been a hotspot due to its contribution to the application of bio-oil (Zhang et al. 2013).

The chemical composition of bio-oil depends on the feedstock, reaction parameters during the pyrolytic liquefaction, and the storage conditions. The pyrolytic liquid, also known as bio-oil, is a complex mixture composed of more than 400 compounds including carboxylic acids, aldehydes, esters, acetals, hemiacetals, alcohols, olefins, aromatics, phenolics, nitrogen- and sulfur-containing heterocycles. Crude bio-oil generally has low heating value, high oxygen content, high viscosity, poor thermal oxidative and storage stability. Due to the deterioration of thermo-

physical properties aforementioned, bio-oils cannot be used directly as a fuel prior upgrading (Dielbold et al. 1999; Branca et al. 2003).

Hydrogen-based processes are generally more expensive than thermal cracking, but they have the advantage of having a higher selectivity for liquid products by reducing the formation of light gases and coke. Catalytic hydrogenation, hydrodeoxygenation (HDO), catalytic cracking, emulsification, and steam reforming are some of the approaches employed to upgrade bio-oil. Among them, HDO has attracted much interest as it effectively lowers the oxygen content without extensive C-C bond breakage and works under relatively less-demanding condition.

Depending on polarity, the solvents are divided into polar aprotic (water, ethanol and methanol), dipolar aprotic (1,4-dioxane and acetone) and non-polar (benzene, toluene, and cyclohexane) solvents. Ethanol is most often used because it can reach a supercritical point at a lower temperature and pressure when compared other solvents. It also dissolves substances that are normally insoluble in the liquid or gas phase. The price of ethanol has been declining due to increased production through biomass fermentation. Ethanol is less harmful than methanol and easier to handle than butanol. Although methanol is also used in the transesterification of bio-oil due to its short chain, its toxicity is a disadvantage over ethanol (Lin and Tanaka 2006; Demirbas et al. 2007 and Demirbas et al. 2009). The supercritical reaction with a polar aprotic solvent is used for biomass pyrolysis of HDO, because supercritical reaction not only increases heat transfer, but also produces high density, low viscosity and high diffusion coefficient reactants and solvents in the system (Zhang et al. 2015; Sharifzadeh et al. 2015). Figure 6.1 shows the path followed for the upgradation of the CSPO.

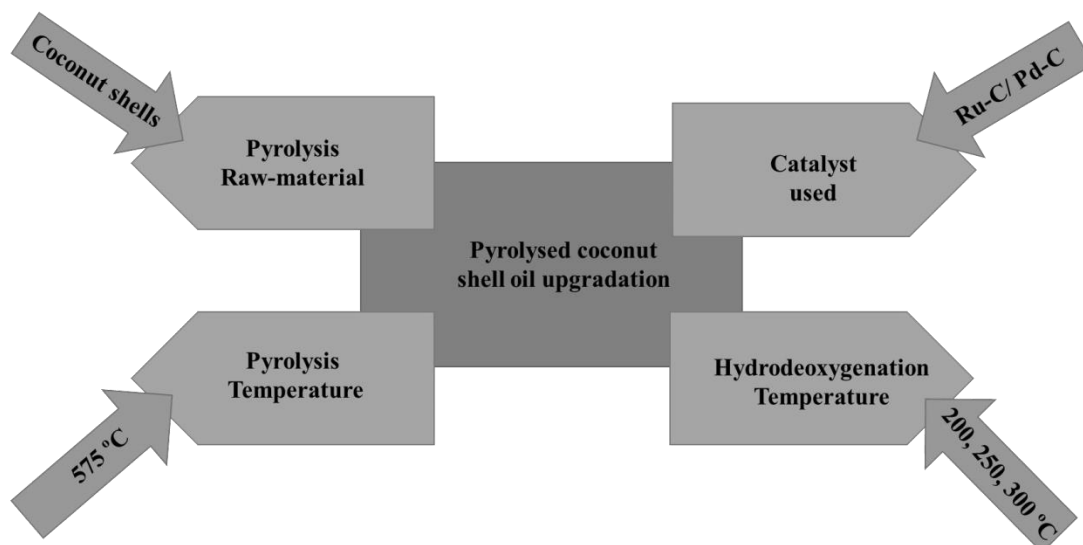


Figure 6.1 Pyrolysed coconut shell oil upgraded tested conditions

6.1 MATERIALS AND METHODS

Crude coconut shell pyrolysis oil (cr-CSPO) was used as the feedstock. The higher heating value of the cr-CSPO was 16.46 MJ/kg (dry basis). Palladium on activated carbon (5 wt.% Pd-C) was purchased from Otto Chemie Pvt. Ltd., and the heterogeneous catalyst was used without any pre-treatment. Absolute Ethanol and Acetone (99%) were purchased from Loba Chemie Pvt. Ltd., and used as received. The elemental analyser was used to determine the composition of the CSPO. The elemental analysis determines the percentage of carbon, hydrogen, and nitrogen. The oxygen was calculated by the difference. The presence of the different compounds present in the CSPO is identified by FT-IR. The spectra of the CSPO were identified in the range of 4000-400 cm^{-1} . To find the chemical composition of the CSPO GC-HRMS was performed. Modified Dulong's formula is used to calculate higher heating value (HHV) based on elemental analysis.

$$\text{HHV} = (33.5 \times \text{C} + 142.3 \times \text{H} - 15.4 \times \text{O}) \times 0.01 \text{ MJ/kg.}$$

6.2 PYROLYSIS OF CSPO

Coconut shell pyrolysed oil (CSPO) was used in this work, obtained by intermediate pyrolysis of coconut shell at 575 °C, in an electrically heated fixed bed batch reactor. The bio-oil is dark brown. CHN analysis of CSPO showed 46.11 wt.% carbon, 5.90 wt.% hydrogen, 0.07 wt.% nitrogen, and 47.95 wt.% oxygen (on dry basis). The approximate molecular formula, based on the experimentally found elemental composition, was $\text{CH}_{1.53}\text{O}_{0.78}\text{N}_{0.001}$.

6.3 REACTION CONDITIONS FOR THERMAL AND CATALYTIC UPGRADING

A Hastelloy-made autoclave (500 ml) fitted with a magnetically-driven gas-inducing impeller was used in this work (figure 6.2). The reactor can withstand a maximum pressure of 20 MPa at 300 °C. A three-blade impeller was used for stirring the content of the reactor. The temperature of the reactor was controlled by the electrically-heated heating mantle with a thermocouple sensor. The reactor was controlled by a control panel.

6.3.1 Experimental procedure

The reactor was loaded with cr-CSPO (2.00 g), 10 wt.% of 5%Pd-C (0.2 g) catalyst, and 50 ml of anhydrous ethanol as a diluent. The reactor was sealed, purged with nitrogen gas three times followed by high purity hydrogen gas. The pressure of hydrogen gas was adjusted to 3 MPa at room temperature. Subsequently, the reactor was heated to 250 °C at a heating rate of 10 °C/min. The temperature was maintained at 250 °C for 3 h with a stirring speed of 350 rpm. After completion of the reaction, the reactor was cooled to ambient temperature. The liquid sample was filtered through a filter paper, and the recovered catalyst was washed with fresh ethanol (2 x 10 ml). No phase separation of the liquid was observed. Ethanol from the liquid product was removed in a rotary evaporator under reduced pressure. The elemental analysis was carried out of the remaining liquid.

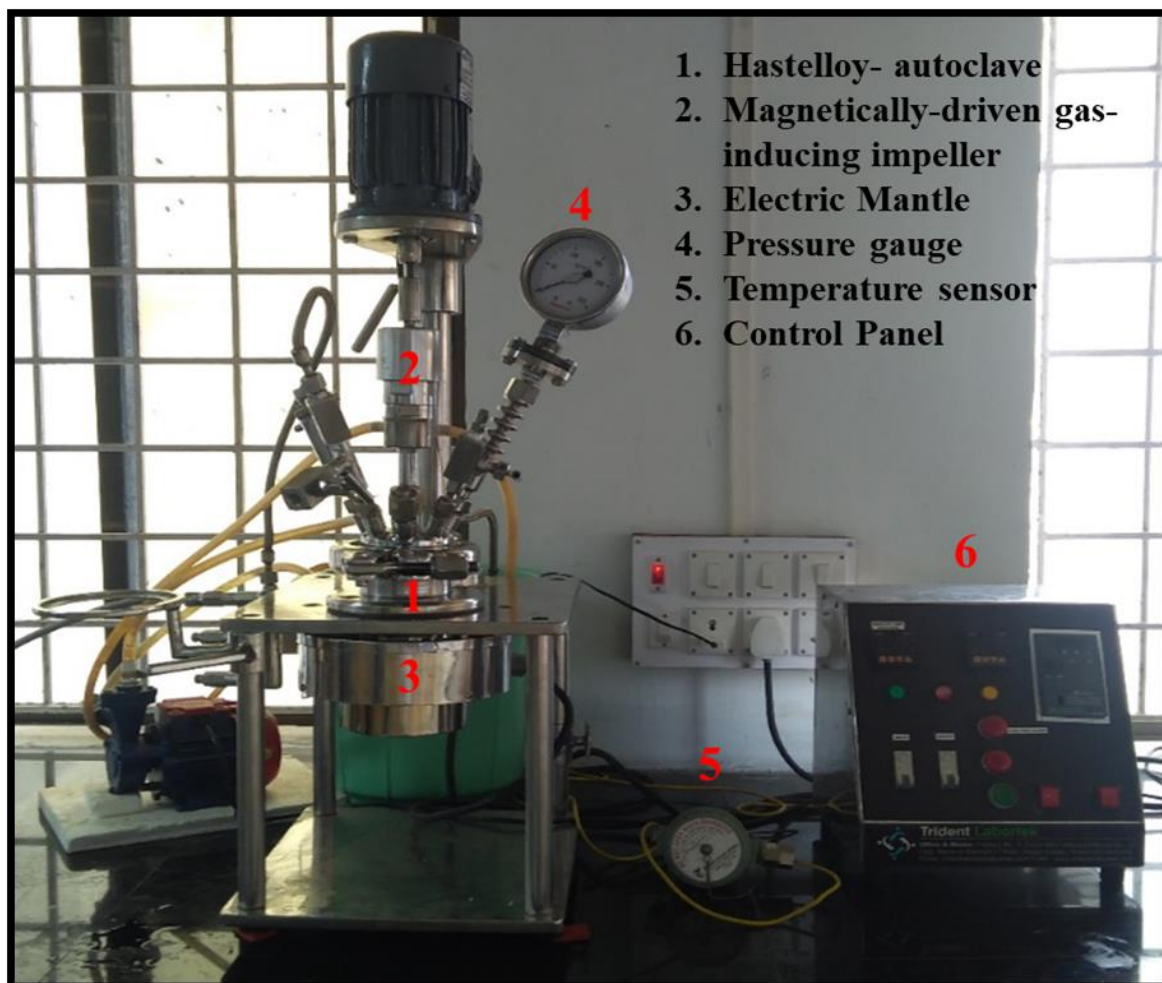


Figure 6.2 High-pressure reactor

6.4 RESULTS AND DISCUSSIONS

6.4.1 Characterization of cr-CSPO, th-CSPO, and ca-CSPO

All the oil samples were characterized by Gas chromatography and mass spectroscopy (GC-MS), Elemental analysis, Fourier transform infrared spectroscopy (FT-IR), and Thermogravimetric (TGA) analysis.

6.4.2 Elemental analysis

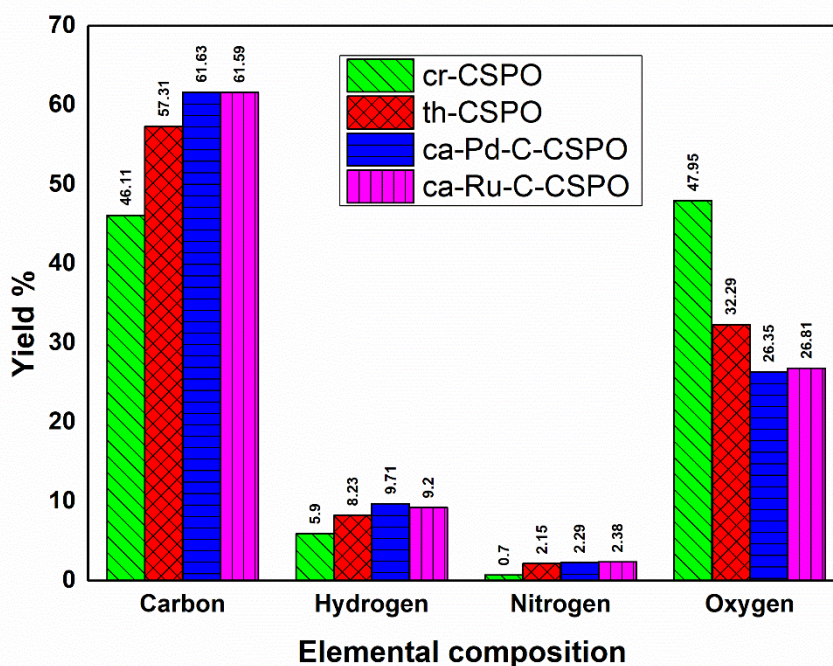


Figure 6.3 Elemental analysis of cr-CSPO, th-CSPO ca-Pd-C-CSPO and ca-Ru-C-CSPO at 250 °C.

Elemental analysis of the crude CSPO (cr-CSPO), thermally upgraded CSPO (th-CSPO) and catalytically upgraded CSPO (ca-CSPO) were carried out to compare and analyse the chemical composition of the three liquid samples. Figure 6.3 shows the elemental analysis of the crude and upgraded (250 °C) pyrolysis oil samples. Whereas the carbon content in the cr-CSPO is only 46.11%, the same in th-CSPO increased to 57.31%. The catalytically upgraded oil ca-CSPO was found to have the carbon content of 61.63%. On the other hand, the oxygen content declined from 47.95% in cr-CSPO to 32.29% in th-CSPO and 26.35% in ca-CSPO. Therefore, the oxygen to carbon ratio decreased from 0.78 in cr-CSPO to only 0.32 in ca-CSPO. The hydrogen to carbon ratio improved from 1.5 in cr-CSPO to 1.8 in ca-CSPO. The above parameters indicate selective oxygen removal in both thermal and catalytic treatments of cr-CSPO, but the catalytic HDO is superior to the thermal route. When compared with petroleum fuels (41-43 MJ/kg) (Lu et al. 2009), the HHV 16.46 MJ/kg of the crude bio-oil is very low. By reducing the oxygen content, the HHV of ca-Ru-C-CSPO and ca-Pd-C-CSPO increased to 29.6 and 30.41 MJ/kg during the HDO process respectively.

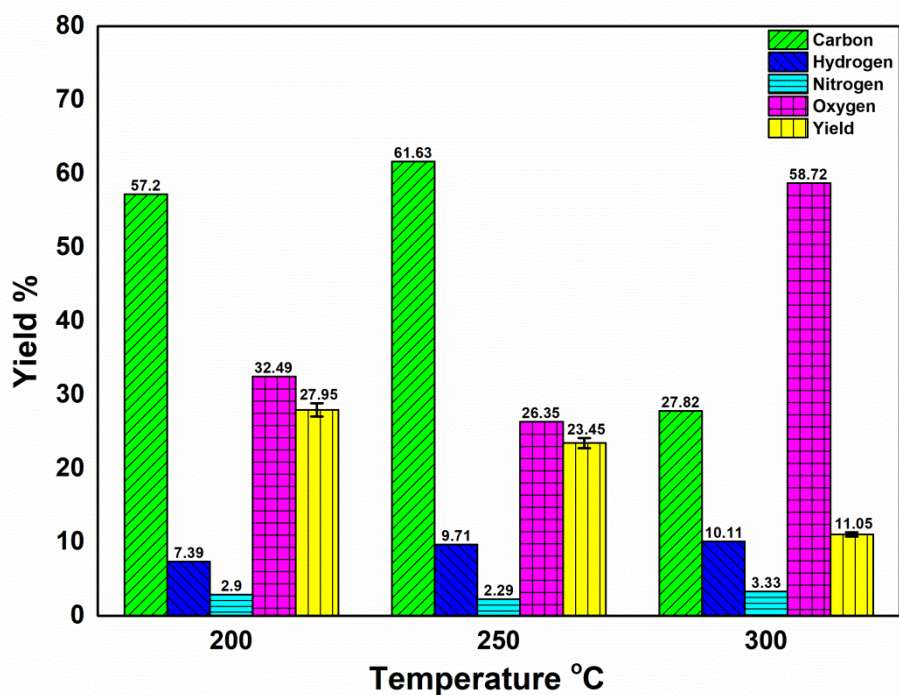


Figure 6.4 Elemental analysis and yield of ca-Pd-C-CSPO at various reaction temperatures.

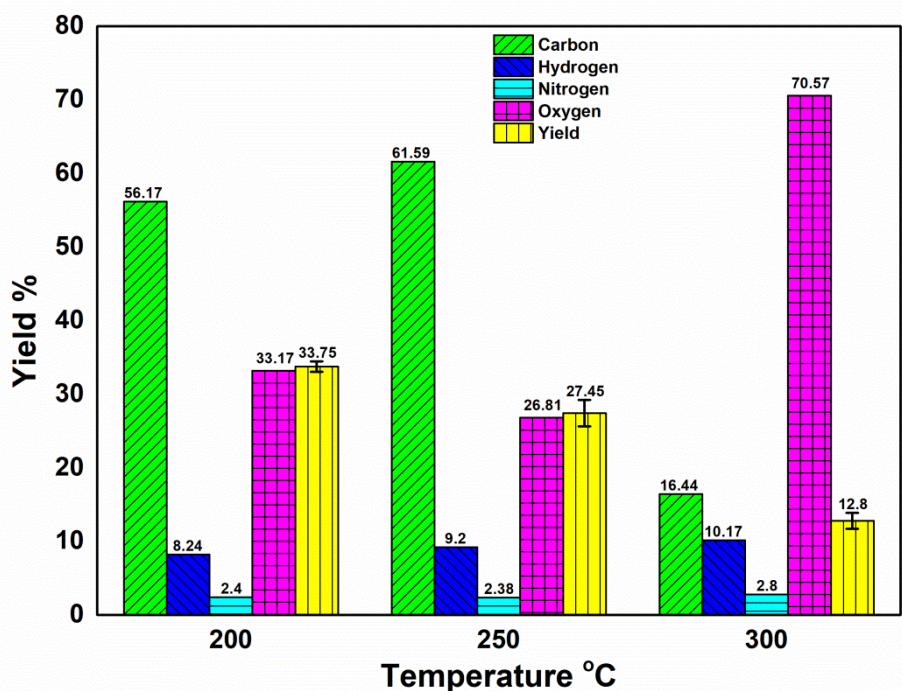


Figure 6.5 Elemental analysis and yield of ca-Ru-C-CSPO at various reaction temperatures.

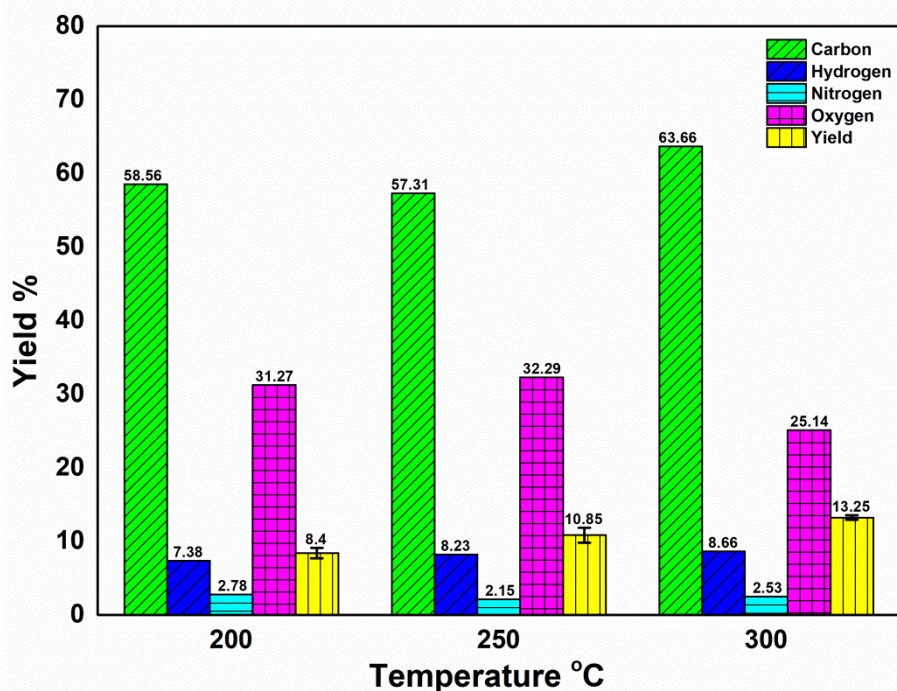


Figure 6.6 Elemental analysis and yield of thermally upgraded CSPO at various reaction temperatures.

Shafaghat et al. (2019) in his work identified that, the carbon content increased to 70.80% and oxygen reduced to 40.10%. The HHV of pyrolysis oil improved (12.61 to 24.72 MJ/kg) by hydrodeoxygenation using nickel catalysts. In addition to ethanol, methanol, and 2-propanol have also been used as organic solvents in HDO bio-oil. When methanol or ethanol (primary alcohol) is used as the solvent, the degree of deoxygenation and higher heating value of the upgraded bio-oil are significantly increased.

The effect of reaction temperature on the catalytic HDO of ca-Ru-C-CSPO and ca-Pd-C-CSPO was further studied. Reaction temperature significantly influenced the elemental properties of the upgraded oil. Figures 6.4, 6.5 and 6.6 shows the elemental analysis and yields of ca-Ru-C-CSPO, ca-Pd-C-CSPO and th-CSPO at various temperatures 200, 250 and 300 °C. At a lower temperature (i.e., 200 °C), the carbon content was improved to 56.17%, in ca-Ru-C-CSPO and 57.2% in ca-Pd-C-CSPO. The carbon content steadily improved up to 61.59% and 61.63% at 250 °C. However, at 300 °C, extensive carbon-carbon bond scission started to happen, and the fuel quality (yield) of liquid product worsened. Gaseous products including CO, CO₂,

and CH₄ form with mass yield approximately 5% of dry lignin (Caballero et al. 1996; Sanna et al. 2015; Alda-Onggar et al. 2019; Ferdous et al. 2002). The increase of reaction temperature from 200-250 °C, the yield of upgraded oil decreased but it was beneficial in improving the elemental properties. Further increasing the reaction temperature from 250-300 °C the yield of the upgraded oil drastically decreased due to the carbon loss and gas formation. Because of the high pressure in the reactor caused by the large amount of gas (methane and carbon dioxide) formation at 300 °C and above, the gasification reactions become important (Elliot and Hart 2009).

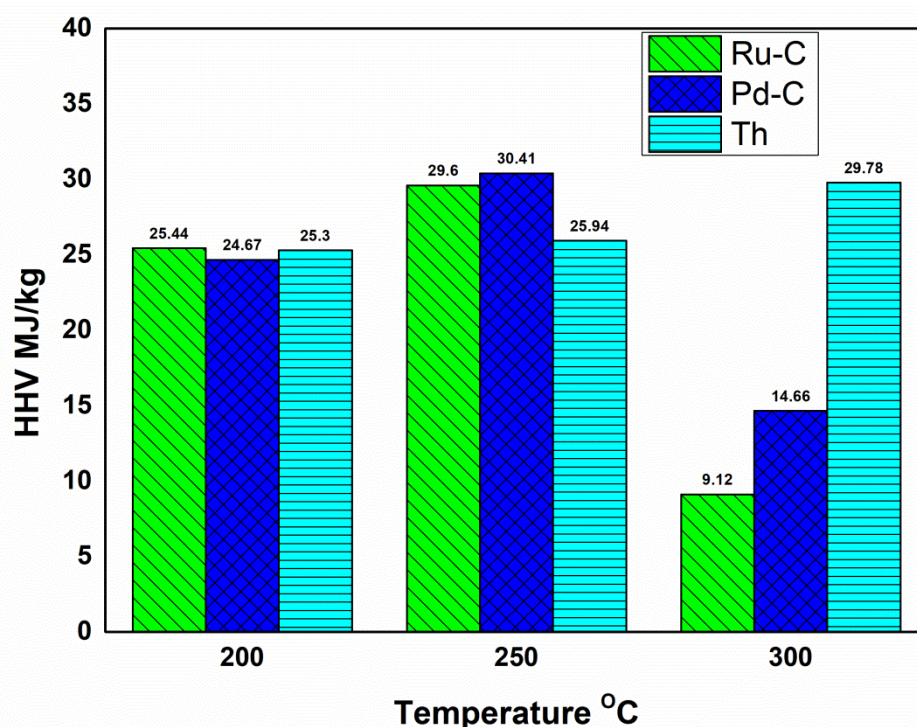


Figure 6.7 Higher heating value of ca-Ru-C, ca-Pd-C and th-CSPO at 200 250 and 300 °C.

When cr-CSPO was treated thermally in the absence of the palladium catalyst, the fuel properties of the upgraded th-CSPO also improved but lower than the catalytically upgraded ca-CSPO. Thermal treatment at 200 °C itself improved the carbon content significantly from 46.11% to 58.56%. Increasing the temperature to 300 °C further improved the carbon content to 63.66%. The hydrogen content also improved from 7.38% at 200 °C to 8.66% at 300 °C, whereas the oxygen content decreased from 31.27 % at 200 °C to 25.14 % at 300 °C. Figure 6.7 represents the

higher heating value with increasing temperatures and figure 6.8 shows the yield value with increasing temperatures.

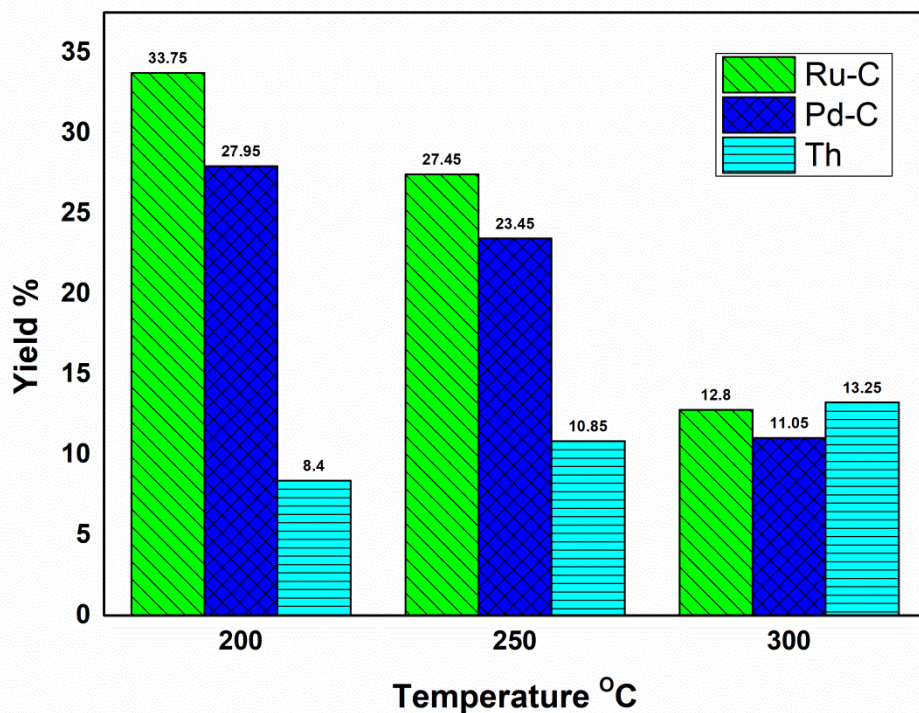


Figure 6.8 Yields of ca-Ru-C, ca-Pd-C and th-CSPO at 200, 250 and 300 °C.

6.4.3 Analysis by fourier transform infrared spectroscopy (FT-IR)

The FTIR spectrum of cr-CSPO is presented in Figure 6.9. The FTIR shows an overwhelming amount of water, phenolic compounds, and carboxylic acids. The O-H stretching vibration between 3200-3600 cm^{-1} of Cr-CSPO indicates the presence of water and phenols. Whereas C=O stretching vibration of 1720 cm^{-1} from a ketone or carboxylic acid. Similarly, the 1600 cm^{-1} and 1380 cm^{-1} indicates the presence of aromatics. The bands at 1270 cm^{-1} with C-O stretching indicates the presence of the alcohol group.

After thermal and catalytic treatment of cr-CSPO, the FTIR spectra of the corresponding upgraded oils appear to be much hydrophobic in nature with minimal or no water in them. The characteristic peaks for various functional groups present in the constituent molecules of the upgraded oil samples were clearly visible (Figure

6.10). The broad peak at 3200-3600 cm^{-1} is still present but of significantly less intensity. The peak corresponds to hydrogen-bonded phenolic $-\text{OH}$ groups. The small peak slightly above 3000 cm^{-1} corresponds to $\text{Csp}^2\text{-H}$ stretching vibration from olefinic and aromatic compounds. The peaks slightly below 3000 cm^{-1} correspond to $\text{Csp}^3\text{-H}$ stretching vibration from aliphatic compounds or aliphatic side chain attached to aromatic compounds. The strong peak at 1620 cm^{-1} corresponds to the $\text{C}=\text{O}$ stretching frequency of various carbonyl functionalities such as ketone, carboxylic acid, and ester in the upgraded oil samples (i.e., th-CSPO and ca-CSPO). The strong peaks around 1050-1200 cm^{-1} range correspond to the C-O stretching in the ethers (aliphatic and phenolic), esters, as well as phenols. Peaks around 750-600 cm^{-1} correspond to various C-H bending vibrations. The major peaks in the FTIR spectra are given in table 6.1.

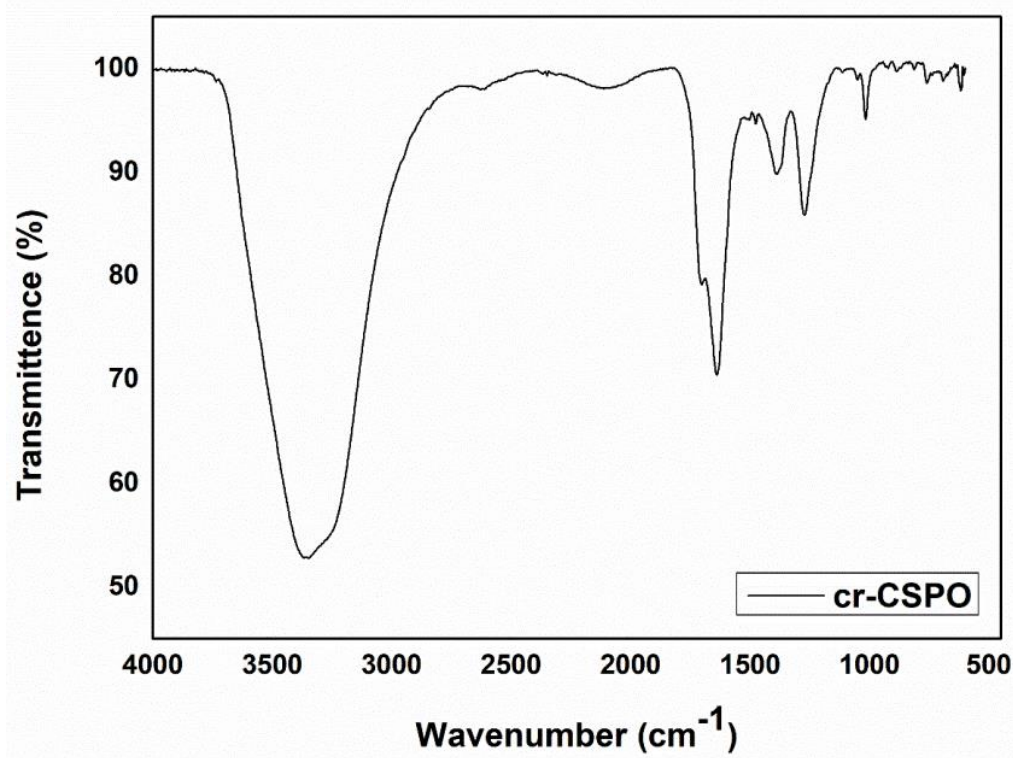


Figure 6.9 FTIR spectrum of cr-CSPO.

Table 6.1 Frequencies of bond vibrations in the FTIR spectra of th-CSPO and ca-CSPO

Wave number (cm⁻¹)	Type of vibration	Functional group
3377	H-bonded O-H stretch (strong, broad band)	Alcohol/phenol
3100	Aromatic and olefinic C-H stretching	Olefins, Aromatic
2950	Aliphatic C-H stretching	Aliphatic compounds
1720	C=O stretch (strong)	Ketone or carboxylic acid
1605	C=C stretch (medium)	Aromatic
1472	C=C stretch (medium)	Aromatic
1372	C=C stretch (medium)	Aromatic
1262	C-O stretch	Phenols
1035	C-O stretch	Aliphatic ether
754	C-H bend	Aromatic
692	C-H bend	Aromatic

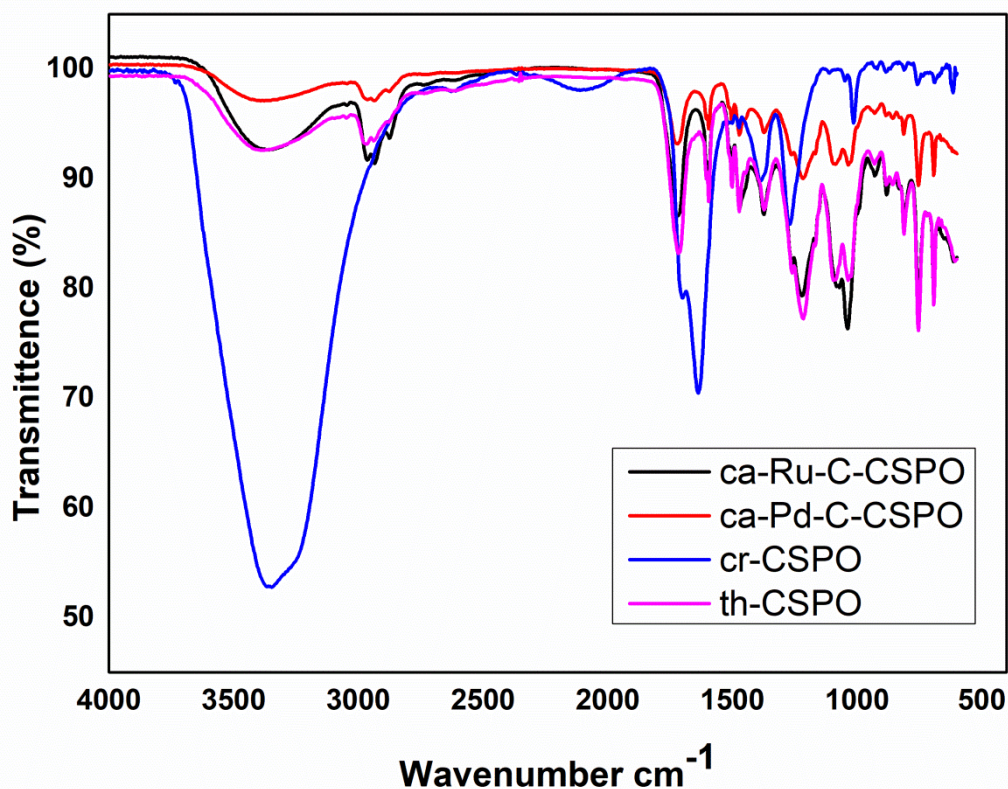


Figure 6.10 Overlaid FTIR spectra of cr-CSPO, th-CSPO, ca-Ru-C-CSPO and ca-Pd-C-CSPO

6.4.4 Thermo gravimetric analysis (TGA)

The thermal behaviour of cr-CSPO, th-CSPO, and ca-CSPO were studied by TGA (figure 6.11). The TGA graph of cr-CSPO showed an overwhelming drop in the mass below 100 °C that supports the FTIR data of having a significant amount of water in the cr-CSPO.

The TGA data of th-CSPO showed noticeably improved thermal behaviour. There was less mass loss below 100 °C compared to cr-CSPO. There is a second mass loss between 100-250 °C due to evaporation of volatiles. The ca-Pd-C-CSPO and ca-Ru-C-CSPO showed much improved thermal behaviour with only marginal mass loss below 100 °C. The mass loss is significant in the range of 100-250 °C due to the evaporation of volatiles. The mass loss above 250 °C is minimal.

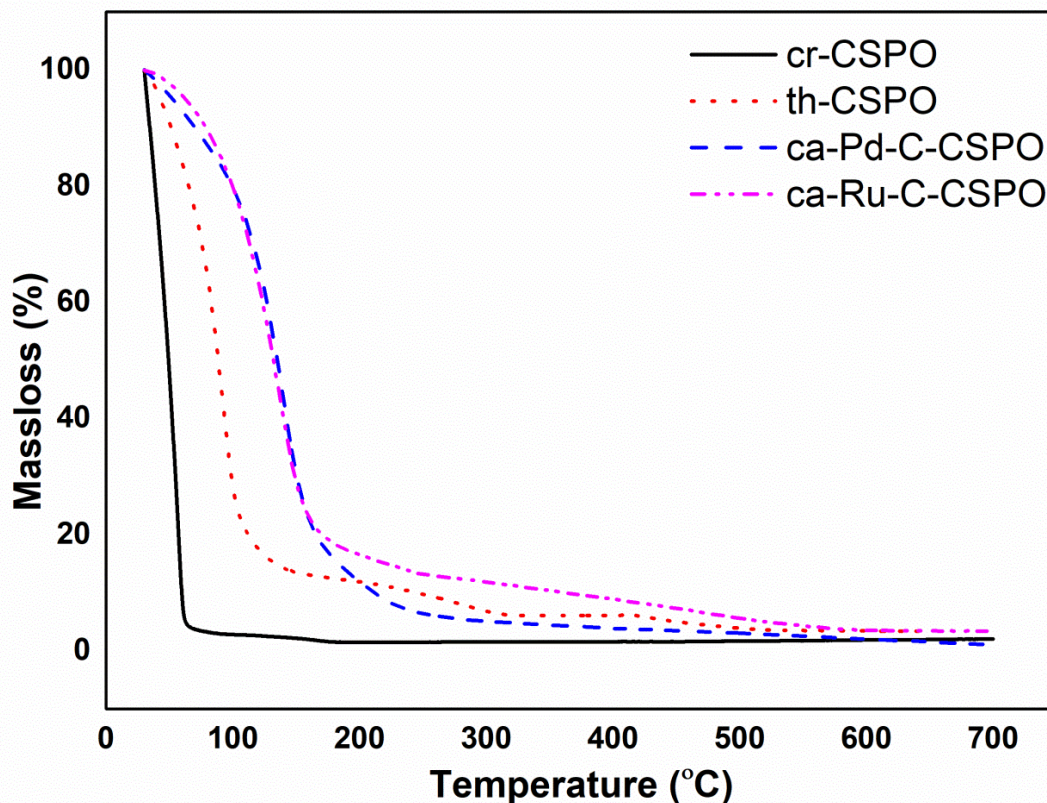


Figure 6.11 Overlaid TGA graph of cr-CSPO, th-CSPO, and ca-CSPO.

The thermo-gravimetric analyses showed significantly less mass loss in the upgraded oil samples compared to the crude oil at temperatures below 100 °C. Evidently, the upgraded oils contained much less moisture as compared to the crude one. The storage stability of the upgraded oils is noticeably better than the crude oil even after months of storage at ambient conditions. The upgraded oils do not stick to the walls of the container unlike the crude oil. A number of studies also identified bio-oil oxygenates as the major cause for its instability, suggesting a correlation between bio-oil oxygen content and stability. In this sense, significant reduction of bio-oil oxygen content would result in enhanced stability (Boucher et al. 2000; Meng et al. 2015).

6.5 CATALYTIC HYDRODEOXYGENATION (HDO) OF PYROLYSIS OIL

6.5.1 Gas chromatography –mass spectroscopic (GC-MS) analysis

The HDO of cr-CSPO was carried out using highly active palladium on activated carbon catalyst. The reaction was performed in a Hastelloy-made batch pressure reactor at 250 °C and 30 bar of hydrogen pressure for 3 h. The cr-CSPO sample before and after the catalytic upgrading were measured and compared using GC-MS. The compounds found in cr-CSPO have been categorized based on the functional groups present in them and in table 6.2.

Table 6.2 Gas chromatography and mass chromatography of CSPO at 575 °C

Retention time (min)	Area wt. %	Chemical compounds	Chemical formula
3.26	4.31	Butanoic acid, 4-hydroxy	C ₄ H ₈ O ₃
3.67	0.67	4-Heptene-3-one,2,5,6-trimethyl-	C ₁₀ H ₁₈ O
3.89	0.99	1,1-Cyclohexanedimethanol	C ₈ H ₁₆ O ₂
4.22	70.81	Phenol	C ₆ H ₆ O
5.23	1.81	N-carbobenzyloxy-l-tyrosyl-l-valine	C ₂₂ H ₂₆ N ₂ O ₆
5.6	12.06	Phenol, 2-methoxy (Guaiacol)	C ₇ H ₈ O ₂
7.23	1.36	Phenol, 2-methoxy-4-methyl (cresol)	C ₈ H ₁₀ O ₂
8.62	0.33	Phenol, 4-ethyl-2-methoxy- (p-ethylguaiacol)	C ₉ H ₁₂ O ₂
9.82	6.22	Phenol, 2-6-dimethoxy- (syringol)	C ₈ H ₁₀ O ₃
11.33	1.04	1,2,4-Trimethoxybenzene	C ₉ H ₁₂ O ₃
12.51	0.39	Methiocarb-anisole	C ₁₀ H ₁₄ OS

Gas chromatography coupled with mass spectroscopy (GC-MS) was used to analyse the chemical composition and the relative amounts of various classes of compounds present in CSPO. Among the major fractions (11 major compounds), 70.81 wt.% was found to be phenolic compounds, 1.03 wt.% ethers, 1 wt.% alcohols, 0.67 wt.% ketones, and 26.46 wt.% of other compounds. The presence of an overwhelming amount of phenol is coming from the thermal or catalytic deconstruction of lignin. In this regard, the phenolic compounds such as methyl phenols (cresols), methoxyphenols (guaiacol), and methoxypropenylphenol (isoeugenol) are seen. The obtained CSPO approximately contains >70% of phenolic

compounds. This may be due to the decomposition of the lignin content present in the coconut shell (Abnisa et al. 2013; Hasanah et al. 2012). The potential applications of the compounds present in the bio-oil could be utilized like phenols for reagents, plastic and resin industries. Syringol in flavors/fragrances industries, 2-methoxy-4-methylphenol and 2,6-dimethoxy-4-methylphenol in flavors industries (Sukhbaatar et al. 2009). The relative proportion of various functional groups of ca-Pd-C-CSPO and ca-Ru-C-CSPO is shown in table 6.3 and 6.4.

Table 6. 3 Gas chromatography and mass chromatography of ca-Ru-C-CSPO

Retention time (min)	Area wt. %	Chemical compounds	Chemical formula
3.16	9.36	Cyclopentanol, 2-methyl- cis	C ₆ H ₁₂ O
3.42	1.27	Butyrolactone	C ₄ H ₆ O ₂
4.37	40.28	Phenol	C ₆ H ₆ O
5.35	7.36	Butanoic acid, 3-methylphenyl ester	C ₁₁ H ₁₄ O ₂
5.66	10.90	Phenol, 2-methoxy (Guaiacol)	C ₇ H ₈ O ₂
6.55	3.42	Phenol,2-ethyl	C ₈ H ₁₀ O
6.78	3.20	Succinic acid, ethyl non-5-yn-3yl ester	C ₁₅ H ₂₄ O ₄
6.84	1.33	1H-Thieline, 2,3,6,7-tetrahydro-4,5-didehydro-3,3,6,6-tetramethyl-,1-oxide	C ₁₀ H ₁₆ OS
7.11	2.87	Phenol,4-ethyl	C ₈ H ₁₀ O
7.27	3.52	Phenol, 2-methoxy-4-methyl (Creosol)	C ₈ H ₁₀ O ₂
8.41	1.35	Pentanedioic acid, diethyl ester	C ₉ H ₁₆ O ₄
8.66	3.53	Phenol, 4-ethyl-2-methoxy- (<u>p-Ethylguaiaco</u>)	C ₉ H ₁₂ O ₂
9.52	3.39	2,5-diethylphenol	C ₁₀ H ₁₄ O
9.92	1.75	Phenol,4,3,5-Diethyl	C ₁₀ H ₁₄ O
10.08	2.25	Phenol, 2-methoxy-4-propyl (<u>p-Propylguaiacol</u>)	C ₁₀ H ₁₄ O ₂
11.41	0.82	Silane,trimethyl(2-methylphenoxy)-	C ₁₀ H ₁₆ OSi
13.17	1.22	Bicyclo[4.3.0]nonan-7-one, 1-(2-methoxyvinyl)-	C ₁₂ H ₁₈ O ₂
21.63	0.41	N-Propyl hexadecanoate	C ₁₉ H ₃₈ O ₂
24.43	0.17	Octadecanoic acid, Propyl ester	C ₂₁ H ₄₂ O ₂
28.2	0.22	1,1'Biphenyl, 5-hydroxy-3,2',3',4'-tetramethoxy-	C ₁₆ H ₁₈ O ₅

Table 6.4 Gas chromatography and mass chromatography of ca-Pd-C-CSPO

Retention time (min)	Area wt. %	Chemical compounds	Chemical formula
3.15	9.12	Phosphonic acid, (p-hydroxyphenyl)-	C ₆ H ₇ O ₄ P
3.49	2.68	Bicyclo[2.2.2]octane-2,6,7-triol, stereoisomer	C ₈ H ₁₄ O ₃
3.74	20.79	propanic acid , 2 methyl-anhydride (Isobutyric anhydride)	C ₈ H ₁₄ O ₃
4.01	23.87	Phenol, 2-methoxy (Guaiacol)	C ₇ H ₈ O ₂
4.63	4.59	Phenol,2-ethyl	C ₈ H ₁₀ O
4.82	6.51	Butanedioic acid, diethyl ester	C ₈ H ₁₄ O ₄
5.12	3.80	(1,4,4-Trimethyl-cyclohex-2-enyl)acetic acid	C ₁₁ H ₁₈ O ₂
5.27	5.41	Phenol, 2-methoxy-4-methyl (Creosol)	C ₈ H ₁₀ O ₂
5.73	2.07	7-Oxabicyclo[4.1.0]heptane, 1-methyl-4-(2-methyloxirany)-	C ₁₀ H ₁₆ O ₂
6.2	2.67	Pentanedioic acid, diethyl ester	C ₉ H ₁₆ O ₄
6.46	6.69	Phenol, 4-ethyl-2-methoxy- (p-Ethylguaiacol)	C ₉ H ₁₂ O ₂
7.02	0.90	propanic acid , 2-[3-methoxyphenyl]-	C ₁₀ H ₁₂ O ₃
7.23	1.14	Cyclohexene, 2-ethenyl-1,3,3-trimethyl-	C ₁₁ H ₁₈
7.42	0.40	1,2,3,4-Tetrahydroisoquinolin-6-ol-1-carboxylic acid	C ₁₀ H ₁₁ NO ₃
7.56	0.58	Cyclohexene, 2-ethenyl-1,3,3-trimethyl-	C ₁₁ H ₁₈
7.75	2.81	Phenol, 2-methoxy-4-propyl (p-Propylguaiacol)	C ₁₀ H ₁₄ O ₂
7.88	0.41	Nonanoic acid, 5-methyl-, ethyl ester	C ₁₂ H ₂₄ O ₂
8.13	1.74	Benzaldehyde, 4-(diethylamino)-	C ₁₁ H ₁₅ NO
8.31	0.33	trans-Z- -Bisabolene epoxide	C ₁₅ H ₂₄ O
8.64	0.27	3-Buten-2-one, 4-(3-hydroxy-6,6-dimethyl-2-methylenecyclohexyl)-	C ₁₃ H ₂₀ O ₂
9	1.11	Benzoic acid, 4-methoxy, ethyl ester	C ₁₀ H ₁₂ O ₃
9.62	0.75	trans-Z- -Bisabolene epoxide	C ₁₅ H ₂₄ O
9.86	0.53	Sipro[2,4,5,6,7,7a-hexahydro-2-oxo-4,4,7a-trimethylbenzofuran]-7,2'(oxirane)	C ₁₂ H ₁₆ O ₃
10.88	0.43	9-Octadecanoic acid (z), phenylethyl ester	C ₂₅ H ₄₀ O ₂
12.55	0.41	1,3,4-Thiadiazol-2-amine, 5-(3,4,5,trimethoxyphenyl)-	C ₁₁ H ₁₃ N ₃ O ₃ S

Among the 25 major compounds found, 2.67 wt.% are alcoholic compounds, 4.58 wt.% phenols, 10.2 wt.% esters, 3.15 wt.% ethers, 1.72 wt.% hydrocarbons, 12.92 wt.% of other acidic compounds, and 64.90 wt.% of other compounds with a

combination of other functional groups. In ca-Pd-C-CSPO upgraded bio-oil, the aromatic compounds seem increased, eg. 23.86% guaiacol, 5.40% of cresol, 6.68% P-ethyl guaiacol, 2.81% P-propyl guaiacol. Also, the organic acids were converted to esters like 6.51% butanedioic acid-diethyl ester, 2.66% Pentanedioic acid-diethyl ester, 0.41% Nonanoic acid-5-methyl-ethyl ester, 1.10% benzoic acid-4-methoxy-ethyl ester, 0.43% Octadecanoic acid-phenylethyl ester. Additionally, In ca-Ru-C-CSPO upgraded bio-oil, the aromatic compounds increased, eg. 10.89 % guaiacol, 3.51 % of cresol, 3.53 % P-ethyl guaiacol, 2.25% P-propyl guaiacol. Also, the organic acids were converted to esters like 7.35% butanoic acid, 3-methyl phenyl ester, 3.19% succinic acid, ethyl non-5-yn-3yl-ester, 1.34% pentanedioic acid, diethyl ester, 0.167% octadecanoic acid-propyl ester.

During the upgrade process, most of the organic acid was removed and the ester content increased significantly 11.11 % (Pd-C) and 12.047 % (Ru-C). It is possible that the detected esters (e.g., phenyl methyl ester, diethyl ester) are produced by esterification with ethanol, and the corresponding acid is present in the crude bio-oil. However, for many of the detected esters, no corresponding acid was found in the crude bio-oil. These higher alkyl esters were found to be the result of the ethanol reaction and the Guerbet oxidation esterification reaction (Huang et al. 2014). The aldehydes detected in the crude bio-oil were completely eliminated during the upgrading process. The main reason is that aldehyde is an active functional group that is easy to convert during the recovery process. For example, vanillin (4-hydroxy-3-methoxybenzaldehyde) can be converted to 4-methyl-2-methoxyphenol by dehydrodeoxygenation of the aldehyde group and guaiacol by cracking reaction (decarbonylation). The aromatic compounds, the main component of the upgraded bio-oil, increased significantly after the upgrade. The increase in aromatics content may be attributed to further depolymerisation of the lignin-derived oligomer during the upgrading process (Zhang et al. 2016). Many literatures support this interpretation.

Yuan et al. (2010) reported that lignin is effectively depolymerized into aromatic compounds in solvent ethanol. Tang et al. (2010) also reported that high yields of aromatic compounds can be obtained from pyrolyzed lignin using ethanol as a reaction solvent. In addition, it can be seen that the carbonyl group and the

unsaturated bond on the substituent of the aromatic compound are successfully hydrogenated. Catalytic Hydrogenation was performed to decrease the oxygen content present in the bio-oil and also to enhance the higher heating value. As envisioned, the HHV value of ca-CSPO obtained at 250 °C had a much higher heating value than cr-CSPO and even th-CSPO treated at the same temperature. In quantitative terms, the HHV of ca-CSPO is 84% higher than Cr-CSPO, whereas the thermal treatment of Cr-CSPO at 250 °C improved the HHV by 57%. The deoxygenation of phenols converted them into other classes of compounds. Significant economic potential in food, pharmaceutical, and paint industries (Horne and Williams 1996; Stoikos et al. 2011).

6.5.2 Nuclear magnetic resonance (NMR) analysis

The bio-oil is a complex mixture of organic compounds containing wide range functional groups. The ¹H NMR spectroscopy of the bio-oil revealed the type of compounds and their relative proportions present in bio-oil. The aromatic compounds including phenolics could easily be identified by the aromatic C-H signals around 7 ppm. In all the samples (i.e., th-CSPO, ca-Ru-C-CSPO, and ca-Pd-C-CSPO), the presence of phenols and phenolic ethers were present in significant proportion. As expected from the calorific value, the amount of oxygenates other than phenolics decreased in ca-Pd-C-CSPO as compared to th-CSPO or ca-Ru-C-CSPO. Specifically, the relative proportion of protons in the oxygenated compounds was only 13.21% in ca-Pd-C-CSPO as compared to 32.11% in th-CSPO (table 6.5). Figures 6.12- 6.14 shows the proton NMR of upgraded oils and the percentage of hydrogen are tabulated (table 6.5) As seen in the NMR analysis, the free phenol has been converted into phenolic ether under the catalytic HDO conditions. The HDO condition led to dehydration and deoxygenation reactions and therefore the protons in the aliphatic region (1.5-0.9 ppm) increased noticeably. This increase also helped in improving the HHV.

Table 6.5 Functional group distribution from ^1H NMR spectral integration using Chemical shift region (ppm)

Chemical shift region (ppm)	Dominant type of Hydrogen	Percentage of Hydrogen		
		(th-CSPO)	(ca-Ru-C-CSPO)	(ca-Pd-C-CSPO)
8.5-6.5	Aromatic	22.48	22.72	23.26
4.5-3.5	CH_3 and CH_2 directly connected to oxygen atoms as in ether	32.11	22.86	13.21
3.0-2.0	CH_3 CH_2 and CH to an aromatic ring	11.86	22.5	23.31
1.6-0.9	β - CH_3 , CH_2 and CH γ to an aromatic ring	33.53	32.16	40.21

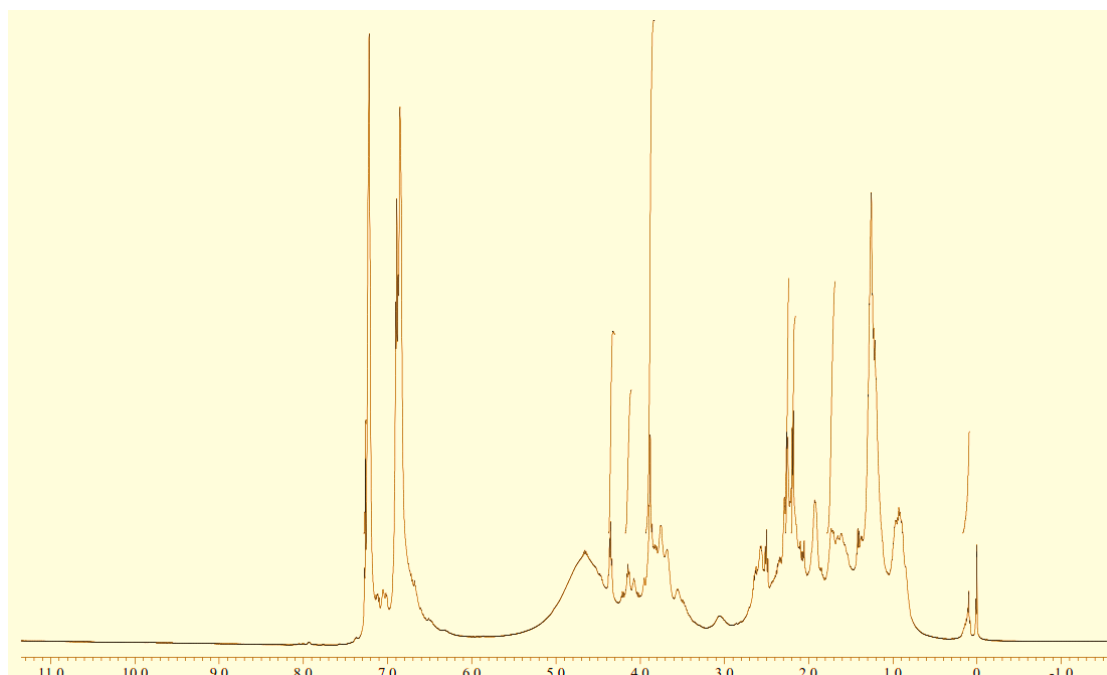


Figure 6.12 Proton NMR of th-CSPO at 250 °C

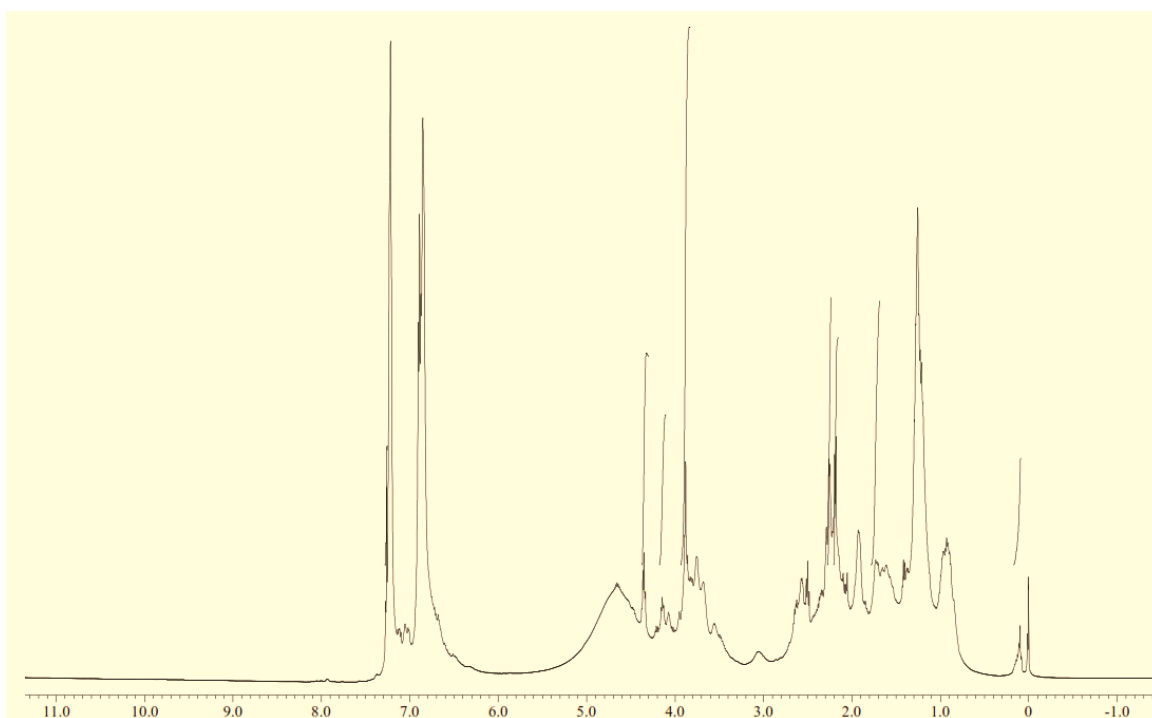


Figure 6.13 Proton NMR of ca-Ru-C-CSPO at 250 °C

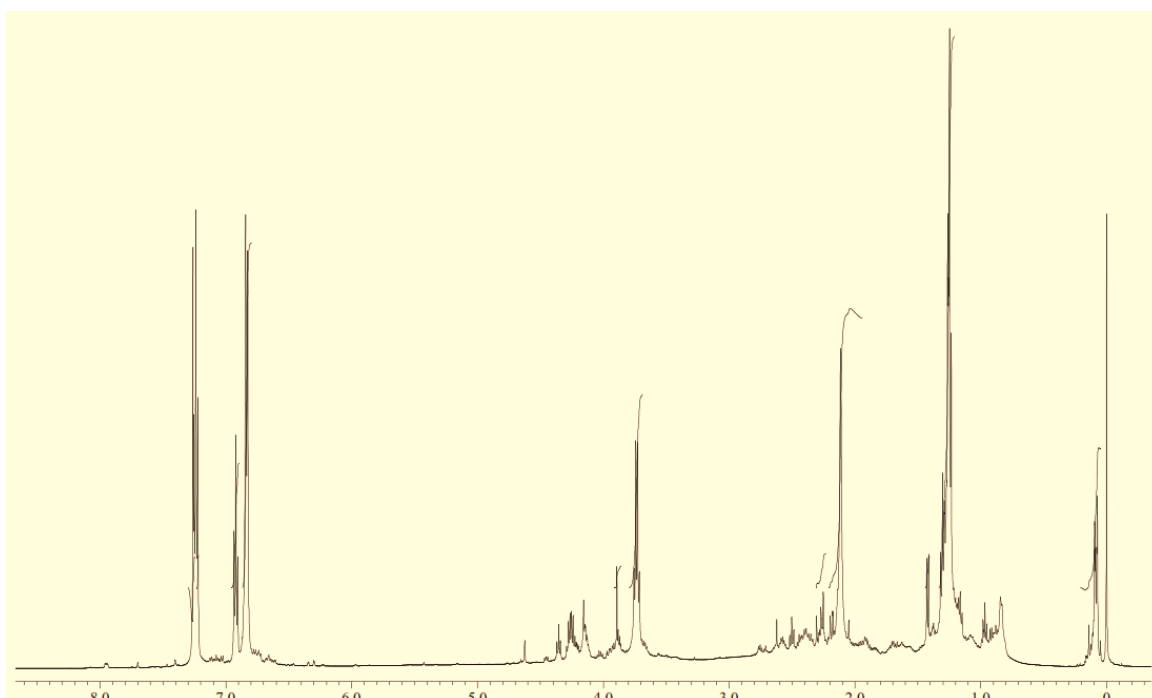


Figure 6.14 Proton NMR of ca-Pd-C-CSPO at 250 °C

CHAPTER 7

COCONUT SHELL ACTIVATED CARBON-BASED DYE-SENSITIZED SOLAR CELL FOR DEVELOPMENT OF HIGHLY SENSITIVE TEMPERATURE AND CURRENT SENSOR

In this chapter, the pyrolysed bio-char is synthesised to activated carbon and used as a counter electrode in the fabrication of dye sensitised solar cell and performed the current voltage characteristics of DSSC with and without optical filters.

INTRODUCTION

To a great extent photovoltaic cells are being intensively used to tap these huge resources and will play key role in future energy systems. Solid-state junction devices usually made of silicon have dominated photovoltaic solar energy converters (Hasan and Sumathy 2010). However, the cost initially investments of photovoltaic electricity production are still too high to compete with fossil energy. The recently developed third generation solar cell called Dye Sensitized Solar Cells (DSSC) by (Kreitman 1991) O'Regan and Gratzel in 1991 mimics the photosynthesis process. The solar cell works by converting photons from solar energy to electrical energy, based on sensitization of wide band gap semiconductor, Dyes (Nazeeruddin et al. 1997; Hwang et al. 207) and Electrolyte (Nazeeruddin et al 2013). The advantages of Dye-sensitized solar cells are that it can be engineered into flexible sheets, ease of fabrication, use of low-cost sensitization materials and low process temperature. Due to the low cost of the overall production of DSSC it has been expected that the DSSC type of solar cells will give a higher return of investment (ROI) when compared to silicon based solar cells (Si-Sc). Recently carbon-based counter electrodes in DSSC are better for developing better cell efficiency, one such material is activated carbon with enhanced surface area. This activated carbon is synthesised by different methods to increase the microporous structures which is highly essential for thin film solar cells.

7.1 EXPERIMENTAL METHODOLOGY

7.1.1 Preparation of TiO₂ photo anode

The used reagents were proper analytical grade and used without further purification. The Indium tin oxide coated conductive glass is prepared by cleaning with the acetone and checked with resistance and obtained near 13 Ω/cm^2 . Omega (Ω) represents the resistivity of indium tin oxide conductive glass. Then 5ml of nitric acid was added to the TiO₂ precursor in drop wise and mixed constantly to result to a consistent paste. Parallely, the conductive glass is arranged for applying TiO₂ paste using doctor knife technique. Then the electrode is allowed to dry by hot air for 15 min and followed by drying in oven for 1h under a controlled temperature of 100 °C. After this the electrode is allowed to cool down gradually with a cooling rate of 2 –3 °C /min to avoid peeling of the coating and the cracking of the electrode.

7.1.2 Preparation of POM dye

One of the major sources of anthocyanin dyes is from pomegranate fruit which belongs to punicea family. The fruit contains several seeds separated by white membrane pericarp and each surrounded by small amount tart and red juice. The plant contains alkaloids, tannin pigments, organic acids, salts in flower, fruit and root. Punicacea is an aromatic dye with high cynin content and pomegranate seed contain high percentage of phenolic derivatives. The sensitisation dye is extracted from pomegranate fruit by separating juice from the fruit and further centrifuged to separate the fiber and minute mixed seed remains in the juice and this juice is directly used for the construction of the DSSC. The fresh extract of pomegranate juice is used to prepare the dye sensitizer for photo electrode and filtered using wire mesh and stored respectively. Then 40 ml of POM extract is taken and transferred in a vial for centrifuging to separate the final pulp fibres from the dye extracts.

7.1.3 Preparation of carbon

The currently used carbon is prepared using pyrolysed coconut shell. The raw material coconut shell charcoal with moisture content of 3.99%, volatile matter of

7.35% and fixed carbon content of 88.16% was used to prepare activated carbon. The steam activation of bio-char was done in a vertical furnace at a pressure of 1.5 kg/cm².

7.1.4 Carbon coated counter electrode

The counter electrodes were prepared by coating carbon on the conductive side of the electrode. Initially, the freshly prepared carbon flakes were directly deposited over the electrode, it was observed that the deposition was not even but the thickness was even. This took to try several methods to effectively deposit the carbon. The synthesized carbon is extremely high surface area has very low affinity to stick to the conductive glass. Finally, the conductive glass is slightly rolled with sticky notes paper and its conductance and resistance of the conductance layer were unaltered. Then a very smooth coating of carbon is coated over the counter electrode. Before assembling any loose carbon is carefully removed. Without any further preparation process the counter electrode is used for counter electrode.

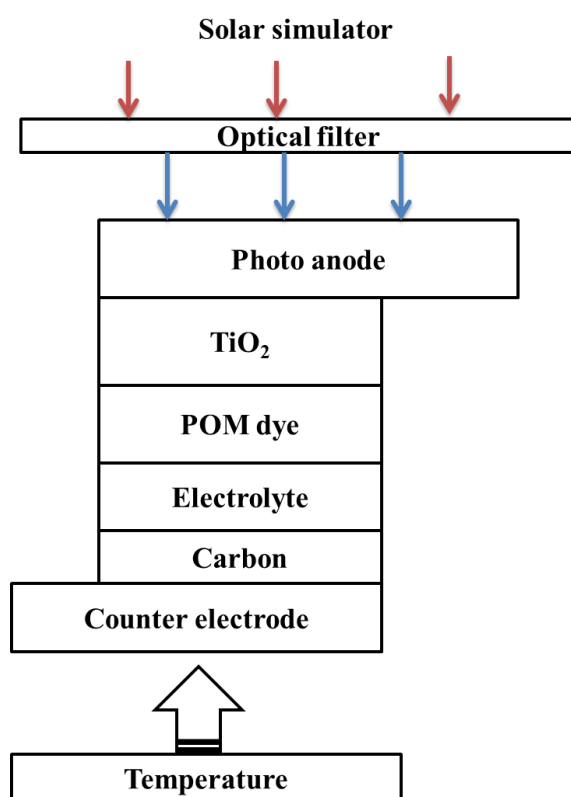


Figure 7.1 Schematic layout of natural POM dye DSSC

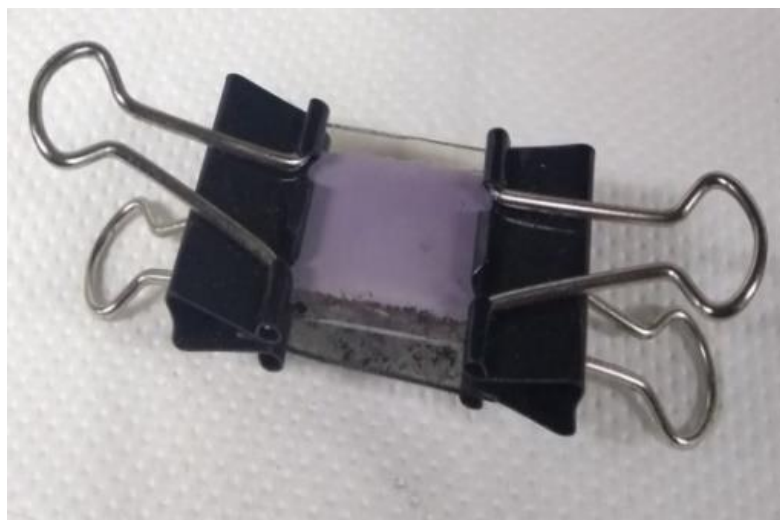


Figure 7.2 Actual photograph of the constructed natural POM dye DSSC

7.2 DSSC ASSEMBLY

Before the complete assembly of the DSSC the TiO_2 coated photo electrode is soaked in the extracts of the POM juice and allowed be immersed for 30 min allows the dye to get adsorbed in TiO_2 active zones. Then the photo anode is cleaned using deionised water to remove the excess dye extracts. Then the photo anode is connected with activated carbon sandwiched to activated carbon counter electrode. It was oriented such a way that the considerable conductive surface is sufficient to locate the sensing probes. The DSSC two electrodes were connected by redox electrolyte and the sides of the glass was blocked by high conductive silver paste and clamped using binder clips. Figure 7.1 shows the schematics of DSSC assembly. The actual fabricated DSSC with POM natural dye is shown in figure 7.2.

7.3 DSSC SENSOR CHARACTERIZATION SETUP

The experimental activity aimed to investigate the performance of current and temperature sensing characteristics of DSSC under real operating condition. The conductive surface of the both anode and counter electrode is connected to the DAC; K-type thermocouple with sensitivity of $0.1\text{ }^\circ\text{C}$ is attached to the DSSC module. Behind the active area of the DSSC a resistance heater is fixed connected to the NI controller using a flux controller. Adjustable stand is fixed to position the optical

filters ranging from 410 nm to 620 nm. Above which the solar simulator is focused on the active area of the DSSC.

7.4 SYNTHESIS AND CHARACTERIZATION OF DSSC MATERIALS

Figure 7.3 presents the surface morphology of photo electrode and counter electrode used in this current investigation. Figure 7.3 (a) shows the sintered TiO_2 coating in the conductive glass. The coating was found uniform with minimal abnormalities. Figure 7.3(b) shows the deposited activated carbon for the preparation of counter electrode. In this case, the deposition was not uniformly distributed as that of photo electrode. Further the addition of activated carbon does not alter the conductance and resistance of the counter electrode. On continuous operation of DSSC worn outs both the electrodes to a great extent shown in figures 7.3(c), (d). Multiple relocations of TiO_2 were observed in the worn-out cell which might severely affect the photo conversion efficiency. In the case of counter electrode serious damage in coating was seen, the possible cause may be due to the activated carbon is mixed with electrolyte. Figures 7.3(e), (f) shows the TiO_2 photo electrode adsorbed with POM dye. It was found that the maximum adsorption of the dye were on porous trenches of TiO_2 . Figures 7.3(g), (h) shows the details of sintered porous trenches in the TiO_2 photo electrode. Figure 4.3(h) highlights the depth of the porous TiO_2 with multiple inner trenches.

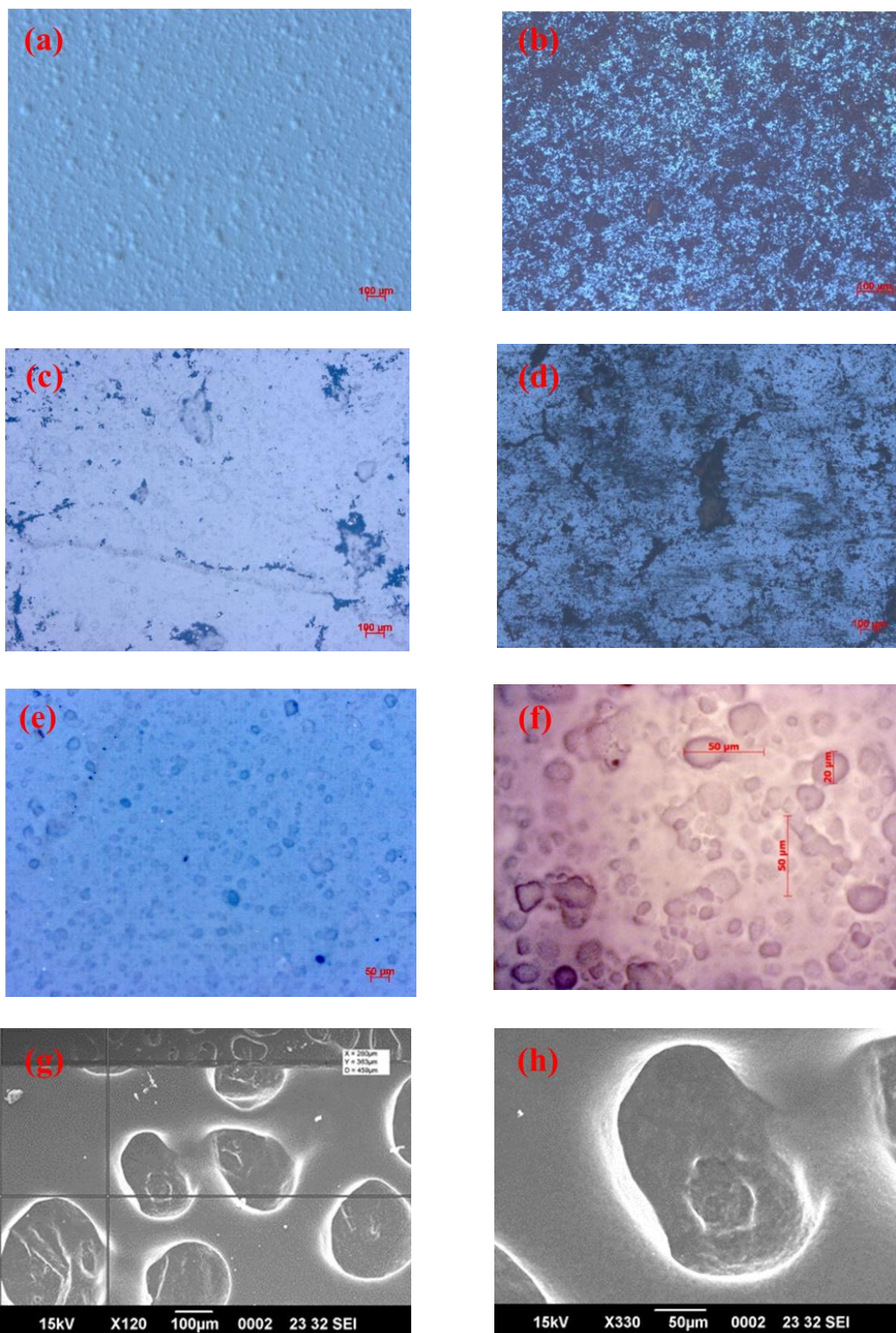


Figure 7.3 Characterization of photo electrode and counter electrode, (a) TiO₂ coating, (b) activated carbon coated counter electrode, (c) worn out photo electrode, (d) worn out counter electrode condition, (e) porous surfaces in photo electrode, (f) TiO₂ photo electrode after POM dye adsorption, (g, h) SEM details of the porous structures.

7.5 CHARACTERISATION OF SEM AND XRD

To find the surface morphology of activated carbon and TiO_2 , scanning electron microscope analysis was performed using JEOL_JSM-6360LV model. SEM is a kind of electron microscope which usually scans the images with high beam of electrons in the scan patterns. Dense agglomeration of nano particles was observed in TiO_2 which looked irregular shape. The agglomeration happens as a result of the TiO_2 is unstable in the nanoparticles as they tend to affix one another till they are comparatively stable (Nasikhudin et al 2018). The formation of pores on the activated carbon is mainly due to the escape of volatile matter during the activation process. Different pores were observed in the samples shown in figure 7.4. The heterogeneous distribution of macro pores and a rough texture obtained could be useful in much liquid-solid adsorption process (Boudrahem et al. 2009). X-ray diffraction (XRD) impression was done using a diffractometer using $\text{Cu K}\alpha$ radiation ($\lambda=1.542$) operating at 40 kV with step size of 0.02° in the range of 10° – 90° . The x-ray diffraction patterns of the raw material i.e., Activated carbon prepared from coconut shell charcoal or char or the solid residue formed by its pyrolysis is shown in figure 7.5. The pattern does not show a basic horizontal line. Absence of sharp peaks in the XRD pattern suggests it is extravagantly amorphous structure which is worthwhile property for well-defined absorbents (Kennedy et al. 2007; Pechyen et al. 2007; Anuradha et al. 2014).

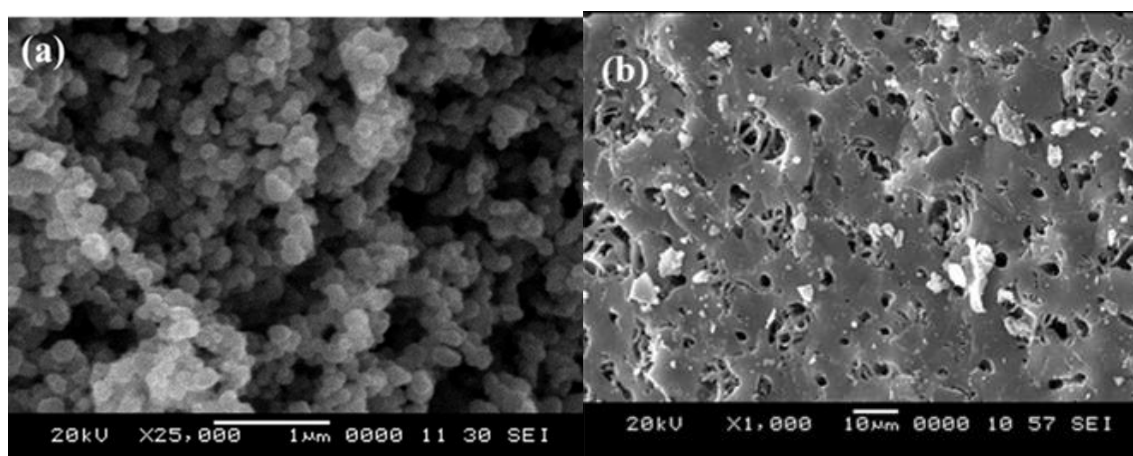


Figure 7.4 Scanning electron microscopic images, (a) TiO_2 and (b) activated carbon

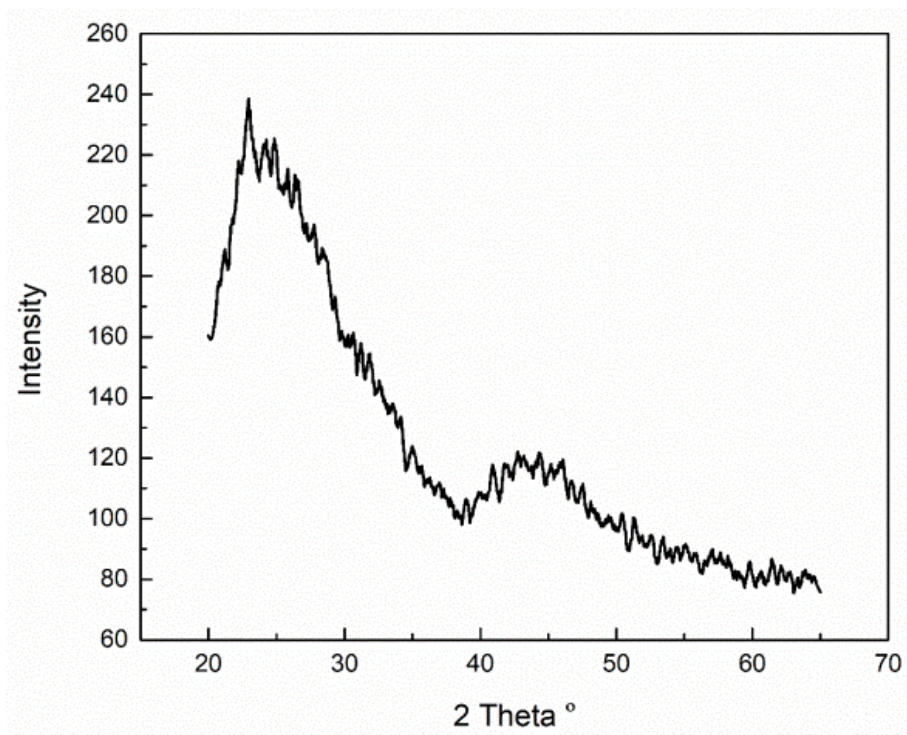


Figure 7.5 X-ray diffraction pattern of activated carbon

7.6 RESULTS AND DISCUSSIONS

7.6.1 Current and voltage characteristics

Figure 7.6 depicts IV (Current and Voltage curve) characteristics of DSSC with and without optical filters. It is observed that the maximum performance was delivered for 443 nm. Moreover, there was no much difference in the results of 470 nm of violet filter. For both of these optical filters the results were more similar and near to the maximum short circuit current of 6 μ A. This is attributed to the effect of maximum absorption range of pomegranate dye. This is near to the range of 443 nm. On other hand short circuit current developed by 515 nm, 545 nm and 620 nm optical filters achieved subsequently lower short circuit current. The DSSC with green optical filter of 545 nm developed the most stable current when compared to all other filters.

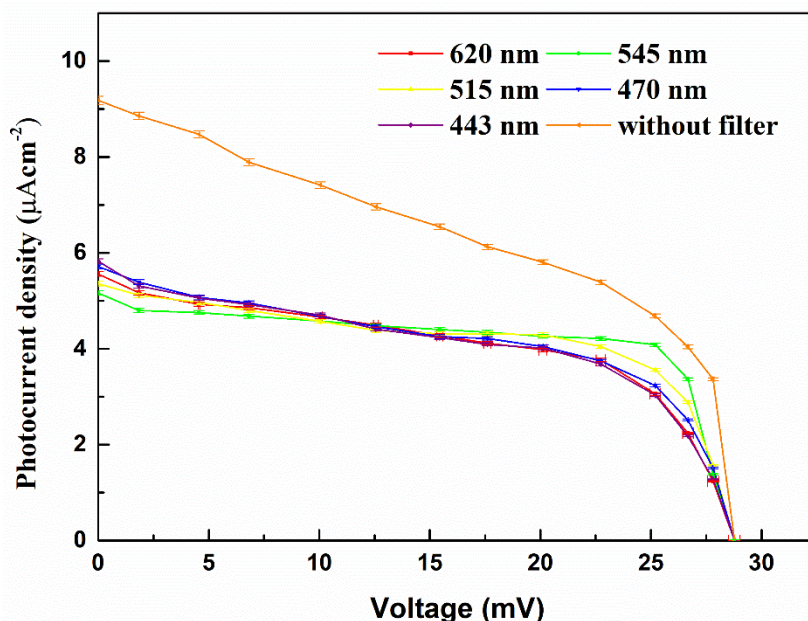


Figure 7.6 I-V characteristic curve of dye sensitised solar cell with different optical filters and one without optical filter

DSSC exhibits nearly $0.856 \mu\text{A}$ of short circuit current which is 50 % more. But POM dye based DSSC suffered high un-stability and drastic reduction in the current is observed. From this study, it is confirmed that DSSC with combined visible spectrum range develops a maximum performance and power. But also develops high un-stability in photo conversion. This un-stability was observed due to higher amount of unstable photo transitions at excited energy state. Due to this, one may observe increase in photocurrent density of the cell initially but the decrement in the current was drastic. In the case of using filters, increase in photo conversion stability was found. Moreover, the used filters were within the emission intensity of natural POM dyes, this maybe one of the reasons which made highly stable photo conversion in the case of with filters.

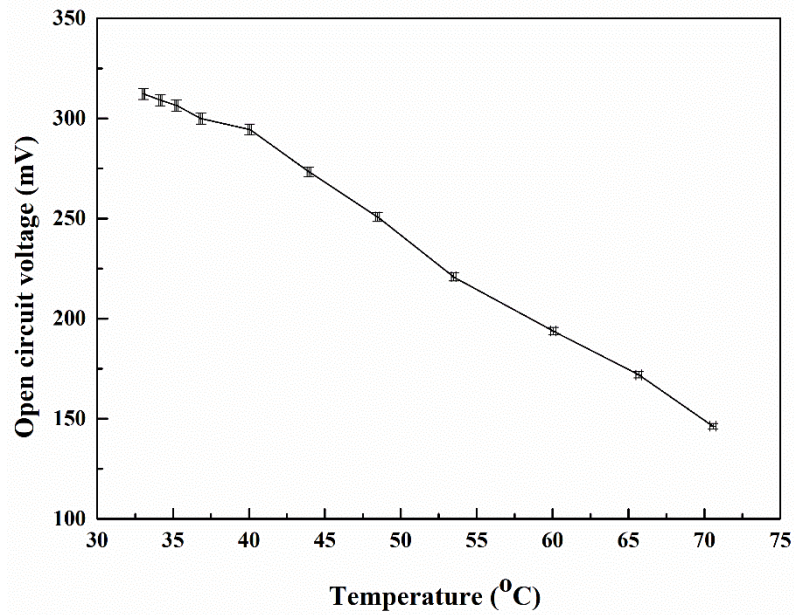


Figure 7.7 Open circuit voltage decrement of POM based dye sensitised solar cell at increased temperatures

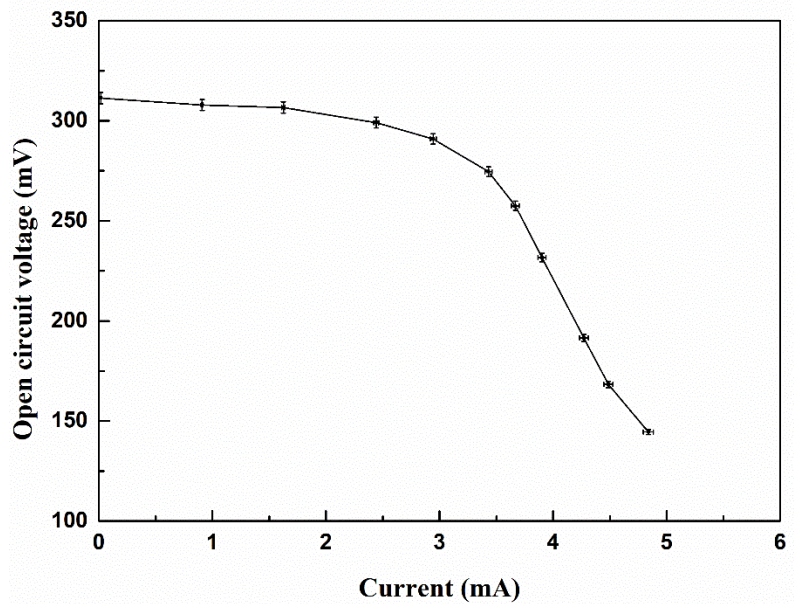


Figure 7.8 Open circuit voltage versus current for dye sensitised solar cell with POM sensitizer.

The figures 7.7 and 7.8 depicts the temperature and current sensor characteristics of the DSSC. Figure 7.7 shows the stability and sensitivity responses at different temperature variations under constant illumination. The electrolyte used in DSSC is temperature-sensitive. It also depicts temperature dependency of the DSSC. To recapitulate the effect of the temperature on DSSC a resistive heater is placed in

vicinity of the cell and temperature increment is made. The raise in cell temperature evaporates the cell electrolyte significantly. Till near the temperature of 40 °C reduction in voltage is less and up-to this temperature the DSSC is considered to be in stable and thereafter drop in open voltage is rapid with temperature increase and this condition is considered to be sensitivity response to temperature. The uncertainties for DSSC are shown in Appendix-A1.5. In this investigation the study limited up to the maximum temperature of 75 °C above which the power characteristics are dropped. It is noticed that up to a lower temperature of 40 °C the open circuit voltage is much similar but on increased temperature, the voltage drastically decreases. This can be attributed to the reduction in total DSSC resistance irrespective to the wave length of light. On other hand increase in temperature steadily accelerates the kinetics of the redox electrolyte thereby increasing dye conductivity. This increased conductivity of the electrolyte is due to the increment in viscosity. Similar effect was observed by (Raga and Fabregat-Santiago 2013). Furthermore, the predominant dye adsorptions were on sintered porous trenches observed on TiO₂. Increase in sintering time allows more porous voids which is more suitable for dye molecules in photo electrode for recombination at higher temperatures. From multiple deposition of TiO₂ and adsorption of dye provide an insight that increased viscosity reduces the diffusion of I₃⁻ at increased temperatures. As observed the decrease in open circuit voltage is gradual for a slight increase in temperature from ambient to 35 °C. But once the temperature exceeds 40 °C the reduction open circuit voltage is very rapid. At temperature above 80 °C the electrolyte started to move rigorously and started to evaporate, but once again the cell worked normally as the fresh electrolyte is applied in DSSC. Moreover, the increase in temperature increases the kinetics of the cell with increased recombination and reduces the device efficiency. Figure 7.8 depicts open circuit voltage compared with the resistance current generated by DSSC for increased temperature. As observed the DSSC breaks at a particular power rating of 0.856μW ($Power = V \times I = 2.944 \times 290.18 = 0.856$) at temperature range near 70.5 °C.

CHAPTER 8

CONCLUSIONS

In this study, coconut shells were chosen as the biomass source. Its pyrolysis was conducted at temperature 575 °C in a fixed bed reactor. Characterization of the bio-oil and bio-char products was studied in order to determine its possibility of being a potential source of renewable fuel and chemical feedstock. The Characterization of the biomass (coconut shell) was carried out. Thermo gravimetric analysis shows the degradation of the coconut shell around 300 °C onwards and hence this is the deciding factor for pyrolysis temperature range. Intermediate pyrolysis of coconut shells was carried out at 575 °C. By increasing the temperature, the yield of the liquid increased up to 575 °C at which highest liquid yield of 33-38 % is obtained. The yield of bio-char decreases continuously while non-condensable part decreased with increase in temperature up to 575 °C, after which it increased. The physiochemical properties of liquid products produced at 575 °C were carried out. The FTIR analysis showed the presence of alcohols or phenols and other functional groups like aldehydes and ethers. The result is consistent with the findings of GC-MS. Phenol is detected in highest amount and many other phenol derivatives were detected. SEM images showed the presence of pores on solid residue (bio-char). This leads to making of activated carbon from the solid residue.

Coconut shell bio-tar (CSBT) was effectively separated using solvent extraction combined with column chromatography to obtain saturated aromatic resin and asphaltene (SARA) fractions. The yields of the four fractions showed saturated (17.17 %), aromatic (18.97 %), resin (16.37 %), asphaltene (24.77 %), and toluene insoluble (1.9 %). In total, 77.28 % of the starting oil was recovered. Asphaltenes are the components of crude oil, which are soluble in toluene but precipitate from solutions of normal paraffins, under specified experimental conditions. Resins are soluble in the liquids that precipitate asphaltene and can be separated from the residue in the maltene mixture by chromatography, and are strongly adsorbed onto the asphaltene. The compositions of the SARA fractions were then characterized using ¹H NMR, elemental analysis and FT-IR. From ¹H NMR the total

hydrogen atoms were in the following order: saturated <aromatic<resin<asphaltene. Further, Bio-asphalt structure showed highest concentration (68.20%) of carbon.

Upgradation of coconut shell pyrolysed oil (CSPO) is carried out by using palladium on activated carbon and ruthenium on activated carbon catalysts. Also, the CSPO was upgraded thermally (without catalyst). The upgrading strategy is performed by hydrodeoxygenation process and compared the elemental properties of the upgraded oil. Hydrodeoxygenation (HDO) is the efficient way of removing oxygen atoms in the bio-oil. The higher heating value of the upgrading oil increased to nearly double of that in cr-CSPO. The oxygen content in cr-CSPO reduced from 47.95 wt.% to 26.35 wt.% in the upgraded oil, whereas the carbon content increased from 46.11% to 61.64 wt.%. Elemental compositions of crude bio-oil (46.11wt% C, 5.9 wt% H and 47.95 wt% O) and upgraded bio-oil ca-RuC-CSPO (1: 20 ratio of bio-oil to ethanol) (61.59 wt% C, 9.2 wt% H and 26.81 wt% O) quantitatively indicates, the carbon content increased to 33.57% and oxygen content declined to 44.08%. Additionally the upgraded bio-oil, ca-PdC-CSPO (61.63 wt% C, 9.71 wt% H and 26.35 wt% O) also shows the carbon content increased to 33.36% and oxygen content declined to 45.04%. As the control, the reaction was performed at the same conditions except the catalyst to explore the effect of heat in the oxygen removal process. It was observed that in th-CSPO, the carbon content increased and the oxygen content decreased to only 24.28% and 32.6%. Therefore, the oxygen-to-carbon ratio dramatically decreased from 0.78 in cr-CSPO to only 0.32. The hydrogen-to-carbon ratio improved from 1.5 in cr-CSPO to 1.7 in ca-RuC-CSPO and 1.8 in ca-PdC-CSPO. After HDO, a significant reduction of water content in the bio-oil is observed. The high water content in bio-oils imparts polarity to the fuel, resulting in immiscibility of bio-oils in fossil fuels. At a lower temperature (i.e., 200 °C), the carbon content was improved to only 21.81 %, in ca-RuC- CSPO and 24.05% in ca-PdC- CSPO. The increase of reaction temperature from 200-250 °C, the yield of upgraded oil decreased, but it was beneficial in improving the elemental properties. Also as oxygen content reduced the degree of deoxygenation increased. Therefore, the above parameters indicate that the selective oxygen removal in catalytic treatments of cr-CSPO by the HDO chemistry was superior to the thermal route. When compared

with petroleum fuels (41-43 MJ/kg), the HHV 16.46 MJ/kg of the crude bio-oil is very low. By reducing the oxygen content the HHV of ca-RuC-CSPO and ca-PdC-CSPO increased to 29.6 and 30.41 MJ/kg during the HDO process respectively. The hydrodeoxygenation of crude oil using Pd-C as catalyst provided upgraded oil with highest HHV. The HDO over Ru-C catalyst also gave fairly good result. However, the thermally upgraded oil had significantly lower HHV

From GC-MS analysis we found that the amount of phenols decreased significantly after catalytic HDO of the cr-CSPO. In particular, ketones were almost completely removed. Most phenols were converted into corresponding esters, and at the same time, new esters, ethers, and hydrocarbons formed. The amount of oxygenates lowered in catalytic HDO and the amount of hydrocarbons increased as seen in the ^1H NMR spectra. The FT-IR analysis GC-MS and NMR analysis of showed that it had significantly lower contents of organic acids, aldehydes, ketones, and ethers than cr-CSPO pointing towards superior storage and thermal stability. . The renewable upgraded CSPO may therefore be used in various blends with diesel for furnace and engine applications.

The solids (bio-char) obtained from intermediate pyrolysis process is synthesised to activated carbon and was used as a counter electrode in the fabrication of dye sensitised solar cell and performed the current voltage characteristics of DSSC with and without optical filters. The developed activated charcoal is implemented in demonstrating Dye Sensitised Solar Cell using naturally available sensitizer. Anthocyanin dye extracted from pomegranate juice generated maximum current of 10 mA. The performance of the DSSC module with TiO_2 photo electrode and active carbon-based counter electrodes was investigated with different optical filters. The characteristics of the cell was performed with different optic filters wavelength ranging 400-600 nm and the maximum efficiency was developed for wave length of 445 nm. It has been observed that the DSSC performance of the module increased for the optical filter of 443 nm with increased stability. Without optical filter, the DSSC performed with the increased current generation and reduced stability. In the effort to develop a highly sensitive thin film temperature sensor, the stability and sensitivity

responses at different temperature variations under constant illumination were also investigated. The study limited upto the maximum temperature of 75°C. It was noticed that upto a lower temperature of 40 °C the open circuit voltage is much similar but on increased temperature, the voltage drastically decreases. The observed results demonstrate the use of DSSC as thin film sensors. The rapid advancement in the field of consumer electronics has drastically reduced the size of the devices with enhanced smartness. As a result, it is redefined our work space with sophistication and smart devices with tremendous level of diversification. The corresponding smart feature of the device predominantly insists to the effective sensors involved in the device. Now days, these sensors are implemented in flexible electronics, wearable technology, opto electronics and electronic bio implants etc. It is pertinent to mention the current devices are predominantly flexible and there is a huge demand for flexible sensors. This makes thin film based DSSC sensor a better solution to the latest compact devices. From all the findings it provides a better insight and to develop a thin film based renewable solar temperature and current sensor for compact electronic devices.

REFERENCES

- Abdelfattah, M. S. H., Abu-Elyazeed, O. S. M., Abd El mawla, E., and Abdelazeem, M. A. (2018). "On biodiesels from castor raw oil using catalytic pyrolysis." *Energy*, 143, 950–960.
- Abnisa, F., Arami-Niya, A., Wan Daud, W. M. A., Sahu, J. N., and Noor, I. M. (2013). "Utilization of oil palm tree residues to produce bio-oil and bio-char via pyrolysis." *Energy Convers. Manag.*, 76, 1073–1082.
- Acikgoz, C., Onay, O., and Kockar, O. M. (2004). "Fast pyrolysis of linseed: Product yields and compositions." *J. Anal. Appl. Pyrolysis*, 71(2), 417–429.
- Acosta, M. J. (2018). "Advances in energy research." Volume 1, Nova Science Publishers, Inc., USA, 1-239.
- Akmaz, S., Iscan, O., Gurkaynak, M. A., and Yasar, M. (2011). "The structural characterization of saturate, aromatic, resin, and asphaltene fractions of batiraman crude oil." *Pet. Sci. Technol.*, 29(2), 160–171.
- Alcaniz-Monge, J., Cazorla-Amoros, D., and Linares-Solano, A. (2001). "Characterization of coal tar pitches by thermal analysis, infrared spectroscopy and solvent fractionation." *Fuel*, 80(1), 41–48.
- Alda-Onggar, M., Maki-Arvela, P., Aho, A., Simakova, I. L., and Murzin, D. Y. (2019). "Hydrodeoxygenation of phenolic model compounds over zirconia supported Ir and Ni-catalysts." *React. Kinet. Mech. Catal.*, 126(2), 737–759.
- Anca-Couce, A. (2016). "Reaction mechanisms and multi-scale modelling of lignocellulosic biomass pyrolysis." *Prog. Energy Combust. Sci.*, 53, 41–79.
- Antal, M. J., and Gronli, M. (2003). "The art, science, and technology of charcoal production." *Ind. Eng. Chem. Res.*, 42(8), 1619–1640.

Anuradha, S., Raj, K. J. A., Elangovan, T., and Viswanathan, B. (2014). “Adsorption of VOC on steam activated carbon derived from coconut shell charcoal.” *Indian J. Chem. Technol.*, 21(5–6), 345–349.

Ardiyanti, A. R., Gutierrez, A., Honkela, M. L., Krause, A. O. I., and Heeres, H. J. (2011). “Hydrotreatment of wood-based pyrolysis oil using zirconia-supported mono- and bimetallic (Pt, Pd, Rh) catalysts.” *Appl. Catal. A Gen.*, 407(1–2), 56–66.

Asadullah, M., Anisur Rahman, M., Mohsin Ali, M., Abdul Motin, M., Borhanus Sultan, M., Robiul Alam, M., and Sahedur Rahman, M. (2008). “Jute stick pyrolysis for bio-oil production in fluidized bed reactor.” *Bioresour. Technol.*, 99(1), 44–50.

Aske, N., Kallevik, H., and Sjoblom, J. (2001). “Determination of saturate, aromatic, resin, and asphaltenic (SARA) components in crude oils by means of infrared and near-infrared spectroscopy.” *Energy and Fuels*, 15(5), 1304–1312.

Ates, F., Putun, E., and Putun, A. E. (2004). “Fast pyrolysis of sesame stalk: Yields and structural analysis of bio-oil.” *J. Anal. Appl. Pyrolysis*, 71(2), 779–790.

Baratieri, M., Baggio, P., Fiori, L., and Grigiante, M. (2008). “Biomass as an energy source: Thermodynamic constraints on the performance of the conversion process.” *Bioresour. Technol.*, 99(15), 7063–7073.

Boscagli, C., Tomasi Morgano, M., Raffelt, K., Leibold, H., and Grunwaldt, J. D. (2018). “Influence of feedstock, catalyst, pyrolysis and hydrotreatment temperature on the composition of upgraded oils from intermediate pyrolysis.” *Biomass and Bioenergy*, 116, 236–248.

Boucher, M. E., Chaala, A., and Roy, C. (2000). “Bio-oils obtained by vacuum pyrolysis of softwood bark as a liquid fuel for gas turbines. Part I: Properties of bio-oil and its blends with methanol and a pyrolytic aqueous phase.” *Biomass and Bioenergy*, 19(5), 337–350.

- Boudrahem, F., Aissani-Benissad, F., and Ait-Amar, H. (2009). "Batch sorption dynamics and equilibrium for the removal of lead ions from aqueous phase using activated carbon developed from coffee residue activated with zinc chloride." *J. Environ. Manage.*, 90(10), 3031–3039.
- Branca, C., Giudicianni, P., and Blasi, C. Di. (2003). "GC/MS characterization of liquids generated from low-temperature pyrolysis of wood." *Ind. Eng. Chem. Res.*, 42(14), 3190–3202.
- Bridgwater, A. V. (1994). "Catalysis in thermal biomass conversion." *Appl. Catal. A, Gen.*, 116(1–2), 5–47.
- Caballero, J. A., Font, R., and Marcilla, A. (1996). "Study of the primary pyrolysis of Kraft lignin at high heating rates: Yields and kinetics." *J. Anal. Appl. Pyrolysis*, 36(2), 159–178.
- Channiwala, S. A., and Parikh, P. P. (2002). "A unified correlation for estimating HHV of solid, liquid and gaseous fuels." *Fuel*, 81(8), 1051–1063.
- Das, D., Samal, D. P., and Bc, M. (2015). "Preparation of activated carbon from green coconut shell and its characterization." *Chem. Eng. Process Technol.*, 6(5), 1415–1420.
- Dasari, K. K. (2019). "Activated carbon-based dye-sensitized solar cell for development of highly sensitive temperature and current sensor." *IOP Publishers, Mater. Res. Express*, 6, 085531.
- Demirbas, A. (2007). "Biodiesel from sunflower oil in supercritical methanol with calcium oxide." *Energy Convers. Manag.*, 48(3), 937–941.
- Demirbas, A. (2009). "Biofuels from agricultural biomass." *Energy Sources, Part A Recover. Util. Environ. Eff.*, 31(17), 1573–1582.
- Deveci, H., and Kar, Y. (2013). "Adsorption of hexavalent chromium from aqueous solutions by bio-chars obtained during biomass pyrolysis." *J. Ind. Eng. Chem.*, 19(1), 190–196.

Dielbold, J., (1999). “A review of the chemical and physical mechanisms of the storage stability of fast pyrolysis bio-oils.” *National renewable energy laboratory, NREL/SR-570-27613*, January, 56, Subcontractor report, Thermalchemie, Inc. Lakewood, Colorado.

Ganapathy, S., and Natarajan, E. (2009). “Pyrolysis of Coconut Shell: An Experimental Investigation.” *J. Eng. Res.* 6(2), 33–39.

Elliott, D. C., and Hart, T. R. (2009). “Catalytic hydro processing of chemical models for bio-oil.” *Energy and Fuels*, 23(2), 631–637.

Fan, Y., Fowler, D., and Norris, C. (2017). “Potential of a pyrolytic coconut shell as a sustainable bio filler for Styrene – butadiene rubber.” *Ind. Eng. Chem. Res.*, 56(16), 4779–4791

Fardiyanti, D. S., Istanto, H., and Anajib, M. K. (2018). “Extraction of phenol from bio-oil produced by pyrolysis of coconut shell.” *J. Phys. Sci.*, 29, 195–202.

Feng, J., Liu, G., Ma, T., Hu, Z., Wu, K., and Zhang, W. (2012). “The performance of dye-sensitized solar cells using different carbon materials as counter electrodes.” *Carbon*, 51, 436.

Ferdous, D., Dalai, A. K., Bej, S. K., and Thring, R. W. (2002). “Pyrolysis of lignins: Experimental and kinetics studies.” *Energy and Fuels*, 16(6), 1405–1412.

Frolander, A., and Rodsrud, G. (2011). “Conversion of cellulose, hemicellulose and lignin into platform molecules: biotechnological approach.” *EuroBioRef Summer Sch.*, Lecce, Italy, September, 18-24

Garca-Perez, M., Chaala, A., and Roy, C. (2002). “Vacuum pyrolysis of sugarcane bagasse.” *J. Anal. Appl. Pyrolysis*, 65(2), 111–136.

Gollakota, A. R. K., Reddy, M., Subramanyam, M. D., and Kishore, N. (2016). “A review on the upgradation techniques of pyrolysis oil.” *Renew. Sustain. Energy Rev.*, 58, 1543–1568.

Government of India. (2018). "All India installed capacity (in Mw) of power stations installed capacity (in Mw) of power utilities in the states / Uts located in." *Cent. Electricity Authority, Minist. power*, 4, 1–7.

Govind Raj, K., and Alias Joy, P. (2015). "Coconut shell based activated carbon–iron oxide magnetic nanocomposite for fast and efficient removal of oil spills." *J. Environ. Chem. Eng.*, 3(3), 2068–2075.

Han, X., Guo, Y., Liu, X., Xia, Q., and Wang, Y. (2019). "Catalytic conversion of lignocellulosic biomass into hydrocarbons: A mini review." *Catal. Today*, 319, 2–13.

Hasan, M. A., and Sumathy, K. (2010). "Photovoltaic thermal module concepts and their performance analysis: A review." *Renew. Sustain. Energy Rev.*, 14(7), 1845–1859.

Hasanah, U., Setiaji, B., and Anwar, C. (2012). "The chemical composition and physical properties of the light and heavy tar resulted from coconut shell pyrolysis." *J. Pure. App. Chem. Res*, 1(1), 26–32.

Hiloidhari, M., Das, D., and Baruah, D. C. (2014). "Bioenergy potential from crop residue biomass in India." *Renew. Sustain. Energy Rev.*, 32, 504–512.

Hogberg, D., Soberats, B., Yoshio, M., Mizumura, Y., Uchida, S., Kloo, L., Segawa, H., and Kato, T. (2017). "Self-assembled liquid-crystalline ion conductors in dye-sensitized solar cells: Effects of molecular sensitizers on their performance." *Chempluschem*, 82(6), 834–840.

Holman JP (2012). "Experimental methods for engineers." 8th edition, *The McGraw-Hill Companies, Inc.*, Copyright ©, New York, NY 10020

Horne, P. A., and Williams, P. T. (1996). "Influence of temperature on the products from the flash pyrolysis of biomass." *Fuel*, 75(9), 1051–1059.

Hornung, A (2014). "Transformation of Biomass -Theory to Practice." First edition published by *John Wiley & Sons, Ltd.*, 1-357.

- Huang, X., Korányi, T. I., Boot, M. D., and Hensen, E. J. M. (2014). “Catalytic depolymerization of lignin in supercritical ethanol.” *ChemSusChem*, 7(8), 2276–2288.
- Hwang, S., Lee, J. H., Park, C., Lee, H., Kim, C., Park, C., Lee, M. H., Lee, W., Park, J., Kim, K., Park, N. G., and Kim, C. (2007). “A highly efficient organic sensitizer for dye-sensitized solar cells.” *Chem. Commun.*, (46), 4887–4889.
- Jeswani, H. K., Gujba, H., Brown, N. W., Roberts, E. P. L., and Azapagic, A. (2015). “Removal of organic compounds from water: Life cycle environmental impacts and economic costs of the arvia process compared to granulated activated carbon.” *J. Clean. Prod.*, 89, 203–213.
- Joardder, M., Islam, M., Beg, M., and Alam, R. (2011). “Pyrolysis of coconut shell for bio-oil.” *Int. Conf. Mech. Eng., ICME2011* December, 18, 1–6.
- Juan, B., Francisco, F., Ivan, M., Germa, G., and Sixto, G. (2009). “Electron lifetime in dye-sensitized solar cells: Theory and interpretation of measurements.” *J. Phys. Chem.*, 113(40), 17278–17290.
- Kabir, G., and Hameed, B. H. (2017). “Recent progress on catalytic pyrolysis of lignocellulosic biomass to high-grade bio-oil and bio-chemicals.” *Renew. Sustain. Energy Rev.*, 70, 945–967.
- Kan, T., Wang, H., He, H., Li, C., and Zhang, S. (2011). “Experimental study on two-stage catalytic hydro processing of middle-temperature coal tar to clean liquid fuels.” *Fuel*, 90(11), 3404–3409.
- Kennedy, L. J., Vijaya, J. J., Kayalvizhi, K., and Sekaran, G. (2007). “Adsorption of phenol from aqueous solutions using mesoporous carbon prepared by two-stage process.” *Chem. Eng. J.*, 132(1–3), 279–287.
- Kreitman, M. and Gratzel, M (1991). “A low-cost high efficiency solar cell based on dye sensitised colloidal TiO₂ films” *Nature*, 353, 412–414.

- Kulkarni, S. J., Tapre, R. W., Patil, S. V., and Sawarkar, M. B. (2013). "Adsorption of phenol from wastewater in fluidized bed using coconut shell activated carbon." *Procedia Eng.*, 51, 300–307.
- Kumar, R., and Bhargava, P. (2015). "Fabrication of a counter electrode using glucose as carbon material for dye sensitized solar cells." *Mater. Sci. Semicond. Process.*, 40, 331–336.
- Kumar, S., Smith, S. R., Fowler, G., Velis, C., Kumar, S. J., Arya, S., Rena, Kumar, R., and Cheeseman, C. (2017). "Challenges and opportunities associated with waste management in India." *R. Soc. Open Sci.*, 4, 1-11.
- Kusy, J., Andel, L., Safarova, M., Vales, J., and Ciahotny, K. (2012). "Hydrogenation process of the tar obtained from the pyrolysis of brown coal." *Fuel*, 101, 38–44.
- Lappas, A. A., Samolada, M. C., Iatridis, D. K., Voutetakis, S. S., and Vasalos, I. A. (2002). "Biomass pyrolysis in a circulating fluid bed reactor for the production of fuels and chemicals." *Fuel*, 81(16), 2087–2095.
- Lee, H., Kim, Y. M., Lee, I. G., Jeon, J. K., Jung, S. C., Chung, J. Do, Choi, W. G., and Park, Y. K. (2016). "Recent advances in the catalytic hydrodeoxygenation of bio-oil." *Korean J. Chem. Eng.*, 33(12), 3299–3315.
- Lehto, J., Oasmaa, A., Solantausta, Y., Kyto, M., and Chiaramonti, D. (2014). "Review of fuel oil quality and combustion of fast pyrolysis bio-oils from lignocellulosic biomass." *Appl. Energy*, 116, 178–190.
- Li, D., Li, W. H., Liu, Q. C., Fan, Z., Li, H., Ma, W., and Yan, S. H. (2015). "Optimization of processing parameters and macro kinetics for hydrodesulfurization of coal tar." *Energy Sources, Part A Recover. Util. Environ. Eff.*, 37(23), 2591–2600.
- Li, Q., Qi, Y., and Gao, C. (2015b). "Chemical regeneration of spent powdered activated carbon used in decolorization of sodium salicylate for the pharmaceutical industry." *J. Clean. Prod.*, 86, 424–431.

Lin, Y., and Tanaka, S. (2006). "Ethanol fermentation from biomass resources: Current state and prospects." *Appl. Microbiol. Biotechnol.*, 69(6), 627–642.

Liu, X., Luo, Y., Li, H., Fan, Y., Yu, Z., Lin, Y., Chen, L., and Meng, Q. (2007). "Room temperature fabrication of porous ZnO photoelectrodes for flexible dye-sensitized solar cells." *Chem. Commun.*, 27, 2847–2849.

Lu, Q., Li, W. Z., and Zhu, X. F. (2009). "Overview of fuel properties of biomass fast pyrolysis oils." *Energy Convers. Manag.*, 50(5), 1376–1383.

Mahajan, G. V, and Femina, A. (2017). "Preparation and characterization of micro porous activated carbon prepared from prosopis juliflora with chemical and thermal activation." *Res. J. Engineering Sci.* 6(1), 5–11.

Meng, J., Moore, A., Tilotta, D. C., Kelley, S. S., Adhikari, S., and Park, S. (2015). "Thermal and storage stability of bio-oil from pyrolysis of torrefied wood." *Energy and Fuels*, 29(8), 5117–5126.

MNRE. (2017). "Financing of renewable energy projects by Indian renewable energy development agency limited." 22nd report, Committee on public undertakings, New Delhi.

Mohammed, I. Y., Abakr, Y. A., Musa, M., Yusup, S., Singh, A., and Kazi, F. K. (2016). "Valorization of bambara groundnut shell via intermediate pyrolysis: Products distribution and characterization." *J. Clean. Prod.*, 139, 717–728.

Mohan, D., Kumar, H., Sarswat, A., Alexandre-Franco, M., and Pittman, C. U. (2014). "Cadmium and lead remediation using magnetic oak wood and oak bark fast pyrolysis bio-chars." *Chem. Eng. J.*, 236, 513–528.

Mohan, D., Pittman, C. U., and Steele, P. H. (2006). "Pyrolysis of wood/biomass for bio-oil: A critical review." *Energy and Fuels*, 20(3), 848–889.

Mohan, D., Rajput, S., Singh, V. K., Steele, P. H., and Pittman, C. U. (2011). "Modelling and evaluation of chromium remediation from water using low-cost bio-char, a green adsorbent." *J. Hazard. Mater.*, 188(1–3), 319–333.

- Mortensen, P. M., Grunwaldt, J. D., Jensen, P. A., Knudsen, K. G., and Jensen, A. D. (2011). "A review of catalytic upgrading of bio-oil to engine fuels." *Appl. Catal. A Gen.*, 407(1–2), 1–19.
- Ranganadham, M. (2018). "Energy statistics 2018" 25th issue, Central statistics office ministry of statistics and programme implementation government of India." New Delhi.
- Mui, E. L. K., Cheung, W. H., Valix, M., and McKay, G. (2010). "Dye adsorption onto char from bamboo." *J. Hazard. Mater.*, 177(1–3), 1001–1005.
- Murugan, S., and Gu, S. (2015). "Research and development activities in pyrolysis - Contributions from Indian scientific community - A review." *Renew. Sustain. Energy Rev.*, 46, 282–295.
- Nasikhudin, Diantoro, M., Kusumaatmaja, A., and Triyana, K. (2018). "Study on photocatalytic properties of TiO₂ nanoparticle in various pH condition." *J. Phys. Conf. Ser.*, 1011, 1–8.
- Natarajan, E. (2009). "Pyrolysis of rice husk in a fixed bed reactor." *World Academy of Science, Engineering and Technology*, 56, 504-508
- Nazeeruddin, M. K., Péchy, P., and Gratzel, M. (1997). "Efficient panchromatic sensitization of nanocrystalline TiO₂ films by a black dye based on a trithiocyanato-ruthenium complex." *Chem. Commun.*, 1(18), 1705–1706.
- Niquille-Rothlisberger, A., and Prins, R. (2006). "Hydrodesulfurization of 4,6-dimethyldibenzothiophene and dibenzothiophene over alumina-supported Pt, Pd, and Pt-Pd catalysts." *J. Catal.*, 242(1), 207–216.
- Nsamba, H. K., Hale, S. E., Cornelissen, G., and Bachmann, R. T. (2015). "Sustainable Technologies for Small-Scale Biochar Production—A Review." *J. Sustain. Bioenergy Syst.*, 05(01), 10–31.
- Onay, O., and Kockar, O. M. (2003). "Slow, fast and flash pyrolysis of rapeseed." *Renew. Energy*, 28(15), 2417–2433.

Onay, O., and Koçkar, O. M. (2004). “Fixed-bed pyrolysis of rapeseed (*Brassica napus* L.)” *Biomass and Bioenergy*, 26(3), 289–299.

Park, H. J., Dong, J. I., Jeon, J. K., Park, Y. K., Yoo, K. S., Kim, S. S., Kim, J., and Kim, S. (2008). “Effects of the operating parameters on the production of bio-oil in the fast pyrolysis of Japanese larch.” *Chem. Eng. J.*, 143(1–3), 124–132.

Patel, A., Sarkar, P., Tyagi, H., and Singh, H. (2016). “Time value of emission and technology discounting rate for off-grid electricity generation in India using intermediate pyrolysis.” *Environ. Impact Assess. Rev.*, 59, 10–26.

Pechyen, C., Atong, D., Aht-ong, D., and Sricharoenchaikul, V. (2007). “Investigation of pyrolyzed chars from physic nut waste for the preparation of activated carbon.” *J. Solid Mech. Mater. Eng.*, 1(4), 498–507.

Perrich, J. R. (1981). “Activated carbon adsorption for wastewater treatment” 1st edition, *Taylor and Francis group, CRC Press*, Boca Raton, FL., 41-60.

Phusunti, N. (2012). “Pyrolytic and kinetic study of *Chlorella vulgaris* under isothermal and non- isothermal conditions.” *Doctoral dissertation, Aston Univ.*, United Kingdom.

Quan, C., Xu, S., and Zhou, C. (2017). “Steam reforming of bio-oil from coconut shell pyrolysis over Fe/olivine catalyst.” *Energy Convers. Manag.*, 141, 40–47.

Radhakrishnan, C., Natarajan, K., Azhagendran, K., Mohanlal, K., Ponraj, P., and Nivas, R. (2016). “Experimental analysis of bio-oil from coconut shell and front by continuous pyrolysis process.” *Int. J. Inno. Res. Sci., Eng. and Tech.*, 5(4), 4841–4846.

Ragauskas, A. J., Beckham, G. T., Bidy, M. J., Chandra, R., Chen, F., Davis, M. F., Davison, B. H., Dixon, R. A., Gilna, P., Keller, M., Langan, P., Naskar, A. K., Saddler, J. N., Tschaplinski, T. J., Tuskan, G. A., and Wyman, C. E. (2014). “Lignin valorization: Improving lignin processing in the biorefinery.” *Science*, 344, 6185.

- Raga, S. R., and Fabregat-Santiago, F. (2013). "Temperature effects in dye-sensitized solar cells." *Phys. Chem. Chem. Phys.*, 15(7), 2328–2336.
- Rangabhashiyam, S., Anu, N., and Selvaraju, N. (2013). "Sequestration of dye from textile industry wastewater using agricultural waste products as adsorbents." *J. Environ. Chem. Eng.*, 1(4), 629–641.
- Rout, T., Pradhan, D., Singh, R. K., and Kumari, N. (2015). "Exhaustive study of products obtained from coconut shell pyrolysis." *J. Environ. Chem. Eng.*, 4, 3696-3705.
- Ruddy, D. A., Schaidle, J. A., Ferrell, J. R., Wang, J., Moens, L., and Hensley, J. E. (2014). "Recent advances in heterogeneous catalysts for bio-oil upgrading via "ex situ catalytic fast pyrolysis: Catalyst development through the study of model compounds." *Green Chem.*, 16(2), 454-490
- Rudzinski, W. E., Aminabhavi, T. M., Sassman, S., and Watkins, L. M. (2000). "Isolation and characterization of the saturate and aromatic fractions of a maya crude oil." *Energy and Fuels*, 14(4), 839–844.
- Ryu, H. W., Lee, H. W., Jae, J., and Park, Y. K. (2019). "Catalytic pyrolysis of lignin for the production of aromatic hydrocarbons: Effect of magnesium oxide catalyst." *Energy*, 179, 669–675.
- Saad, A., Ratanawilai, S., and Tongurai, C. (2015). "Catalytic conversion of pyrolysis tar to produce green gasoline-range aromatics." *Energy Procedia*, 79, 471-479.
- Sahu, J. N., Acharya, J., and Meikap, B. C. (2010). "Optimization of production conditions for activated carbons from Tamarind wood by zinc chloride using response surface methodology." *Bioresour. Technol.*, 101(6), 1974–1982.
- Sanna, A., Vispute, T. P., and Huber, G. W. (2015). "Hydrodeoxygenation of the aqueous fraction of bio-oil with Ru/C and Pt/C catalysts." *Appl. Catal. B Environ.*, 165, 446–456.

Satya Sai, P. M., et al. (1997). "Production of activated carbon from coconut shell char in a fluidized bed reactor..." *Ind. Eng. Chem. Res.*, 36(9), 3625–3630.

Saxena, R. C., Adhikari, D. K., and Goyal, H. B. (2009). "Biomass-based energy fuel through biochemical routes: A review." *Renew. Sustain. Energy Rev.*, 13(1), 167–178.

Sharifzadeh, M., Richard, C. J., Liu, K., Hellgardt, K., Chadwick, D., and Shah, N. (2015). "An integrated process for biomass pyrolysis oil upgrading: A synergistic approach." *Biomass and Bioenergy*, 76(0), 108–117.

Singh, L. K., and Koiry, B. P. (2018). "Natural dyes and their effect on efficiency of TiO₂ based DSSCs: A comparative study." *Mater. Today Proc.*, 5(1), 2112–2122.

Sinha, D., De, D., Goswami, D., and Ayaz, A. (2018). "Fabrication of DSSC with nanostructured ZnO photo anode and natural dye sensitizer." *Mater. Today Proc.*, 5(1), 2056–2063.

Sirichote, O., Innajitara, W., Chuenchom, L., Chunchit, D., and Naweekan, K. (2002). "Adsorption of Iron (III) Ion on activated carbons obtained from bagasse, pericarp of rubber fruit and coconut shell." *Songklanakarin J. Sci. Technol.*, 24(2), 235–242.

Stamatov, V., Honnery, D., and Soria, J. (2006). "Combustion properties of slow pyrolysis bio-oil produced from indigenous australian species." *Renew. Energy*, 31(13), 2108–2121.

Stoikos, T. (1991). "Upgrading of biomass pyrolysis liquids to high-value chemicals and fuel additives." *Biomass pyrolysis liquids upgrading and utilization*, London: *Elsevier Applied Science*, 227–241

Sukhbaatar, B., Steele, P. H., Ingram, L. L., and Kim, M. G. (2009). "An exploratory study on the removal of acetic and formic acids from bio-oil." *BioResources*, 4(4), 1319–1329.

Sun, M., Ma, X. X., Yao, Q. X., Wang, R. C., Ma, Y. X., Feng, G., Shang, J. X., Xu, L., and Yang, Y. H. (2011). "GC-MS and TG-FTIR study of petroleum ether extract and residue from low temperature coal tar." *Energy and Fuels*, 25(3), 1140–1145.

Sun, Z., and Zhang, W. (2017). “Chemical composition and structure characterization of distillation residues of middle-temperature coal tar.” *Chinese J. Chem. Eng.*, 25(6), 815–820.

Swaminathan, M. (2018). “How can India’s waste problem see a systemic change.” *Econ. Polit. Wkly.*, 53, 16.

Tang, Z., Zhang, Y., and Guo, Q. (2010). “Catalytic hydrocracking of pyrolytic lignin to liquid fuel in supercritical ethanol.” *Ind. Eng. Chem. Res.*, 2040–2046.

Thangalazhy-Gopakumar, S., Al-Nadheri, W. M. A., Jegarajan, D., Sahu, J. N., Mubarak, N. M., and Nizamuddin, S. (2015). “Utilization of palm oil sludge through pyrolysis for bio-oil and bio-char production.” *Bioresour. Technol.*, 178, 65–69.

Ting, T. L., Jaya, R. P., Hassan, N. A., Yaacob, H., Jayanti, D. S., and Ariffin, M. A. M. (2016). “A review of chemical and physical properties of coconut shell in asphalt mixture.” *J. Teknol.*, 78(4), 85–89.

Tinwala, F., Mohanty, P., Parmar, S., Patel, A., and Pant, K. K. (2015). “Intermediate pyrolysis of agro-industrial biomasses in bench-scale pyrolyser: Product yields and its characterization.” *Bioresour. Technol.*, 188, 258–264.

Trinh, T. N., Jensen, P. A., Kim, D. J., Knudsen, N. O., and Sørensen, H. R. (2013). “Influence of the pyrolysis temperature on sewage sludge product distribution, bio-oil, and char properties.” *Energy and Fuels*, 27(3), 1419–1427.

Tripathi, M., Sahu, J. N., and Ganesan, P. (2016). “Effect of process parameters on production of biochar from biomass waste through pyrolysis: A review.” *Renew. Sustain. Energy Rev.*, 55, 467–481.

Tsai, W. T., Lee, M. K., and Chang, Y. M. (2007). “Fast pyrolysis of rice husk: Product yields and compositions.” *Bioresour. Technol.*, 98(1), 22–28.

Vasanth Kumar, personal communication, August 3rd 2017; Vasanth K unpublished internal report (M/s Vayu Gases, Oils and Carbons Bengaluru- 560091), August 2017

- Venkatesan, K., and Senthilkumar, M. (2015). "Comparative analysis of performance and emission characteristics of diesel engine fuelled with emulsified coconut shell pyro oil." *Int. J. Appl. Mech. Prod. Eng.*, 1(2), 19–23.
- Wang, S., Dai, G., Yang, H., and Luo, Z. (2017). "Lignocellulosic biomass pyrolysis mechanism: A state-of-the-art review." *Prog. Energy Combust. Sci.*, 62, 33–86.
- Warnijati, S., Agra, I. B., and Sudjono. (1996). "Pyrolysis of coconut shells in a concentric three tubes reactor." *Renew. Energy*, 9(1–4), 934–937.
- Wildschut, J., Melian-Cabrera, I., and Heeres, H. J. (2010). "Catalyst studies on the hydrotreatment of fast pyrolysis oil." *Appl. Catal. B Environ.*, 99(1–2), 298–306.
- Xiao, X., and Zhang, P. (2015). "Numerical and experimental study of heat transfer characteristics of a shell-tube latent heat storage system: Part I - Charging process." *Energy*, 79, 337–350.
- Yahya, M. A., Al-Qodah, Z., and Ngah, C. W. Z. (2015). "Agricultural bio-waste materials as potential sustainable precursors used for activated carbon production: A review." *Renew. Sustain. Energy Rev.*, 46, 218–235.
- Yan, R., Yang, H., Chin, T., Liang, D. T., Chen, H., and Zheng, C. (2005). "Influence of temperature on the distribution of gaseous products from pyrolyzing palm oil wastes." *Combust. Flame*, 142, 24–32.
- Yang, H., Yan, R., Chen, H., Lee, D. H., and Zheng, C. (2007). "Characteristics of hemicellulose, cellulose and lignin pyrolysis." *Fuel*, 86(12–13), 1781–1788.
- Yang, K., Peng, J., Srinivasakannan, C., Zhang, L., Xia, H., and Duan, X. (2010). "Preparation of high surface area activated carbon from coconut shells using microwave heating." *Bioresour. Technol.*, 101(15), 6163–6169.
- Yang, Y., Brammer, J. G., Mahmood, A. S. N., and Hornung, A. (2014). "Intermediate pyrolysis of biomass energy pellets for producing sustainable liquid, gaseous and solid fuels." *Bioresour. Technol.*, 169, 794–799.

- Yella, A., Lee, H.W., Tsao, H.N., Nazeeruddin, M.K., and Gratzel, M. (2013). "Porphyrin-sensitized solar cells with cobalt (II/ III)-based redox electrolyte exceed 12 percent efficiency." *Science*, 334(6056), 629-634.
- Yorgun, S., Sensoz, S., and Kockar, O. M. (2001). "Flash pyrolysis of sunflower oil cake for production of liquid fuels." *J. Anal. Appl. Pyrolysis*, 60(1), 1-12.
- Yuan, Z., Cheng, S., Leitch, M., and Charles, C. (2010). "Hydrolytic degradation of alkaline lignin in hot-compressed water and ethanol." *Bioresour. Technol.*, 101(23), 9308-9313.
- Zhang, L., Liu, R., Yin, R., and Mei, Y. (2013). "Upgrading of bio-oil from biomass fast pyrolysis in China: A review." *Renew. Sustain. Energy Rev.*, 24, 66-72.
- Zhang, Q., Xu, Y., Li, Y., Wang, T., Zhang, Q., Ma, L., He, M., and Li, K. (2015). "Investigation on the esterification by using supercritical ethanol for bio-oil upgrading." *Appl. Energy*, 160, 633-640.
- Zhang, X., Zhang, Q., Wang, T., Li, B., Xu, Y., and Ma, L. (2016a). "Efficient upgrading process for production of low-quality fuel from bio-oil." *Fuel*, 179, 312-321.
- Zhang, Y., Yao, A., and Song, K. (2016b). "Torrefaction of cultivation residue of *Auricularia auricula-judae* to obtain biochar with enhanced fuel properties." *Bioresour. Technol.*, 206, 211-216.
- Zhao, H. Y., Li, D., Bui, P., and Oyama, S. T. (2011). "Hydrodeoxygenation of guaiacol as model compound for pyrolysis oil on transition metal phosphide hydro processing catalysts." *Appl. Catal. A Gen.*, 391(1-2), 305-310.
- Zheng, J. lu, Yi, W. ming, and Wang, N. na. (2008). "Bio-oil production from cotton stalk." *Energy Convers. Manag.*, 49(6), 1724-1730.
- Zhu, J., Meng, X., and Xiao, F. (2013). "Mesoporous zeolites as efficient catalysts for oil refining and natural gas conversion." *Front. Chem. Sci. Eng.*, 7(2), 233-248.

APPENDIX-1

A1.1 SENSITIVITY ANALYSIS

Table A1.1.1 Sensitivity analysis of pyrolysed products

Parameters	Activated Carbon	Bio-Oil	Bio-Tar	Power
Yield	150 (kg)	260 (l)	40 (l)	1330 (units)
Selling Price (Rs.)	70	8	80	5.6
Margin at 35% of selling price (Rs.)	24.5	2.8	28	1.96
Revenue (Rs.)	10500	2080	3200	7280
Margin amount (Rs.)	3675	728	1120	2548
gross profit (Rs.)	6825	1352	2080	4732
SG&A (Rs.)	1100	1100	1100	1100
Operating profit (Rs.)	5725	252	980	3632

*(SG&A) Selling general and administrative expenses (Assumed)

SG&A includes all non-production expenses incurred by a company in any given period. This includes store rent and labor charges.

The data for range of products extracted from pyrolysis has been given by Vayu Gases oils & carbon as per the standardized experiments carried out.

Table A1.1.2 Approximate estimation of pyrolysed products at different costs

Activated Carbon				Bio-Oil			
Operating profit(Rs.) (5725)	125 (kg)	150 (kg)	175 (kg)	Operating profit(Rs.) (252)	240 (l)	260 (l)	280 (l)
Rs. 90	7087.5	8725	10362.5	Rs. 10	628	772	916
Rs. 80	5837.5	7225	8612.5	Rs. 9	388	512	636
Rs. 70	4587.5	5725	6862.5	Rs. 8	148	252	356
Rs. 60	3337.5	4225	5112.5	Rs. 7	-92	-8	76
Rs. 50	2087.5	2725	3362.5	Rs. 6	-332	-268	-204
Rs. 40	837.5	1225	1612.5	Rs. 5	-572	-528	-484

A1.2 PROPERTIES OF BIO-OIL AND BIO-CHAR DERIVED FROM COCONUT SHELL

A1.2.1 Calorific value by bomb calorimeter

1. Weight of the sample
2. Water equivalent weight
3. Length of thread
4. Nichrome wire
5. Constant temperature (T_1) = _ °C (achieved during experiment after 11 mins)
6. Highest temperature (T_2) = _ °C (achieved during experiment after 11 mins)

$$\text{Calorific value} = \left(\frac{\text{Water equivalent}}{\text{Weight of the sample}} \right) \times T_2 - T_1 \quad \text{cal/gm}$$

A1.2.2 Moisture content %

1. Weight of petridish (W_1)
2. Weight of charcoal (W)
3. Weight of dish + charcoal (W_2)
4. Weight after drying (W_3)
5. Weight of sample after drying

$$\text{Moisture content \%} = \left(\frac{W_2 - W_3}{W} \right) \times 100$$

A1.2.3 Volatile matter

1. Empty weight of crucible (W_1)
2. Weight of sample (W)
3. Weight of crucible and sample (W_2)
4. Weight after drying for 9 mins (W_3)

$$\text{Volatile matter} = \left(\frac{W_2 - W_3}{W_2 - W_1} \right) \times 100$$

A1.2.4 Ash content

Weight of sample after heating till ash is left (W_4)

$$\text{Ash content} = \left(\frac{W_2 - W_3}{W_2 - W_1} \right) \times 100$$

$$\text{Fixed carbon content} = 100 - (\text{Moisture} + \text{volatile matter} + \text{ash content})$$

A1.2.5 Density

1. Empty Weight
2. Weight of filled sample
3. Weight of sample
4. Volume of sample

$$\text{Density} = \frac{\text{Weight}}{\text{Volume}}$$

A1.2.6 Viscosity of bio-oil @ 40 °C

$$\text{Viscosity} = \left(\frac{1.79}{T} \right) \times 0.00260 \times T$$

A1.2.7 H/C and O/C molar ratio

$$\text{Hydrogen} = \frac{\text{Weight percent of Hydrogen}}{\text{Atomic Weight of Hydrogen}}$$

$$\text{Oxygen} = \frac{\text{Weight percent of Oxygen}}{\text{Atomic Weight of Oxygen}}$$

Atomic Weight Carbon=12.011; Hydrogen=1.008; Nitrogen=14.007; Oxygen=15.999

A1.3 UNCERTAINTIES IN HIGH PRESSURE REACTOR

Table: A1.3.1 Uncertainties of measuring instruments in high pressure reactor

Instruments	Absolute uncertainty
Pt-100 KNS terminal head (RS [®] Components)	±0.5 °C (20 – 450 °C)
Pressure gauge (Adarsh)	± 1 bar

For an 95% confidence interval the normal distribution lies within $\pm 2\sigma$, the relative error of individual equipment's is expressed as follows

$$\delta = \left(\frac{\text{Absolute error} \times 2}{\text{Measured value}} \right) \times 100 \quad (\text{A1})$$

The relative error of the temperature measurement (Pt-100 KNS terminal head (RS[®] Components) in the high-pressure reactor was based on maximum trial temperature of 300 °C. Therefore,

$$\frac{\delta_T}{T} = \left(\frac{0.5 \times 2}{300} \right) \times 100 = \pm 0.3\%$$

The relative error of the pressure gauge which is used to measure the maximum pressure of 30 bar in the experiment.

$$\frac{\delta_P}{P} = \left(\frac{1 \times 2}{30} \right) \times 100 = \pm 6.6\%$$

The relative error of the high-pressure reactor based on individual measuring equipment's for maximum operating temperature and pressure of 300 °C and 30 bar. The uncertainty of the high-pressure reactor can be obtained by the uncertainty propagation analysis, as shown in the following equation. (Xiao and Zhang 2015; Holman JP 2012),

$$\frac{\delta_y}{y} = f(T, P) \quad (\text{A2})$$

Therefore,

$$\frac{\delta_y}{y} = \sqrt{\left(\frac{\delta_T}{T} \right)^2 + \left(\frac{\delta_P}{P} \right)^2} \quad (\text{A3})$$

$$\frac{\delta_y}{y} = \sqrt{(0.3)^2 + (6.6)^2} = \pm 6.6\%$$

Table: A1.3.2 Other Equipment's used

Equipment's	Accuracy
Rotary evaporator (IKA [®])	± 1 °C
Ultrasonic Bath (GT Sonic [®])	± 3%

A1.4 UNCERTAINTIES FOR THE EXPERIMENTS IN HIGH PRESSURE REACTOR

Measurements can be precise, which means the measured value is the same as the actual value; they can be precise, which means that the multiple measurements give almost identical values; they can be both exact and precise or they can be neither exact nor precise. The aim is to obtain measured values that are both accurate and precise. Three replicates for each temperature (200°C, 250°C, and 300°C) for samples Ru-C, Pd-C and thermal are used in the study.

The average value of all the measurements

$$Average = \frac{Sum\ of\ measurements}{Number\ of\ measurements} \quad (A4)$$

The deviation of each measurement, which is absolute value of the difference between each measurement and the average value:

$$Deviation = |Measurement - average| \quad (A5)$$

Where | | means absolute value (i.e., convert any negative number to a positive number).

Next, adding all the deviations and divide by the number of measurements to obtain the average deviation:

$$\text{Average} = \frac{\text{sum of deviations}}{\text{number of measurements}} \quad (\text{A6})$$

Now, we can express the precision as a percentage by dividing the average deviation by the average value of the measurements and multiplying the result by 100.

Example: For Pd/C at temperature 200 °C

For three trials the readings were:

Trail 1: 27.95;	Trail 2: 27.05;	Trail 3: 28.85
By using equation (A4)		
$\text{Average} = \frac{27.95 + 27.05 + 28.85}{3} = \frac{83.85}{3} = 27.95$		
The deviations are calculated by using equation (A5)		
$\text{Deviation Trial 1} = 27.95 - 27.95 = 0;$ $\text{Deviation Trial 2} = 27.05 - 27.95 = 0.9;$ $\text{Deviation Trial 3} = 28.85 - 27.95 = 0.9$		
The average deviation is $0.9 + 0 + 0.9 \div 3 = \mathbf{0.6}$		
The precision of this set of measurements is therefore calculated by equation (A6)		
$\text{Precision} = \frac{0.6}{27.95} = 0.0214 \times 100$ $\text{Precision} = 2.14\%$		

For Pd/C at temperature 250 °C

For three trials the readings were:

Trail 1: 23.45;	Trail 2: 22.75;	Trail 3: 24.15
By using equation (A4)		
$\text{Average} = \frac{23.45 + 22.75 + 24.15}{3} = \frac{70.35}{3} = 23.45$		
The deviations are calculated by using equation (A5)		
$\text{Deviation Trial 1} = 23.45 - 23.45 = 0;$ $\text{Deviation Trial 2} = 22.75 - 23.45 = 0.7;$		

$$\text{Deviation Trial 3} = |24.15 - 23.45| = 0.7$$

The average deviation is $0 + 0.7 + 0.7 \div 3 = \mathbf{0.46}$

The precision of this set of measurements is therefore calculated by equation (A6)

$$\text{Precision} = \frac{0.46}{23.45} = 0.0196 \times 100$$

$$\text{Precision} = 1.96\%$$

For Pd/C at temperature 300 °C

For three trials the readings were:

Trail 1: 11.45;	Trail 2: 10.66;	Trail 3: 11.05
By using equation (A4)		
$\text{Average} = \frac{11.45 + 10.66 + 11.05}{3} = \frac{33.16}{3} = 11.05$		
The deviations are calculated by using equation (A5)		
$\text{Deviation Trial 1} = 11.05 - 11.05 = 0.4;$		
$\text{Deviation Trial 2} = 10.66 - 11.05 = 0.39;$		
$\text{Deviation Trial 3} = 11.05 - 11.05 = 0$		
The average deviation is $0.4 + 0.39 + 0 \div 3 = \mathbf{0.26}$		
The precision of this set of measurements is therefore calculated by equation (A6)		
$\text{Precision} = \frac{0.26}{11.05} = 0.0235 \times 100$		
Precision = 2.35%		

A1.5 UNCERTAINTY FOR DSSC

Measuring instruments	Accuracy
Voltmeter (Fluke 115)	± 1.5 volts
K-type thermocouple (RS® Components)	0.1°C

For an 95% confidence interval the normal distribution lies within $\pm 2\sigma$, the relative error is expressed as follows

$$\delta = \left(\frac{\text{Absolute error} \times 2}{\text{Measured value}} \right) \times 100$$

The relative error of the temperature measurement K type thermocouple (RS[®] Components) in the performance analysis of DSSC was based on maximum trial temperature of 70.5 °C. Therefore,

$$\frac{\delta_T}{T} = \left(\frac{0.1 \times 2}{70.5} \right) \times 100 = \pm 0.28\%$$

The relative error of the voltmeter which is used to measure the voltage

$$\frac{\delta_V}{V} = \left(\frac{1.5 \times 2}{311.3} \right) \times 100 = \pm 0.9\%$$

The measured power in the DSSC is a function of temperature and voltage,

$$P = f(V, T)$$

$$\frac{\delta_P}{P} = \sqrt{\left(\frac{\delta_T}{T} \right)^2 + \left(\frac{\delta_V}{V} \right)^2}$$

$$\frac{\delta_P}{P} = \sqrt{(0.28)^2 + (0.9)^2} = \pm 0.94\%$$

List of Publications and Conference Contributions

(A) Research Articles in Peer-reviewed International Journals

Kiran Kumar Dasari and Veershetty Gumtapure, “Activated carbon-based dye-sensitized solar cell for development of highly sensitive temperature and current sensor” IOP Publishers, Mater. Res. Express 6 (2019) 085531. <https://doi.org/10.1088/2053-1591/ab23b7>.

Kiran Kumar Dasari, Veershetty Gumtapure and Saikat Dutta “Upgrading of coconut shell-derived pyrolytic bio-oil by thermal and catalytic deoxygenation” Energy Sources, Part A: Recovery, utilization, and environmental effects <https://doi.org/10.1080/15567036.2019.171146>

Kiran Kumar Dasari and Veershetty Gumtapure, “Intermediate pyrolysis of coconut Shells - Economics related to power generation” In: Singh S., Ramadesigan V. (eds) Advances in Energy Research, Vol. 1. Springer Proceedings in Energy. Springer, Singapore

(B) Oral Conference Contributions

Kiran Kumar Dasari and Veershetty Gumtapure, “Intermediate pyrolysis: Activated carbon-based dye-sensitized solar cell for development of highly sensitive temperature and current sensor” International Conference on advance materials, energy and environmental sustainability (ICAMEES-2018). UPES, Dehradun, India, December 14–15, 2018.

Kiran Kumar Dasari and Veershetty Gumtapure, “Intermediate pyrolysis of coconut shell: Isolated fractions of bio-tar” 12th International conference on thermal engineering: Theory and applications, PDPU Gandhinagar, India, February 23-26, 2019.

(C) Poster and Discussion Symposia Conference Contributions

Kiran Kumar Dasari and Veershetty Gumtapure, “Intermediate pyrolysis of coconut shells - Economics related to power generation” 6th International conference on advances in energy research (ICAER) 2017, Department of energy science engineering, IIT Bombay, Powai Mumbai, Maharashtra, India, 400076. December 12–14, 2017.

Kiran Kumar Dasari and Veershetty Gumtapure, “Intermediate pyrolysis: chemical composition of coconut shell bio-oil” 3rd International conference on sustainable energy and environmental challenges (ISEES-2018), IIT Roorke, India, December 18-21, 2018.

Kiran Kumar Dasari, Veershetty Gumtapure and Saikat Dutta, “Catalytic and thermal hydro-deoxygenation of coconut-shells derived pyrolytic bio-oil” 1st International symposium on analytical and applied pyrolysis (PYROASIA-2019), IIT Madras, December 12-13, 2019.

BIO-DATA

KIRAN KUMAR DASARI

Email ID: kk2kiran@gmail.com and Contact no: +91-9986007700

Personal Details:

Fathers Name: Late Obaleshappa Dasari

Date of Birth: 18 May, 1987

Gender: Male

Nationality: Indian

Permanent Address: KC road, RK apartments, Ground floor G2, Bellary-583101

Educational qualification:

❖ **Ph.D.** (Pursuing) in Mechanical Engineering, 26-12-2014 – Present

Department of Mechanical Engineering,

National Institute of Technology Karnataka Surathkal, Mangalore, Karnataka, India

❖ **M.Tech** in Thermal Engineering, 2011-2013.

Department of Mechanical Engineering,

National Institute of Technology Karnataka Surathkal, Mangalore, Karnataka, India

❖ **B.E.** in Mechanical Engineering, 2005-2009.

Department of Mechanical Engineering

UBDT College of Engineering, Davangere, Karnataka, India

Declaration:

I hereby declare that the above-written particulars are true to the best of my knowledge.

Place: Surathkal, India

()

Date:

KIRAN KUMAR D